Diana Filipa Carmo Guimarães

M. Sc. in Physics Engineering

Measurement of lead concentration in biological tissues by atomic spectroscopy techniques

Dissertation for the degree of Doctor of Philosophy in Physics

Supervisor: José Paulo Moreira dos Santos, Professor, FCT/UNL
Co-supervisor: Maria Luísa Carvalho Leonardo, Professor, FCUL/UL

Evaluation committee:

Chair: Professor Pedro Manuel Corrêa Calvente Barahona
Examiner (s): Professor Luís Manuel Cerqueira Lopes Alves
Professor Mário Emanuel Campos de Sousa Diniz

Other Members: Professor Maria Isabel de Sousa Rocha
Professor Joaquim Marques Ferreira dos Santos

FACULDADE DE CIÊNCIAS E TECNOLOGIA
UNIVERSIDADE NOVA DE LISBOA

December 2011

Diana Filipa Carmo Guimarães

Measurement of lead concentration in biological tissues by atomic spectroscopy techniques

Dissertation for the degree of Doctor of Philosophy in Physics

FACULDADE DE CIÊNCIAS E TECNOLOGIA
UNIVERSIDADE NOVA DE LISBOA

December 2011

To my dear parents.

Acknowledgments

Finally! After four years of continuous battle this war has come into an end. Long and difficult has been the pathway to achieve this final result but in the end what does not kill you makes you stronger. However, this journey was not made alone and this dissertation would not have been possible without the help, support and collaboration of the following persons and institutions.

My supervisor, Professor José Paulo Santos, who I thank for his advice, guidance, patience and extreme rigour from the preliminary to the concluding level, as well for allowing me the room to work in my own way and to grow as a student, a researcher and a scientist want to be.
I also offer my sincerest gratitude to my co-supervisor, Professor Maria Luisa Carvalho, whose support, advices, encouragement, friendship and unsurpassed knowledge of X-ray Fluorescence, had a crucial role during all the work.

I gratefully acknowledge Instituto de Medicina Molecular, namely Professor Isabel Rocha and M. Sc. Vera Geraldes, who have provided all the samples covered in this dissertation, and were always available to explain in detail the sampling procedures.
To the Institute for Analytical Sciences in Dortmund, namely Doctor Alex Von Bohlen and Maria Becker a deepest thank you for giving me the opportunity to work with Total Reflection X-ray Fluorescence. The impressive skills of Maria will not be forgotten as well as the interesting conversations with Alex, who made us deep in the world of Photoshop while discussing physics and eating delicious "kuchen".
I would also like to record my gratitude to Professor Luís Cerqueira, from Instituto Tecnológico Nuclear (ITN), who gave a useful guidance in the use of the Proton Induced X-ray emission spectrometer, always promoting a stimulating and welcoming environment.
To Professor José Capelo-Martinez, Chemistry Department (University of Vigo) an indebted thank you by his valuable advices in science discussion and supervision in atomic absorption spectrometry and ultrasonic solid-liquid extraction.
A big thank you to Professor Mário Diniz, Chemistry Department (FCT/UNL), who introduced me to the world of metallothioneins, histology and histochemical analysis. Thank you for smoothing the path into biology, for your precious help, encouragement and kind supervision.

I will not forget the help and technical support of Carla Rodrigues and Nuno Costa, from REQUIMTE, since my first day working with the graphite furnace and strongly encouraging me until the last. With you I learnt that analytical spectrometers have strong personalities and you have to treat them with love and patience in order to get some results back.

I also would like to make a special reference to Professor Isabel Natário, from the Mathemathics Department (FCT/UNL), for her clarifications about non-parametrical statistics.

I would like to acknowledge the academic and technical support of the Faculdade de Ciências e Tecnologia - Universidade Nova de Lisboa, namely the Physics Department for their assistance since the start of my Graduation in 2001, especially the head of Department Professor Adelaide de Jesus. I convey special acknowledgement to the technical assistants Mrs. Maria Helena Rodrigues, Mrs Fátima Vicente, Mrs Luiza Oliveira, Mrs Paula Correia and Mrs. Hortense Silva for their tenderness, optimism, and indispensable help dealing with administration and bureaucratic matters.
I also express my appreciation to the financial support of the Fundação para a Ciência e Tecnologia (FCT) for the PhD Grant (SFRH/BD/38788/2007) and for the Project No. PEstOE/FIS/UI0303/2011, financed by the European Community Fund FEDER through the COMPETE – Competitiveness Factors Operational Programme.

I am heartily thankful to Professor Lourdes Costa, who has always been the person I appealed in the most difficult times. Thank you for hearing me, for being always available despite your busy schedule, for your kindness, friendship, advices and for being a lovely Human being.
To Doctor Cláudia Quaresma, a big thank you, for the enriching discussions about statistics and also for your support and friendly smile, full of hope and cheer, every time you saw us straggling with our research work.

To my dear friends and PhD colleagues, M.Sc. Rui Pinto, M. Sc. Mauro Guerra, Doctor Pedro Amaro, M.Sc. Diogo Almeida and Doctor Rodrigo Antunes, a sincere thank you! Thank you for giving me my sanity back discussing about Physics (which sometimes seemed to be nothing more than a distant dream) for creating such a great friendship at the office, at the table-tennis, and many places in between. Thank you for your help during all these years, for cheering me up during my stressful stages (almost all of them), and making part of my life. An even more special thanks to M.Sc. Rui Pinto and M.Sc. Mauro Guerra. Guys, without our laughs, our trips, our pints and our friendship this journey would have been way more difficult.
Talking about friendship, trips and pints, I cannot forget to thank Doctor Grant Jobbra Copeland, my Scottish mate, who followed up close this journey helping me many times with the english translation of some reports. I hope next time you see me talking in an conference, the lights don't go out and the fire protections are not activated!

I would also like to thank my colleagues and friends, Doctor Marta Manso, M.Sc. Sofia Pessanha, M. Sc. Ana Guilherme, Doctor Tânia Magalhães, Doctor Pedro Custódio, Doctor Jorge Sampaio, M.Sc. Ana Cavaco and M.Sc. Gonçalo Picado for all the support and for the inspiring phD/master

dissertations, which helped me to increase my knowledge on X-ray Fluorescence. A special thanks to Doctor Marta Manso, M. Sc. Sofia Pessanha and M.Sc. Ana Guilherme, who often had to bear the brunt of my frustration against spectrometers that insisted not to work and for the amazing, professional and friendly working environment. You have been invaluable on both academic and personal level, for which I am extremely grateful. Although it has been a great road trip, I still hate Eyjafallajokull.

To my colleagues and chemists friends Doctor Gonçalo Vale, Doctor Ricardo Carreira and Doctor Marco Galésio a huge thank you. The stimulating science discussions, the dry humor about scientist's life, the growing friendship…all the time spent together was refreshing, cheering and provided me a pleasant time during my work at the Chemistry Department. A special thanks to Doctor Gonçalo Vale, it was a pleasure to work with you, you are really an atomic absorption geek!

Above all, I would like to thank my family. My dear parents, Pedro Guimarães and Cecília Guimarães, for their unflinching encouragement, support, and for their gently and caring love, without which I would not be the person I am today. Thank you for your patience and for always believing in me. This work is dedicated to you! My dear grandparents, Armando Guimarães and Maria Tomásia Guimarães, for their indissoluble support and prayers, love and tenderness. Also to my uncles, Victor Guimarães and Fernando Carmo, and aunts, Maria José da Silva and Fernanda Pimentel, and to my beloved sister, Sara de Oliveira, a big thank you for being an inspiration in my life and making me stronger each day. To my other half, Bruno Dias Guedes, a thank you for showing me that there are far much more important things in life. Your confidence in me, patience, friendship and love have taken the load off my shoulder. It is a pleasure to share my future with you.

To all my friends, and they know who they are, a big thank you for all the relaxing times, fun and support, as well as my apology that I could not mention personally one by one. However a special mention has to be made to Diana Eugénio and Maria Pereira. Diana, thank you from the heart for your dedication, constant support and care. You make me a stronger person and your friendship is irreplaceable. Maria, you are simply the best! Thank you for making me laugh constantly and for being such a good friend. An exceptional thanks as well, to that special Friend that is always with me.

Abstract

Lead is a toxic element that has no biological role. To increase the knowledge of the mean lead concentrations accumulated and excreted by the organism, a study was developed to measure lead concentrations, using different atomic spectrometry techniques, in several tissues and excretions of Wistar rats. These rats were divided in two groups: one exposed to lead since foetal period, by lead acetate in drinking water, and a control group, not exposed to lead. By collecting samples of rats with different ages it was also studied the influence of age in lead concentrations. The studied organs and excretions were: iliac bone, tibia-fibula, femur, skull, liver, kidney, urine and faeces.

When conducting a study like this, the analytical techniques used the knowhow and the ability to understand the physical processes occurring are also of major relevance. In this work it was used the Energy Dispersive X-ray Fluorescence (EDXRF) technique to analyze the solid samples and the Electro Thermal Atomic Absorption Spectrometry (ETAAS) technique to analyze the urine. To carry on with the urine analysis it was developed an Ultrasound Solid-Liquid Extraction (USLE) procedure. This procedure was also applied to analyse brain samples. The Total Reflection X-ray Fluorescence (TXRF) technique was also used to study urine samples and to assess some of the results obtained with ETAAS.

In this work, several correlations between the different tissues were found. A possible evidence of pre-natal exposure was verified because the samples belonging to rats with 1 month old presented much higher mean lead concentrations than the concentrations, measured in works of other authors, of rats exposed to lead but not from foetal period. Furthermore, this study seems to corroborate that lead ingestion decreases with age, once it was measured a decrease of lead excretion by faeces with age. It was observed that lead concentration in tissues depends on the type of tissue. Mean lead concentrations measured were higher in bones (iliac, femur, tibia-fibula>skull) - hundreds of ppm, then in kidney - dozens of ppm and finally in liver on the order of ppm. The urine samples had the lowest mean lead concentrations on the order of hundreds/thousands of ppb, and faeces the highest mean lead concentrations, with values of dozens of thousands of ppm. One of the main contributions of this work was to show that lead accumulation and excretion decreases with age by plateaus in all tissues except in the kidneys.

Key words: EDXRF, ETAAS, TXRF, USLE, lead, biological samples, age dependency.

Resumo

O chumbo é um elemento tóxico sem função biológica no organismo. Para melhorar o conhecimento relativamente às concentrações acumuladas e excretadas pelo organismo, foi elaborado um estudo para medir a concentração de chumbo, utilizando diferentes técnicas de espectrometria atómica, em vários tecidos e excreções de ratos Wistar. Estes ratos foram divididos em dois grupos: um exposto ao chumbo desde o período fetal, através de acetato de chumbo dissolvido na água que ingeriam, e um grupo controlo, não exposto ao chumbo. A recolha de amostras de ratos com idades diferentes permitiu também estudar a influência da idade na concentração de chumbo. As concentrações de chumbo foram medidas e quantificadas nos ossos ilíacos, tíbia-perónio, fémur, crânio, fígado, rim, urina e fezes.

Quando se conduz um estudo com esta dimensão é necessário ter em conta as técnicas de análise utilizadas, o know-how e a capacidade de compreender os processos físicos que ocorrem. Neste trabalho utilizou-se a técnica de Fluorescência de Raios-x Dispersiva em Energia (EDXRF) para analisar as amostras sólidas e a técnica de Espectrometria de Absorção Atómica Electrotérmica (ETAAS) para analisar a urina. Para se efectuar a medição das amostras de urina foi necessário desenvolver um procedimento de Extracção Assistida por Ultra-Sons (USLE). Este procedimento foi também usado na análise de amostras de cérebro. A técnica de Fluorescência de Raios-x por Reflexão Total (TXRF) foi também utilizada para medir amostras de urina e verificar alguns dos resultados obtidos por ETAAS.

Neste trabalho, constatou-se a existência de várias correlações entre os diferentes tecidos. Foi também observada uma possível evidência da exposição materna durante a gravidez, uma vez que as amostras pertencentes a ratos com 1 mês de idade apresentaram concentrações médias de chumbo muito maiores que as concentrações encontradas em trabalhos de outros autores feitos em ratos expostos ao chumbo, mas não desde período fetal. Verificou-se uma diminuição, ao longo da idade, da concentração de chumbo excretada nas fezes o que poderá corroborar o facto de que a quantidade de chumbo ingerida diminui com a idade. Constatou-se que a concentração de chumbo nos tecidos depende do tipo de tecido. As concentrações médias de chumbo medidas foram mais altas nos ossos (ilíaco, fémur, tíbia-perónio > crânio) - centenas de ppm; seguindo-se o rim - dezenas de ppm; e, finalmente, o fígado na ordem dos ppm. A urina apresentou a menor concentração de chumbo medida, na ordem das centenas/milhares de ppb, e as fezes a mais alta, com valores nas dezenas de milhares de ppm. Uma das principais contribuições deste trabalho foi mostrar que, ao longo do tempo, existe um a diminuição na acumulação e excreção de chumbo que é feita por patamares em todos os tecidos, excepto nos rins.

Palavras-chave: EDXRF, ETAAS, TXRF, USLE, chumbo, amostras biológicas, dependência com a idade.

Table of contents

List of Figures

List of Tables

Acronyms and abbreviations

AAS - Atomic Absorption Spectrometry

ATSDR -Agency for Toxic Substances and Disease Registry

AXIL - Analysis of X-ray Spectra by Iterative Least Squares

BCR - Community Bureau of Reference

BDH - British Drug Houses

BDL - Below Detection Limit

BQL - Below Quantification Limit

c.f. - *confer* (consult)

CV -Coefficient of Variation

CVAAS - Cold Vapour Atomic Absorption Spectrometry

DATTPIXE - Data Analysis Thick Target Proton Induced X-ray Emission

DFC - Digital Film Camera

DL - Detection Limit

DPX - Distyrene Plasticizer Xylene

e.g. - *exempli gratia* (for example)

EDL - Electrodeless Discharge Lamps

EDXRF - Energy Dispersive X-ray Fluorescence

EPA - Environmental Protection Agency

et al. - *et alii* (and others)

ETAAS - Electrothermal Atomic Absorption Spectrometry

FAAS - Flame Atomic Absorption Spectrometry

FCT/UNL - Faculdade de Ciências e Tecnologia/Universidade Nova de Lisboa

FCUL/UL - Faculdade de Ciências/Universidade de Lisboa

FWHM - Full Width at Half Maximum

GFAAS - Graphite Furnace Atomic Absorption Spectrometry

HCL - Hollow Cathode Lamp

HDA - Hypothalamic Defense Area

HGAAS - Hydride Generation Atomic Absorption Spectrometry

HPGe - High Purity Germanium

ICP-AES - Inductively Coupled Plasma Atomic Emission Spectrometry

ICP-MS - Inductively Coupled Plasma Mass Spectrometry

ICP-OES - Inductively Coupled Plasma Optical Emission Spectrometry (same as ICP-AES)

IQ - Intelligence Quotient

ISAS - Institute for Analytical Sciences

IUPAC - International Union of Pure and Applied Chemistry

LOD - Limit of Detection

LOQ - Limit of Quantification

m/m - mass (of solute) per mass (of solvent)

m/v - mass (of solute) per volume (of solvent)

MWD - Microwave Digestion

NBS - National Bureau of Standards

NTS - Nucleus Tractus Solitarius (or Nucleus of the Solitary Tract)

PIXE - Proton Induced X-ray Emission

ppb - parts per bilion

ppm - parts per milion

PTFE- Polytetrafluoroethylen

ROI - Region of Interest

RSD - Relative standard deviation

SD - Standard deviation

SDD - Silicon Drift Detector

SRXRF - Synchrotron Radiation X-ray Fluorescence

TXRF - Total Reflection X-ray Fluorescence

USLE - Ultrasound Solid-Liquid Extraction

v/v - volume (of solute) per volume (of solvent)

w/v - weight (of solute) per volume (of solvent)

w/w - weight (of solute) per weight (of solvent)

WHO - World Health Organization

XRF - X-ray Fluorescence Spectrometry

XRFAES - X-ray Fluorescence Automatic Evaluation System

Symbols

K - A series of orbitals with the principal quantum number equal to 1

L - A series of orbitals with the principal quantum number equal to 2

n_i - refractive index of the medium *i*

v_i - velocity of the radiation in the medium *i*

c - velocity of the radiation in vacuum

θ_i - incidence angle

θ_i^* - reflection angle

θ_r - refraction angle

β - imaginary component of the refracting index for X-ray radiation

δ - decrement of the refracting index for X-ray radiation

N_A - Avogadro's number

r_e - classical electron radius

ρ - density

Z - atomic number

A - mass number

λ - wavelength

μ - linear absorption coefficient

θ_c - critical incidence angle

α_c - glancing angle

E - energy of incident beam

I' - intensity of characteristic lines from the X-ray tube

V_C - critical voltage

V - applied X-ray tube voltage

i' - current through the X-ray tube

γ - constant that depends on the emission characteristic X-ray radiation

λ_{min} - short wavelength limit for the X-ray tube continuous radiation

I'' - total intensity of the continuum X-ray spectrum

k - constant that includes the current of the X-ray tube

χ^2 - Chi square function

K_α - the more intense lines of K series

K_β - the second more intense lines of K series

L_α - the more intense lines of L series

L_β - the second more intense lines of L series

I_{P_i}- intensity of a characteristic peak of an element *i*

I_0 - intensity of incident beam

K_i - calibration factor

c_i - concentration of the element i

m - sample thickness

C_i - self attenuation factor

α_i - factor that encloses the attenuation of incoming radiation and outgoing characteristic radiation

$\mu_m\left(E_{1,j}\right)$ - mass attenuation coefficient for element *j* at the incident X-ray energy

$\mu_m\left(E_{i,j}\right)$ - mass attenuation coefficient for element *j* at the characteristic X-ray energy for element *i*

φ_1 - angle for incoming radiation on the sample

φ_2 - angle for emitted radiation from sample

σ_{X_i}- ionization cross section of an element *i*

ω_i - fluorescent yield for element *i*

$P_{n\to m}$ - transition probability from level *n* to *m*, in element *i*

C'_i - absorption of radiation in air and detector window for element *i*

ε_i - detector efficiency for element *i*

Ω - detector solid angle

N_T - total accumulated counts of X-ray photons corresponding to a certain region of interest

σ_N - standard deviation associated to N_T

σ_p - standard deviation associated to the element peak counts

σ_B - standard deviation associated to the background

N_P - counts referring to the element peak

N_B - counts referring to the background

N_i - net intensity of the principal peak of the analyte i

B_i - absolute sensitivity particular of element i

S_i- the relative sensitivity of element i

rf - reference element

w - volume of the internal standard

V - volume of the sample

is - internal standard

σ_{blank} - standard deviation associated to the peak counts of a blank sample

T - transmittance

I - intensity of attenuated beam

A - absorbance

b - thickness of the sample

a - absorptivity

$\Delta\lambda_{1/2}$ - linewidth

$\bar{X}$ - mean value of the variable X

R^2 - coefficient of determination

r_s - Spearman rank correlation coefficient

CHAPTER I - INTRODUCTION

1.1. General study: outline and goals

Lead has no physiological function in the organism and represents a problem to the public health [1]. Its toxicity is mainly due to the affinity for sulfidric groups, inhibiting enzymes activity, and its ability to replace calcium. Lead intoxication symptoms range from common symptoms, as nausea and fatigue in the beginning of intoxication, to severe manifestations as peripheral neurophaty, saturnine colic, dementia and even death.

Lead is a soft, ductile and malleable material with high density and very resistant to corrosion. Due to these properties it plays a significant role in modern industry, being the most widely used nonferrous metal [2]. Generally, human exposure to lead comes from the following main sources: leaded gasoline, lead-based paint; lead pipes in water supply systems; processes such as lead mining, smelting, and coal combustion. It is also used in ceramic glazes, batteries, and cosmetics [3, 4].

Even with the recent efforts being made to reduce the lead (Pb) concentrations in the environment, intoxication by this poisonous element is still a current problem. Several recommendations/regulations have been developed by agencies of environmental and public health protection, such as Environmental Protection Agency (EPA), World Health Organization (WHO) and Agency for Toxic Substances and Disease Registry (ATSDR). These agencies have established limit values of mean lead concentration in blood, water, air and soil. The established threshold concentration of lead for children in blood is 10 $\mu g\ dL^{-1}$ while for exposed workers is 30 $\mu g\ dL^{-1}$. The lead concentration in public air should be no higher than 1.5 $\mu g\ m^{-3}$ averaged over 3 months, while in workroom the limit is 50 $\mu g\ m^{-3}$ for an 8-hour workday. Regulations also limit lead in drinking water to 1 000 $\mu g\ dL^{-1}$, although the goal is drinking water free of lead. For residential soils, the value is 400 $\mu g\ g^{-1}$, although only soils with concentrations below 50 $\mu g\ g^{-1}$ are considered not contaminated [5].

The debate on the level from which the concentration of lead ingested starts producing adverse effects has not reached an agreement. With increasingly sensitive methods, lower and lower doses effects have been identified, suggesting there is no threshold for lead toxicity [6].

Besides all the studies made there is still a major lack of information concerning the correlation of lead concentration in the several biological tissues and its effects.

The main goal of this work is to increase the knowledge of lead accumulation and excretion in the organism, through the analysis of lead concentrations in several tissues and excretions of exposed rats, developing new sample treatment methodologies whenever needed. Comparing the mean lead concentration values of the exposed rats with control rats, finding relations between the several

excretions and tissues and study the influence of age and pre natal exposure in lead concentrations are the principal objectives.

The novelty of this study lies in the fact that it is assessed, for the first time, the influence of age in such large number of organs and excretions on the same group of rats exposed since the foetal period.

Two groups of Wistar rats were used, one exposed to lead since foetal period (n=30) and other, a control group (n=20), not exposed to lead. The measurements were made in several tissues and excretions of rats ageing between 1 and 11 months, with about 1 month interval. To determine mean lead concentrations of the samples two principal techniques were used Energy Dispersive X-ray Fluorescence (EDXRF) for liver, kidney, bones (skull, iliac, femur, tibia-fibula) and faeces, and Electrothermal Atomic Absorption Spectrometry (ETAAS) for the urine samples.

ETAAS was also used in some analysis made in brain, namely two specific brain areas Nucleus Tractus Solitarius (NTS) and Hypothalamic Defence Area (HDA), responsible for the arterial pressure control. This last study was made without considering the age of the rats and mainly to develop a method to extract lead from brain tissues using ultrasonic solid-liquid extraction.

The liquid urine samples were analyzed by ETAAS and Total Reflection X-ray Fluorescence (TXRF) essentially due to the small volume and amount of lead concentrations present in the samples.

The TXRF technique provides multi-elemental and non-destructive analysis, and it is of common use in trace element determinations in environmental and biomedical samples study. Due to the high reflectivity of the sample holder almost eliminating the spectral background, the detection limits of this technique are in the order of $\mu g\ L^{-1}$ [7-10].

The most widely used technique to measure lead in urine is the ETAAS, and several analytical methods have been described for urine analysis using this technique [11-13]. Nevertheless, it was developed a sample treatment method based in the ultrasonic solid-liquid extraction [14-16], to assure that the measurement of the lead concentration concerns not only the liquid part, but also the solid part (precipitation) of the urine. The detection limits of this technique are in the order of 0.1 $\mu g\ L^{-1}$.

The EDXRF is a widespread fully matured instrumental analytical method. This analytical method plays an important role in biological samples analysis once it provides multi-elemental analysis, for all the elements with atomic number higher than 13, in a wide range of concentrations [17]. The EDXRF has the advantages of performing non-destructive analysis independently of the chemical form of the samples, rapidly at relatively low costs and high precision. To improve the accuracy of the EDXRF analysis triaxial geometry was used [7, 18] and detection limits in the order of $\mu g\ g^{-1}$ were achieved.

This dissertation is divided into six main Chapters: Chapter I consists in some general facts about lead and an introduction to the work and main goals; Chapter II is dedicated to the history of lead, its intake and distribution in the organism, toxicity in the main organs and excretions studied in this work, as well as a review about the current spectroscopic techniques for lead analysis in biological samples; Chapter III relies in the fundamental principles of X-ray Spectrometry, giving especial attention to EDXRF and TXRF; Chapter IV contains the fundamental principles and main features but of Atomic Absorption Spectrometry (AAS), giving emphasis to ETAAS, more specifically to graphite furnace devices; Chapter V contains the description of the experimental procedure and includes the sample collection, sample treatment procedure development, experimental setups and a small introduction to the statistical tests used, and finally Chapter VI that comprehends the results and conclusions of this study.

CHAPTER II - LEAD

2.1. Lead in the Environment: A worldwide problem

Lead occurs naturally in the Earth crust, and is usually found combined with other elements to form lead compounds, for example lead sulphide (PbS) and more rarely lead carbonate ($PbCO_3$) and lead sulphate ($PbSO_4$) [5]. Due to its valence shell configuration $6s^2$ $6p^2$, lead can be found in three oxidation states: Pb^0, the metal; Pb^{2+} that exists primarily in the environment; and Pb^{4+} that is only formed under extremely oxidizing conditions [19].

This heavy metal was widely used by mankind for 6000 years. The history of lead poisoning is nearly 2500 years old with the earliest written accounts of lead toxicity found in Egyptian papyrus [20]. It was also commonly used by the Romans and Greeks for glazing pottery, kitchenware, lead seals attached to messages and merchandise and for plumbing [19]. During the Middle Ages lead was commonly used for medicinal purposes and alcoholic beverages, in which large amounts of lead were added intentionally to sweeten the wine and ciders [19, 21]. The use of lead continued to spread over the centuries and only in the 15th century appeared the first prohibition laws, with the Spanish and the French governments prohibiting the use of lead in wine, despite it continued being used with other purposes as paint pigments and moveable type for the printing press. This heavy element continued being used through the centuries and it is appointed as the main cause of death of several famous painters, as for example the Spanish painter Francisco Goya (18th-19th centuries) and the Dutch painter Van Gogh (19th century), who used lead pigments on their paintings [22, 23]. With the industrial revolution the amount of industrial waste increased, in particular waste products with high concentrations of heavy metals from mining and sewage sludge. These waste water sludges are still commonly used in agriculture as fertilizers that contaminate the soils and increase the exposure to lead in the environment (*c.f.* Figure 1).

In the last decades, a lot of efforts have been done in order to reduce the high lead levels that humans are exposed to. Safety procedures as the withdrawal of lead in gasoline, the removing of lead solder in food-containing, the prohibition of household paints with high lead concentrations, the control in the process of producing and recycling batteries, the improvements in vigilance guidelines to detect lead in toys, in plastics and in cosmetics, as well as the severe legislation in the use of hazard substances to produce electrical and electronic equipment, have been implemented in the more industrialized countries [3, 5, 24].

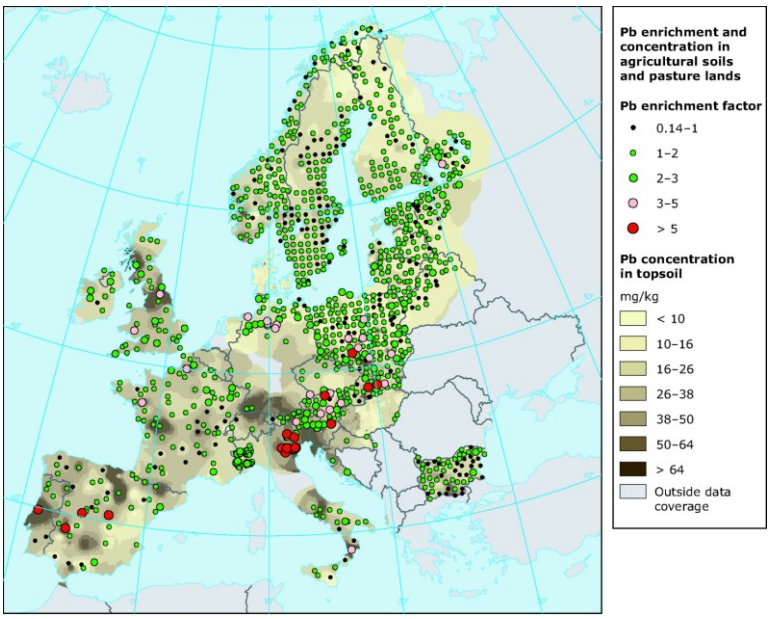

Figure 1: Soil contamination by lead in 2005 25].

However, lead blood levels are usually greater than 10 µg dL^{-1} in children younger than 2 years of age that live in urban areas of developing countries [26]. In China a review of 17 studies from different industrial and heavy traffic areas of the country found that between 65% and 99.5% of children had blood lead levels above 10 µg dL^{-1}. Even outside of those high-risk areas, about 50% of China's children had high blood lead levels [27]. In Nigeria, despite the lower levels of industrialization and car usage, it is estimated that 15% to 30% of the children living in urban areas have blood lead levels greater than 10 µg dL^{-1} [28].

Despite the efforts to reduce lead exposure, the human being is still exposed to lead levels 100- to 1000-fold higher than pre-industrial humans [29]. Saturnism, intoxication by lead, is still one of the most significant occupational and environmental health problems.

2.2. Lead intake and distribution

The absorption of lead into the body has three main intake routes: through the skin, by inhalation and by ingestion. The intake of lead by dermal exposure is a much less efficient route than inhalation and ingestion. In exposure through the skin several layers of cells have to be crossed to reach the capillary vessels where the absorption of lead occurs. Consequently, this process is much more effective for liposoluble substances, such as organic lead compounds (tetraethyl lead and tetramethyl) [30].

In air, metals may occur as aerosols and, in some instances, as vapour. The amount of lead inhaled depends on the number of breaths per minute, the volume breathed per day (an increase in workload will determine a greater absorption of lead) and age-related factors that determine breathing patterns (*e.g.*, nose breathing vs. mouth breathing and air-stream velocity within the respiratory tract) [31]. After inhalation, the metal will be deposited on the walls of the airways. The amount deposited will depend on the particle size and solubility. Lead in submicron size particles can be almost completely absorbed through the respiratory tract, whereas larger particles may be swallowed [32]. In general, particles larger than 2 μm are trapped in the mucus of the respiratory system and are removed to the mouth, or through the glottis into the stomach. Smaller particles, less than 1 μm, are deposited in the bronchiolar and alveolar regions of the respiratory tract and absorbed into the systemic circulation. The very small particles, less than 0.01 μm, can penetrate deep into the lungs but end up being almost in its entirety, expelled by exhalation [5]. The absorption via respiratory system is about 10 times more efficient than the absorption in the gastrointestinal tract, about 50% of the inhaled lead is absorbed by blood in adults [33].

In contrast to the extensive studies in the lung, absorption of metal in the gastrointestinal tract is less well understood. In general population, the contribution of the gastrointestinal route to the total lead absorbed is greater than the respiratory one and is the responsible for most of children intoxications.

Several factors may affect absorption and consequently the fraction of metal that is absorbed, such as the chemical form of the compounds ingested, the pH of the stomach, the size of the contaminated particles, the age (children absorbs ~40% and adults ~10%; absorption rate is also higher in younger animals [34-36]), the meal status (*e.g.* fed vs. fasted) and the simultaneous ingestion of nutrients that affect the solubilisation and binding of Pb (Fe and Ca deficiency may result in higher absorption of lead) [5, 37].

Once lead has been taken into the gastrointestinal tract through food or drinking water, the process of absorption is initiated in the stomach, where food is digested by enzymatic hydrolysis to produce small molecules that are easily absorbed. The digested material moves into the duodenum and small intestine. The materials on the surface of the gastrointestinal tract can be absorbed into the walls and hence the blood chain [38].

After being absorbed to the blood, lead is distributed to all the organs. Blood contains lead bound to erythrocytes, as a non-diffusible form, and in plasma as a diffusible form. Over 90% of total blood lead is bound to erythrocytes cells because of its high affinity and capacity to hold lead. However, it is the interstitial plasma that contains the biologically available fraction of lead and the main role on its distribution to the different tissues [19, 24]. The half-time of lead in blood is approximately 30 days [39]. Once distributed by blood, lead is accumulated in body organs and mainly in bones. Bone represents more than 90% of total body lead in adults, and approximately

70% in young children, with a half-life in the order of years to decades [40-44]. Lead competes with Ca for the formation of the primary crystalline matrix of bone, hydroxyapatite. The fixation of this heavy metal in bone is seen as a protective mechanism that limits its distribution to more sensitive tissues [44-46]. However, accumulation is still made in the soft tissues, though in a minor scale and with lead biological half-times of approximately 3-4 weeks [35, 39]. In general, among soft tissues, the higher percentage of lead is accumulated in kidney followed by liver and other organs as heart and brain [19]. However, skeleton can't be considered an inert repository for lead. Gradual release from the bone serves as a persistent source of toxicity even after the end of external exposure. This mobilization can be increased by several factors like age, sex, nutritional status and by some special conditions associated with bone turnover, such as pregnancy, lactation, menopause, osteoporosis, immobilization, and hyperthyroidism and bone fractures [47, 48].
Absorbed lead that is not stored in the tissues is filtered and excreted through the main excretory routes: kidney to urine (about 76%), and liver to bile and then to faeces (about 16%). Small amounts are also excreted through other minor routes of excretion, such as sweat, saliva, hair, nails (about 8%). Lead is also excreted in breast milk. [5, 49, 50].

There are several models of lead toxicokinetics that have been proposed to characterize parameters as retention of lead in various tissues and relative rates of distribution among the tissue groups. However, there is no consensus among researchers regarding the use of a certain metabolic model.
The daily exposure limit for lead with no increases in the body lead load corresponds to the absorption of 600 μg in adults, and 300 μg in children. Below this threshold, there appears to exist a balance, between absorption and excretion, so that the amount of lead excreted corresponds to the amount absorbed [38].

2.3. Lead toxicity and intoxication

Lead toxicity is mainly due to three biochemical factors. The first is lead ability to bind to important molecules, namely the sulfhydryl (-SH) and amide groups, common components of enzymes, changing their configuration and decreasing their activities. Two of the enzymes in the heme biosynthetic pathway that are inhibited by lead are the δ-aminolevulinic acid dehydratase (ALAD) and the mitochondrial enzyme ferrochelatase that catalyzes the incorporation of Fe in the porphyrin ring. Their inhibition will be reflected in the accumulation of intermediates of the heme pathway, respectively, aminolevulinic acid (ALA) and erythrocyte zinc protoporphyrin because the incorporation of Fe is substituted by Zn. A t high blood lead level, the inhibition of these enzymes

may reflect in a decrease in heme synthesis and consequently in hemoglobin [5, 19].
The second factor is lead ability to compete with essential metallic cations for binding sites inhibiting their action. This behaviour is particularly concerning in the case of Ca due to the increase of lead affinity to the bone tissue. The third factor is lead capacity to interfere with vitamin D metabolism, inhibiting the production of the active form of this vitamin [51].

Depending on the exposure period, lead poisoning intoxication can be described as acute (less than 15 days), intermediate (15-364 days) and chronic (more than 365 days) [5].
One of the principal problems concerning lead intoxication is that the early symptoms are common to other diseases. This increases the difficulty of diagnose without medical testing, what suggests that subclinical lead toxicity can be more prevalent than is recognized. Differences in the IQ of children and in their behaviour [52], in hearing thresholds and in height [53, 54], fatigue, sleep disturbances and headaches, irritability, loss of appetite and nausea are some of the subclinical symptoms already detected [55]. These symptoms are only considered signs of intoxication if the blood test analysis, or work conditions, indicate an increased exposure to lead.

After a long exposure time, or exposure to abnormally high lead concentrations, the symptoms became clinical and may cause severe impairments in hematopoietic, central nervous, reproductive, gastrointestinal, cardiovascular, renal and hepatic systems [36, 56, 57]. Among the clinical symptoms there are: acute gastrointestinal colic and abdominal pain known as saturnine colic [58]; peripheral neuropathy - wrist and foot drops [59]; Burton's Line - bluish line in the bottom of the gum resulting of lead sulphite accumulation [60]; functional and morphological renal changes [61]; fertility problems [62] and lead encephalopathy (delirium, seizures and even lapse into coma) [63]. There are also some studies that indicate appearance of malignant and benign tumours in rats and mice. However, there is no conclusive evidence of carcinogenic properties of lead in humans [64-66].

In the following Sections it will be referred the effects of lead poisoning in all the tissues studied in this work as well as some particularities of lead excretion by faeces and urine.

2.3.1. Lead in faeces

The mechanisms for faecal excretion of absorbed lead are still not clear. However, it is believed that pathways of excretion may include secretion into the bile and passing directly by blood to intestine walls [67]. Faeces have normally the highest lead concentrations, corresponding to the majority of the lead that is not absorbed into the blood. It is known that, in adults more than 90% of the amount of lead taken into the human body will be expelled within a couple of weeks in the

waste [5]. The upper limit of lead concentration considered acceptable in humans is about 50 μg g^{-1} in dry faeces [68].

2.3.2. Lead in urine

The lead excretion in urine is mainly through glomerular filtration [69]. Due to the easy non-invasive sample collection and to the absence of health risk, urine is one of the most convenient samples for human biomonitoring [70-72]. However, urine mean lead concentration measurements do not reflect the body lead burden. This is in part due to the wide variation in renal excretion rates, the large dilution effects in the bladder and the high nephrotoxic lead exposures that may induce potential alterations in kidney function on excretion [12, 73]. Thus, the 24 h urinary lead is an important aspect of monitoring recent exposure lead poisoning. Nevertheless, the urine complex composition, the variability of the matrix and the tendency for some constituents to precipitate out of solution also contribute to difficult lead analysis in this sample [12, 74]. The upper limit of acceptable lead concentration in human urine is 10 μg dL^{-1} [68].

2.3.3. Lead in kidneys and liver

Among the soft tissues, liver and kidneys are the ones that show substantially higher lead concentrations [35, 75]. These organs, which play a vital part in the detoxification and metabolism of toxic substances, are under risk of damage due to the oxidative reaction of lead [76, 77]. The lipid peroxidation of cellular membranes has a crucial role in the mechanisms of hepato- and nephrotoxic action of lead, and is a consequence of accumulation of δ-aminolevulinic acid (δ-ALA), which undergoes a process of inducing free radicals [77, 78]. The accumulation of δ-ALA is a reflection of the inhibition of the sulfhydryl-containing enzyme δ-aminolevulinate dehydratase (δ-ALAD) caused by the strong affinity of lead to the thiol groups (SH) of aminoacids [76, 79].

The lead intoxication in the kidneys may cause proximal tubular dysfunction or irreversible nephropathy depending on the exposure regimens. These facts, along with the oxidative stress, have been implicated as a contributing factor in lead-associated renal injury and dysfunction [76, 77, 80]. Intranuclear inclusion bodies have been observed in kidneys at lead concentrations of 10 μg g^{-1} [81, 82].

Liver is responsible for the detoxification and biotransformation of toxic substances, and morphological lesions were found in rats exposed sub chronically to low doses of lead, confirming the hepatoxicity of lead [83].

Despite the lack of information about lead dose-relationships in liver and kidneys, concentrations of 5-10 μg g^{-1} are considered to be indicative of acute intoxication in animals and humans [84].

2.3.4. Lead in bones

Due to the continuous remodelling process of bone, this tissue is considered not only as a target of lead contamination from the environment (referred to as external dose) but also as a source of lead contamination due to the mobilization of lead stores to soft tissues, resulting in toxic manifestations (referred to as internal dose). This fact is particularly dangerous during pregnancy because lead accumulated in bone is transferred to the foetus during the resorption of maternal bone for the production of the foetal skeleton [85, 86]. Approximately 80% of cord blood lead appears to be from maternal bone lead stores [87]. Once lead is slowly eliminated from bone, bone lead concentration may serve as a long-term exposure biomarker, and also a better predictor of some health effects than blood lead (approximately 30 days half life) [39].

The distribution of lead in bone, however, is not homogeneous and depends on the type of bone: trabecular (spongy) or cortical (compact). In childhood lead accumulation will occur predominantly in trabecular bone, and during adulthood in both cortical and trabecular bone [88]. Nevertheless, the cortical bone may be a better indicator of long-term cumulative exposure to lead than trabecular bone, once the last exchanges lead more actively with blood [39, 89].

Bone lead has been associated with several health problems, namely elevations in blood pressure and hypertension [90, 91], increased risk of Parkinson's disease [92] and poor cognitive test performances [93]. It is also known that bone lead accumulation may impair bone growth and remodelling with occurrence of decreased bone density and increased bone resorption activity [94-96].

Although there is no defined limit for the lead concentration in bones and health outcomes, recent studies provide evidence for adverse effects of lead concentrations above 10 $\mu g\ g^{-1}$ [5].

2.4. Current spectroscopic techniques for the analysis of lead in biological samples

To overcome the insufficient knowledge about lead metabolism in the organism, studies concerning human biomonitoring, lead concentrations in several organs and their relation, and the influence of several factors, are useful tools. New insights about factors that influence the bioaccumulation of lead in the organism, such as age, dietary constituents, exposure regimen and nutrient-lead interactions, should be provided.

To achieve these goals, the choice of the most appropriate spectroscopic technique and analytical method is an important step. Normally, the technique used depends on the volume and type of

sample. In some samples, such as blood or urine, direct lead determination is possible, whereas for others, such as soft tissues, hair and bones, a preliminary step of sample treatment may be necessary. Depending the amount of the samples there are also more adequate methods than others. Another important parameter is the detection limit, once the level of lead present in biological samples often varies between ppm to ppb, and sometimes the use of a more sensitive analytical techniques is needed [19, 32].
For the determination of lead total concentration, the most commonly used spectroscopic techniques are AAS, inductively coupled plasma mass spectrometry (ICP-MS), inductively coupled plasma atomic emission spectrometry (ICP-AES, also known as ICP-OES inductively coupled plasma optical emission spectrometry) and X-ray Fluorescence spectrometry (XRF).

Several works have been conducted using AAS and have demonstrated the suitability of this technique in determining the mean lead concentration of several biological samples. Multiple studies were made using the Flame Atomic Absorption Spectrometry (FAAS): analysis of human nails using them as bio-indicators of exposure to heavy elements [97]; analysis of lead content in hair of exposed workers [98]; development of new procedures for determination of Pb and Cd in hair samples [99]; improvement of a rapid method (less than 5 minutes) to determine lead in blood [100]; study of the age influence in teeth lead accumulation [101] and of the relation between skull and femur in rat bone samples, measured after microwave digestion [46]. The simplicity, effectiveness, and relatively low cost make this elemental technique very appealing. However, the sensitivity is usually insufficient for many samples, about 10-100 $\mu g\ L^{-1}$ for lead. Thus, it is convenient to use ETAAS that has lower detection limits, about 0.05-0.5 $\mu g\ L^{-1}$ for lead and allows lead determination in samples of small portions (20 µL) [102].
There are several studies measuring lead in blood using ETAAS [103-105]. Actually, it is the most used technique in the diagnosis of workers lead poisoning. Studies made in urine range from the development of a fast analytical method to determine lead in this sample [106], the participation in an interlaboratory study to determine urine lead concentration [12], and to the direct measurement of these samples with no digestion procedure [107]. Lead concentration study in the hair of young children has also been conducted using ETAAS [108, 109], as well as in other routes of excretion of humans and animals (nails, urine, hair, faeces) [110-112]. This technique has also been used for the analysis of soft tissues and bones, namely in the determination of cadmium and lead in several porcine [113], in kidney and liver of silver foxes to observe the content of lead, cadmium and mercury in relation to age and reproduction disorders [114], in several soft tissues and bones of rats that were ashed in order to measure the increase of lead retention in rats when exposed to lead in early stages of life [47], and in different types of bone of non-exposed workers concerning their sex, age and living area (urban or rural) [115].

The use of ICP-MS in the biological field studies, namely in trace analysis, is very popular due to the excellent detection limits (ng L^{-1}) and its ability to analyze multiple metals and performing isotopic measurements. However, its applications may be more sparse than AAS because of the high cost of the instrumentation [5, 102]. The ICP-MS has been applied in the study total lead and cadmium mean concentration and lead isotope ratios in whole blood [116-118]. It was also used in the measurement of Cd, Cu, Mn, Ni, Pb and Zn in nails [111] and in the study of nails as a biomarker of metal exposure [119]. Other studies relate the use of this technique in hair lead determination and hair suitability as a tool for biomonitoring [120], as well as the relationship between continuous lead exposure and the concentration of this metal in rat fur [121]. Several urine lead concentration measurements have also been made using this technique [12, 122, 123]. It was also used in archaeological bones analysis with the aim to use trace elements as indicators of dietary habits, nutrition and disease [124] and in multi-elemental characterization of soft biological tissues [125].

With a sensitivity lower than ICP-MS, but higher than FAAS, the ICP-AES is also a powerful tool for lead analysis. It is normally used for multi-elemental measurements, being very economical for a large quantity of samples. A major study made by Hee and Boyle [126] showed the suitability of this technique in multi-elemental analysis of a large amount of samples: leaded paint, human blood and excretions and Sprague Dawley rat soft tissues and excretions. The ICP-AES as also been used to analyze hair for lead in children of two Sardian towns [127] and in the study of the relation with cognitive functioning tests [128]. Hair, nails and teeth Pb and Cd concentrations in environmentally exposed people were also conducted by ICP-AES [129]. The concentration of lead in blood, as also been determined as a part of an environmental impact study about a lead smelter in Sweden [130]. Analysis of 14 elements in Taiwanese bones was also successfully achieved with the use of this technique [131].

The XRF has also given great contribution to the analysis of lead in biological samples with minimal sample pre-treatment. With detection limits in the order of μg g^{-1},the EDXRF has been applied to study trace elements in liver, brain and kidneys of patients with cirrhosis [132], and other human tissues as blood, bone, hair, liver and kidney [133-135]. Once this technique is non destructive, it is widely used in vivo studies to analyse the distribution of lead in bone [136-138] and even it relation to Parkinson disease [92]. With lower detection limits, in the order of ng g^{-1}, the TXRF has also been largely used in the study of lead in biological samples. Elemental constitution of cancerous tissues, namely colon, breast, uterus [139], lung, prostate and intestinal tissue, rectum and stomach [140], and also the analysis of human soft tissues for cancer recognition [141] have been performed giving importance to lead. Other studies also have been reported among which measurements made in freshwater microcrustaceans, using a portable TXRF spectrometer [142]

and in human amniotic fluid and placenta in order to study child weight and maternal age dependence [143].

Synchrotron radiation X-ray Fluorescence (SRXRF), with detection limits between EDXRF and TXRF ones, was used to determine multi-element concentration of lead and several elements in of the small mammals diet and tissues [144], in humans placenta, blood and hair, and animal hair, gallstones and muscular tissues [145, 146].

CHAPTER III - X-RAY SPECTROMETRY

3.1. X-ray production

X-rays are electromagnetic radiation, with wavelengths between gamma rays and ultraviolet radiation, ranging from 0.01 nm to 10 nm (approximately from 120 keV to 0.12 keV) [17]. They were discovered by Wilhelm Conrad Röntgen in 1985 at the University of Würzburg. Röntgen observed that the radiation from the discharge tubes caused a fluorescent effect on a small cardboard screen painted with barium salts, even when the tube was covered with a black paper. This type of radiation was called X-rays, once it presented characteristics different from any known type [147].

X-ray analysis is based on the fact that all the elements emit characteristic radiation when submitted to an excitation source. For analytical purposes, X-rays are produced by two mechanisms: i) deceleration of high-energy charged particles (electrons, protons alpha particles and ions) or ii) by electronic transitions of electrons in the inner orbital of atoms caused by the interaction of high-energy particles or photons. There is also a third process, which will not be discussed in is work, resulting from the decay process of radioactive sources that emit in the X-ray energy range.

The first mechanism results in the emission of a broad wavelength band called the white radiation or Bremsstrahlung. It is produced due to the deceleration of the high energy particles, losing energy and resulting in a continuous spectrum of radiation [102]. For example, Figure 2 illustrates the emission of Bremsstrahlung radiation due to deceleration of a particle close to the atomic nucleus.

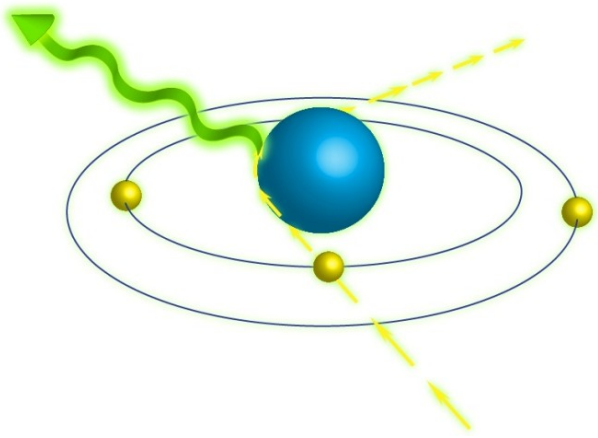

Figure 2: Deceleration of high energy particle illustration with emission of a photon (green).

The second mechanism occurs when the interaction between an incident particle, or photon, and a bound electron (inner shell electron, K or L, see Annex 1 and 2) results in the ionization of the

atom, creating a vacancy in one of the fully occupied inner shells. Then an electron from an outer shell fill the vacancy causing the emission of a X-ray photon (*c.f.* Figure 3) or of another electron, called Auger electron. The emitted X-ray photon has a well-defined energy, which is equal to the difference between the binding energies of the two shells [148].

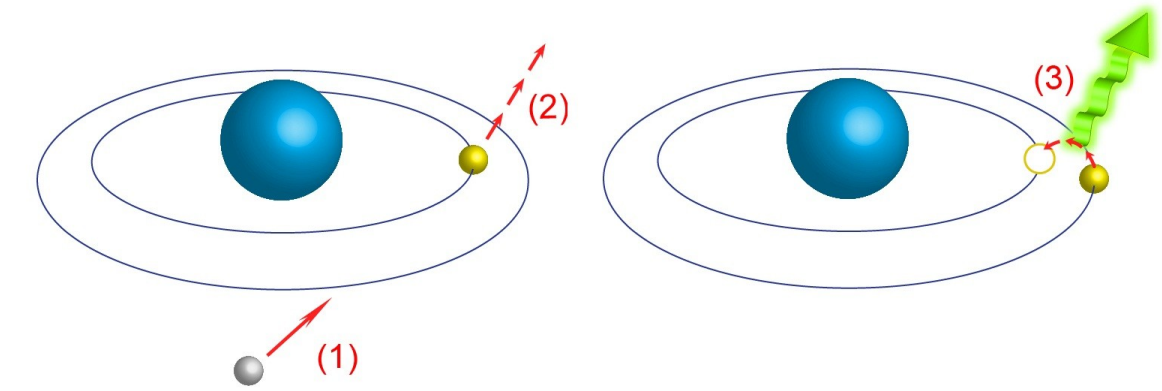

Figure 3: Characteristic X-ray emission illustration. 1) incident electron; 2) inner shell electron ejection; 3) outer to inner shell electron transition with characteristic X-ray emission (green).

The decay through the Auger channel competes with the emission of a characteristic X ray photon and occurs predominantly in elements of light atomic number ($Z < 40$). For elements of higher atomic number, the emission of characteristic X-ray is the more probable phenomenon [148].

3.2. X-ray interaction with matter

The interaction of electromagnetic radiation with matter depends on the energy of the photons and on the atoms that compose the medium. For energies less than 1 MeV the main interactions of a X-rays beam with matter are photoelectric absorption and scattering.

The photoelectric effect, mentioned in Section 3.1., happens when a photon with energy equal or greater than the binding energy of the electron interacts with a bound electron. The incident photon is absorbed and an electron (photo-electron) is ejected with an energy equal to the difference between the original photon energy and the binding energy [17]. The probability of this process to

occur is maximum for photon energies in the order of the binding electron energy [148], and its probability depends on Z^4 for low energy photons and Z^5 to high energy photons [17].

When a X-ray photon interacts with a substance it is scattered by its nucleus and/or electrons. Two different types of scattering can occur: elastic coherent scattering and inelastic incoherent scattering.

The first, also known as Rayleigh scattering, results in a scattered photon with the same energy as the incoming photon (apart from the small loss of energy due to the nucleus recoil). It takes place between photons and bound electrons and the atom remains in its ground state.

Rayleigh scattering occurs mostly at low energies and for high Z materials, being the probability of this process function of Z^2 [17, 149].

The inelastic incoherent scattering, also known as Compton scattering, results in a decrease in energy of the incoming photon. Part of the energy of the photon is transferred to a scattering electron. The Compton scattering cross-section increases with the energy of the incident photons, the scattered angle, and with the decrease of the atomic number. The probability of this phenomena to occur is a function of Z [17].

The scattering processes don't contribute to the identification of the sample made by the emission of characteristic radiation after the photoelectric effect. However, these processes are responsible for increasing background in the detector.

Both the photoelectric effect and the scattering interactions (Rayleigh and Compton), contribute to the X-ray radiation attenuation. The intensity of an X-ray beam passing through a layer is reduced according to the well-known law of Lambert–Beer (that will be described in detail in section 3.1). This reduction depends on the mass attenuation coefficient, μ_m ($cm^2\ g^{-1}$), which consists of the various interactions that contribute to the attenuation of the beam.

In the X-ray radiation energy range, the photoelectric absorption coefficient is much higher than the sum of two diffusion coefficients (Compton and Rayleigh) and usually represents about 95% of the mass attenuation coefficient [148] (*c.f.* Figure 4).

Abrupt discontinuities in the photoelectric mass absorption coefficient (absorption edges) occur where the energy of the photons became higher than the binding energy of a particular shell [17] (*c.f.* Figure 4).

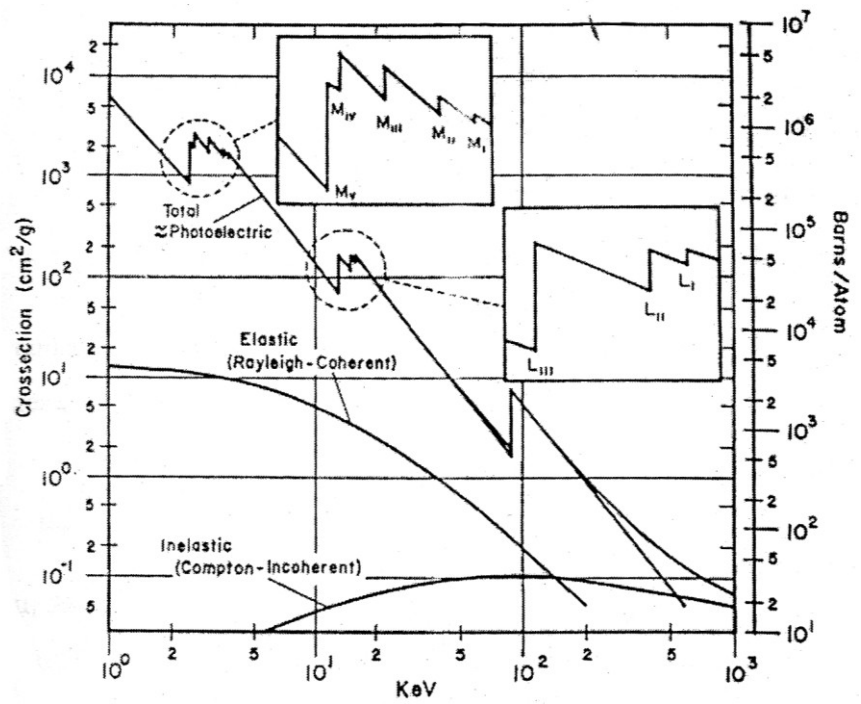

Figure 4: Variation of Pb mass attenuation cross section for several effects with the energy of the incident photon [150].

3.2.1. Reflection and Refraction

The refractive index of a substance is a measure of the speed of light in that substance and is defined by

$$n_i = \frac{c}{v_i} \ , \tag{III.1}$$

where n_i is the refractive index of a specific medium i, v_i (m/s) is the velocity of the radiation in the medium i, and c (m/s) is the velocity of the radiation in vacuum [151].

When radiation passes from a medium to another of differing physical density, i.e. different refractive indices, two things may occur (*c.f.* Figure 5). An incident ray interacting with the interface at an angle, θ_i, between a line perpendicular to the interface and the propagation direction of the incident ray, will be reflected off the interface at the same angle θ_i^*. In other words the angle of reflection is equal to the angle of incidence. If the radiation enters the substance it is observed an abrupt change in direction of the beam, at an angle θ_r, as a consequence of differences in the velocity of the radiation in the two media. This is called refraction and is given by the Snell's law [151]

$$n_1 \sin\theta_i = n_2 \sin\theta_r \ . \tag{III.2}$$

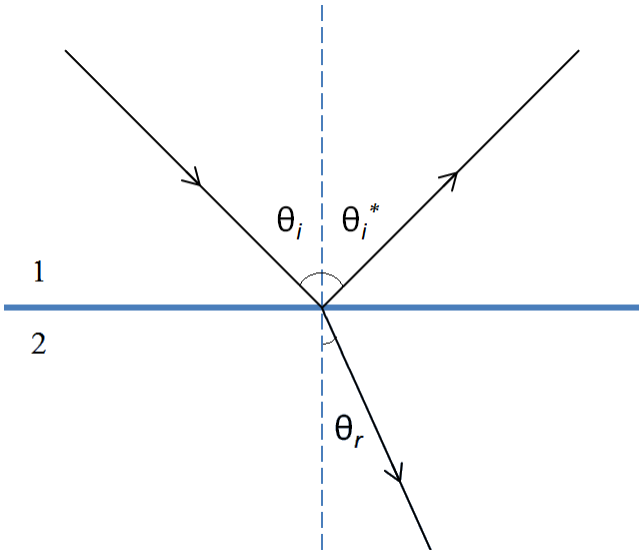

Figure 5: Reflection and refraction of an incident beam.

Once X-rays are electromagnetic waves of very short wavelength the refractive index for all materials is smaller than unity by only a small decrement, and can be written as a complex quantity

$$n = 1 - \delta - i\beta \,,$$

(III.3)

where $1 - \delta$ represents the real part of the refractive index, and the imaginary component β is the absorption index, a measure of the attenuation [8]. The variation of δ (called the decrement) with the X-ray energy, for energies above the absorption edge of the material, is given by

$$\delta = \frac{N_A}{2\pi} r_e \rho \frac{Z}{A} \lambda^2 \,,$$

(III.4)

where N_A is the Avogadro's number (6.022×10^{23} atoms mol^{-1}), r_e the classical electron radius (2.818×10^{-13} cm), ρ the density of the element (in g cm^{-3}), $Z$and A the atomic and mass numbers of the element, and λ the wavelength of the incident beam (in cm) [8].

The component β is given by

$$\beta = \frac{\mu\lambda}{4\pi} \,,$$

(III.5)

where μ is the linear absorption coefficient (in cm^{-1}) [8].

These quantities are strongly dependent on the wavelength of the X-ray radiation and the material where refraction is occurring. An increase in the wavelength means a decrease in penetration and a strong absorption of radiation. Values of δ remain very small throughout the X-ray regions, being

generally in the order of 10^{-6}, with the consequence that radiation is weakly refracted by any material.

As seen in Equation (III.3), for X-ray radiation any medium is optically less dense than vacuum and air, so the refracted beam will be deflected toward the boundary plane. If the angle of refraction, θ_r, is 90º, the refracted beam will emerge tangentially to the boundary surface. The angle of incidence is then called critical, θ_c, and, according to Equation (III.2), is given by

$$sin\ \theta_c = 1 - \delta\ .$$

(III.6)

If the angle of incidence is greater than this critical angle, all the radiation is reflected back into the first medium, and total refection occurs. Since δ is very small, θ_c is very close to 90°. The angle of incidence is customarily measured from the tangent to the surface rather than from the normal, and the angle $\alpha_c = 90 - \theta_c$ is termed the glancing angle of incidence. Thus, using basic trigonometry, the prior Equation can be written as

$$\cos \alpha_c = 1 - \delta\ .$$

(III.7)

Once the glancing angle is small, its cosine can be approximated by

$$\cos \alpha_c \approx 1 - \frac{\alpha_c^2}{2}.$$

(III.8)

Equation (III.8) together with Equation (III.7) and (III.4), leads to the simple relation

$$\alpha_c \approx \sqrt{2\delta} = \frac{1.65}{E}\sqrt{\frac{Z\rho}{A}},$$

(III.9)

where E stands for the energy of the incident beam and has to be given in keV [8].

For angles lower than the glancing angle total reflection occurs. These angles are typically in the range of 0.1º-1º. For example, for quartz glass the critical angle for an incident energy of 17.44 keV (Mo K_α) is 5.9 minutes, i.e. ~ 0.098º [17].

There are two important quantities that characterize total reflection: the reflectivity, which is defined by the intensity ratio of the reflected and the incident beam, and is increased to 100% below the critical angle; and the penetration depth, defined as the depth of a homogeneous medium that a beam can penetrate while its intensity is reduced to 37% of its initial value, which is reduced to a few nanometres when total reflection occurs. Both these parameters depend on the energy of the primary beam, the angle of incidence and the material being irradiated. For quartz glass, at an

incident energy of 17.44 keV (Mo K_α) and at the critical angle, the reflectivity is 93.4% and the penetration depth is 83 nm [8].

3.3. X-ray Spectrometry Techniques

To produce a characteristic X-ray spectrum, which allows us to identify the various elements of the sample, it is necessary to have an excitation source. The most used source in X-ray spectrometry is electromagnetic radiation, which may come from synchrotron facilities, radioactive sources or X-ray tubes and it is known as XRF spectrometry [151]. This is the main analytical technique used in this work and will be discussed in detail.

Another method used in X-ray spectrometry to produce the characteristic spectra of the samples is with a beam of ions (charged particles) as excitation source, usually a beam of protons, i.e. Proton Induced X-ray Emission (PIXE) spectrometry [152].

The other technique rely on the use of an electron beam to create vacancies in the internal atomic layers, such as, for example, the electron microprobe [148].

3.3.1. X-ray Fluorescence

The X-ray fluorescence typically uses a polychromatic beam to excite the characteristic lines (see Annex 2) of the sample to be analyzed. This technique allows multi-elemental analysis promoting qualitative and quantitative information about the sample, straightforward sample preparation, high throughput and low cost per determination [102].

Modern X-ray spectrometers are wavelength or energy dispersive. The wavelength dispersive spectrometers use the diffracting power of a single crystal, placed after the sample, to isolate a narrow wavelength band of the excited sample radiation. With this setup it is not possible to measure more than one element at once. The energy dispersive spectrometers use a high resolution Si(Li) detector connected to a multichannel analyser, allowing to detect a very wide range of energies simultaneously. Once the system used in this work is an energy dispersive X-ray spectrometer only this case will be referred in detail [151].

3.3.1.1. Energy Dispersive X-ray Fluorescence

The conventional energy dispersive spectrometer consists on the excitation source, the sample holder and the detection system. In these spectrometers the resolution equates directly from the

resolution of the detector, typically a semiconductor detector of high intrinsic resolution, such as Si (Li) devices [102]. The most used excitation source is a X-ray tube, which will be discussed in detail. Using this configuration, all X-rays emitted by the sample are simultaneously detected and measured, giving great speed in the acquisition and display of data, unlike wavelength dispersive systems.

There are two main modes of operation: the primary mode of operation and secondary mode, used in this work. In the primary mode the source directly excites the sample, contributing to a high photon flux and a more complex and confusing X-ray spectrum. In the secondary mode, a carefully selected pure element target is interposed between the primary source and the sample in such a way that only a selectable energy range of secondary photons enters the detector. While this configuration does not completely eliminate the count rate and resolution limitations of the primary system it certainly does reduce them. However, due to the lower photon flux, the exposition time must be higher than in EDXRF operating in primary mode [149].

3.3.1.1.1. The X-ray Tube

The radiation obtained directly from the anode of an X-ray tube is nowadays the most often used excitation source in XRF. Electrons are emitted by a heated cathode (usually an incandescent filament), accelerated by a high voltage and focused in a water cooled metal target (anode). The electrons reach the anode with the kinetic energy corresponding to the voltage difference between anode and cathode. The resulting X-rays are emitted passing through a Be or glass window [148].

The typical spectrum resulting from the X-ray tube is formed by the characteristics lines of the tube anode element, resulting from its direct ionization, and by the continuous white radiation (*c.f.* Figure 6).

The characteristic spectrum is only observed if the applied voltage is higher than the critical voltage (V_C, corresponding to the binding energy of the electrons of the anode). The intensity of the characteristic lines (I') is proportional to the tube current and is a nonlinear function of the applied voltage (V)

$$I' = C\ i'(V - V_C)^{\gamma}\ ,$$

(III.10)

where C is a constant, i' is the current through the tube and γ a constant that depends on the emission line ($1.5 \leq \gamma \leq 2$) [148].

The continuous radiation can vary from zero up to the kinetic energy of the electrons striking the target. The short wavelength limit (λ_{min}) is given by the kinetic energy of the electrons. Thus, the shape of the continuum spectra only depends on the energy of the accelerated electrons and not on the nature of the target (*c.f.* Figure 6). If the temperature of the filament varies, keeping the voltage

constant, the beam intensity will increase as more electrons are produced by thermionic effect. The λ_{min} however, remains the same for different temperatures as the voltage does not vary. The total intensity of the continuum spectrum (I'') increases with the atomic number of the anode, as well as the applied voltage

$$I'' = kZV^2, \tag{III.11}$$

where k is a constant that includes the current [148].

It is also known that the energy correspondent to the maximum intensity of the spectrum is given by 2/3 of the energy correspondent to the λ_{min} [153].

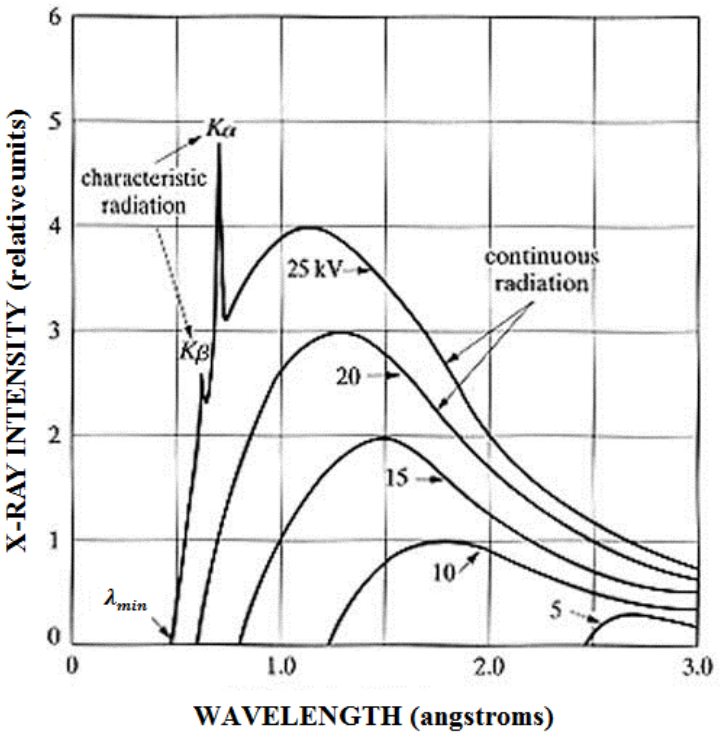

Figure 6: Mo anode X-ray tube spectrum as a function of the applied voltage at a constant filament temperature (adapted from [154]).

3.3.1.1.2. The secondary target method and tri-axial geometry

In 1973 Porter [155] described for the first time a method of quasi-monochromatic excitation obtained when positioning a thick target, called secondary target, between the X-ray source and the sample.

In this excitation method, the primary beam produced by the X-ray tube interacts with a secondary target to produce a secondary beam that contains the scattered Bremsstrahlung radiation from the X-ray tube as well as the characteristic lines of the secondary target. This secondary beam will

excite the sample, however, with a significant decrease in the intensity of the radiation due to the interaction with the secondary target. This is the main reason why in these systems a high voltage tube is normally required.
The X-ray tube produces continuous radiation that can excite efficiently different secondary target materials. This enhances the possibility of selecting several secondary targets, with different characteristic lines, to choose along a wide range of X-ray energies to excite the sample [17].
The combination anode - secondary target is very important and should be determined by the compromise between the energy of the X-rays emitted from the anode and the energy needed to ionize *K* shells electrons of the secondary target. The ionization cross section for an atomic level is greatest when the exciting X-ray energy, corresponding to the maximum intensity, is close to the binding energy of the electron in that level [148]. While this configuration does not completely eliminate the count rate and sensitivity limitations of the primary systems it certainly does reduce them.

The employment of filters is also used to reduce the signal-to-noise ratios. Filters placed in the path between the X-ray tube and the secondary target, depending on the thickness and composition of the filter, can stop radiation below a certain energy and selectively filter part of the tube spectrum. However, a compromise has to be reached as the increase of the filter thickness also decreases the intensity of the spectrum [17].

However, even with the use of filters and secondary targets, some of the Bremsstrahlung photons scattered out from the secondary target are scattered a second time by the sample into the detector, increasing the background and decreasing the sensitivity of the spectrometer. To reduce this contribution to the background radiation a tri-axial system is used.

It was demonstrated by Barkla that X-ray radiation could be polarized by scattering [156, 157]. For an unpolarized primary beam, scattering at an angle of $\pi/2$ results in a nearly complete plane polarization of the scattered X-rays [18, 158]. By using collimators to define the three orthogonal beams, Barkla demonstrated that signal-to-noise ratios were improved.
According to Barkla's experiment [159], when a a source of X-ray radiation is incident on the secondary target, the Bremsstrahlung component with the direction of radiation propagation, can be eliminated when the beam is scattered at an angle of exactly $\pi/2$ (*c.f.* Figure 7). Scattering this radiation from the secondary target by the sample to the detector (also through $\pi/2$ relative to the first scatter plane) will annihilate the remaining radiation. Thus, almost none Bremsstrahlung radiation from the tube would interact with the detector, what improves the signal-to-noise ratio [18].

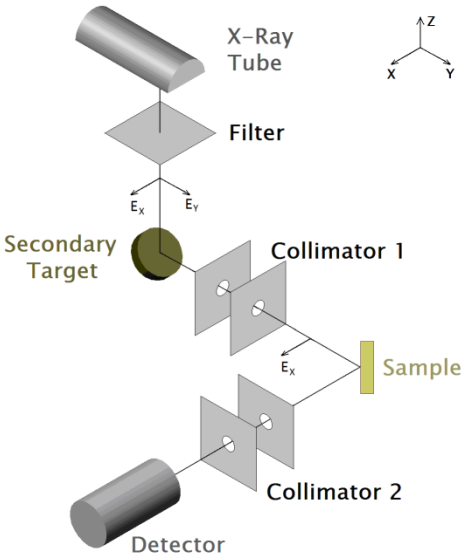

Figure 7: EDXRF with triaxial geometry, elimination of the Bremsstrahlung radiation from the X-ray tube due to the 90º arrangement.

However, to achieve these exact angles, the beams must be highly collimated, approaching zero divergence. In this situation the beam intensity would undesirably approach zero, thus a compromise has to be done between the collimator apertures and the analyte intensities. The extending of the apertures involves a decrease in the degree of polarization, which is compensated by the increase in X-ray flux.

This geometry also causes low energy background because Compton scattered radiation has a minimum of intensity to a diffusion angle of $\pi/2$, which decreases the intensity of the secondary radiation that arrives to the detector [18, 160].

The use of collimators, despite reducing the intensity of the beam, allows the collimation of the beam to the central active region of the detector, reducing some phenomena such as incomplete charge collection and the escape peaks (described in Section 3.3.1.1.3.) resulting from the excitation of the detector material. The collimator must be made from a material that absorb radiation in the range of low energies and, if excited, should have an X-ray spectrum of simple identification.

The Figure 8 compares the spectra of an EDXRF spectrometer working on the primary and on the secondary mode, with and without triaxial geometry.

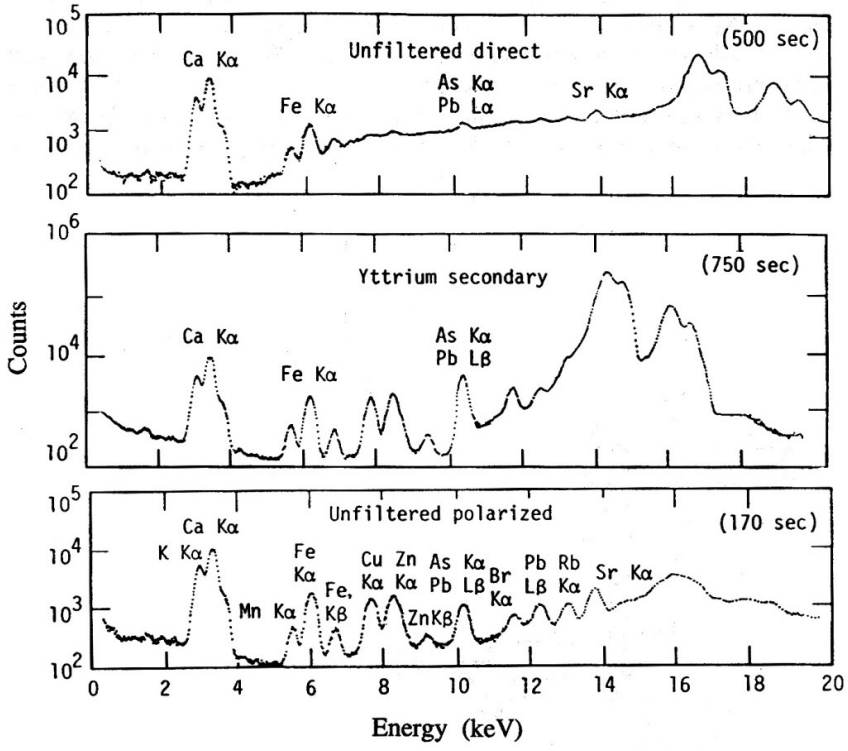

Figure 8: EDXRF spectrum measured in primary mode; in secondary mode with no triaxial geometry and a Y secondary target, and with triaxial geometry and boron carbide as secondary target [17].

3.3.1.1.3. The detection system

Energy dispersive X-ray detectors are high efficiency detectors that enable simultaneous multi-elemental analysis and operate under the basic principle of photoionization.

Besides the energy range in which the detector can work properly, there are other characteristics that define a good detector: proportionality, the voltage pulse must be proportional to the energy of the respective incoming photon; linearity, the incoming photons and the output pulses must be in the same counting rate; energy resolution that describes the dispersion of the voltage pulse produced by the detector around its average value; and the detection efficiency, given by the ratio between the number of pulses recorded and the number of radiation quanta emitted by the source (absolute efficiency), or the number of pulses recorded and the number of quanta incident on the detector (intrinsic efficiency) [102, 161]. The last feature is related to the thickness and material of the detector window, which determines the efficiency in the low energy region, and also with thickness of the detector crystal that determines the efficiency in the high energy region.

Resolution is also very important especially when choosing a detector an experimental assembly once high resolution enables the spectrometer to separate two X-ray lines that are close to each other. The resolution of the detector is determined by the full width at half maximum (FWHM),

defined as the width of the distribution at a level which is just half the maximum ordinate of the peak (maximum number of counts). The energy difference correspondent to the FWHM is the detector absolute resolution. It is usually measured at the K_α line of Fe or Mn [161].

The X-ray detectors most used in EDXRF systems are the Si(Li), the Ge(Li),the high purity germanium (HPGe), and the most recent and fastest growing detector technology, the Peltier cooled silicon drift detector (SDD).
All these detectors have adequate energy resolution to resolve the lines from adjacent elements with atomic numbers greater than 10. In the Si(Li) and SDD detector the applicable energy range is from about 1 to 50 keV, while the Ge(Li) and HPGe detector are better suited from about 6 to 200 keV range due to its higher atomic number [158, 161]. Concerning resolution, the worse detectors are the Ge(Li) (about 450 eV @ 14 keV) and the HPGe (about 180 eV @ 5.9 eV and 400-500 eV @122 keV), followed by the Si(Li) (about 145 eV @ 5.9 keV), and finally the SDD (that can reach values of 127 eV @ 5.9 keV) [7, 161, 162]. This new detector with amazing resolution is also very used due to its high counting rate and consequently high throughput [163]. However, the most used semiconductor detector in EDXRF spectrometers remains being the Si(Li) and it is the one used in this work.

The Si (Li) detector consists of a small cylinder of p-type silicon compensated by Li to increase its electrical sensitivity. Because Li has a high electropositivity, its presence converts the p-type region into a n-type region. A DC voltage, forward biased, applied across the crystal causes the withdrawal of electrons from the Li layer and holes from the p-type layer. When reverse biased, a current across the pn junction causes migration of Li ions into the p layer, electrons into the n layer, and the formation of an intrinsic layer, originating a p-i-n type diode detector. This area is called the depletion area [102, 151, 161]. To inhibit the mobility of the lithium ions and to minimize the electronic noise, the diode and its preamplifier are operated at the liquid nitrogen boiling temperature (77 K).
Incident X-ray photons interact in the deplection area to produce a specific number of electron-hole pairs. The number of electron-hole pairs created, or in other words, the total electric charge released is proportional to the energy of the detected photon. The charge produced is swept from the diode by the bias voltage to a charge-sensitive preamplifier. The preamplifier is responsible for collecting this charge on a feedback capacitor to produce an output pulse whose voltage amplitude is proportional to the original X-ray photon energy. After this, the signal undergoes the pulse processor where it is shaped and the energy of the incoming X-ray accurately measured [102, 158].
Finally, a multichannel analyzer, converts the analog voltage to a digital number, and each time a pulse is produced, a number is generated that represents the channel to be incremented by one, each

channel corresponds to a small range of energy of the incident photon. Thus, the energy spectrum is accumulated [164].

From the several artifacts that may possible be generated during the detecting process, it is important to emphasize the ones that more frequently occur: sum peaks, escape peaks and incomplete charge collection. These processes can give rise to a degraded signal from the detector, which can increase the background level in the spectrum.
Sum peaks occur when two X-ray photons impact the detector almost simultaneously and the pulse created and measured is the sum of the two photon energies. This process occurs when the count rates are moderate to high.
The escape peaks in a Si(Li) detector are 1.74 keV (Si-K_{α}) lower in energy than the incident X-ray photons, and they occur when the characteristic X-ray photon from Si escapes from the detector, not being collected.
Incomplete charge collection occurs when all the electron-hole pairs generated by an X-ray are not swept to the electrical contacts, resulting in a charge signal measured lower than expected, and, consequently, in a energy measurement lower than the energy of the incident X-ray (detected peaks with low energy tail) [161].

3.3.1.1.4. Data Analysis: X-ray spectra

A typical X-ray spectrum obtained with an EDXRF spectrometer can be divided into three sections, as can be seen in Figure 9.

The high energy region consists of the elastically and inelastically scattered peaks of the excitation radiation, which corresponds to about 90% of the total number of counts. The higher intensity of the Compton in comparison with the Rayleigh peak is because this sample is majority consisted of light elements, namely C, H and O.
The lower energy region is mainly due to the escape effects inside the detector and to a high contribution of the electronic noise of the detector.
The intermediate energy region is composed by the characteristic *K* and *L* lines of the sample and the background. The identification of the different elements of the sample by their characteristic lines consists in the qualitative analysis of the spectrum.

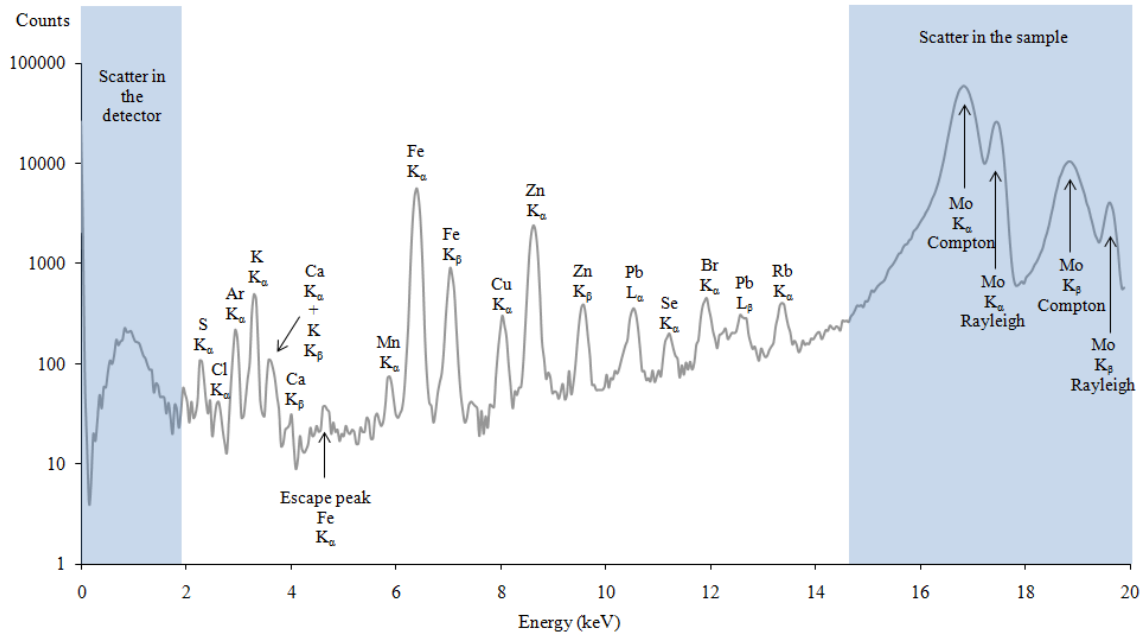

Figure 9: Spectrum from a liver sample of a Pb contaminated Wistar rat obtained by a tri-axial EDXRF spectrometer with a Mo secondary target (Centro de Física Atómica FCUL/UL).

3.3.1.1.5. Quantitative Calculations

Quantitative analysis is used to obtain information about the relative amount of elements present in the sample in terms of their concentration (*e.g.* µg of analyte per g of sample).

Each of the methods used to obtain quantification has its advantages and disadvantages, and the choice between them relies mainly in the particular application. If the objective of the quantitative analysis is the determination of a single or several elements in an unknown but constant matrix or in a sample with negligible matrix effects, comparative methods, such as standard addition and internal standard, are used. If the matrix effects are variable from one sample to another and multi-elements determination is required, the use of the so called "mathematical methods" is mandatory. Included in this category are the influence coefficient correction method and the fundamental parameter method. The first tend to be used in combination with more standards than the fundamental parameter methods [17, 102]. In this work it was used the fundamental parameters method that will be described next.

The first step to perform quantitative X-ray fluorescence analysis from a multi-elemental sample is an accurate and reliable deconvolution procedure of the spectral data, in order to determine the intensity of each characteristic X-ray radiation emitted by the elements present in the sample. This

requires knowing the total number of counts obtained by integrating the area corresponding to each peak, after subtracting the background.

The characteristic X-ray lines are defined by a Lorentzian distribution [149]. Peak profiles observed with a semiconductor detector are the convolution of the Lorentz distribution with the nearly Gaussian detector response function originating a Voight profile [165]. However, since the Lorentz width is of the order of 10 eV for elements with atomic number below 50, while the width of the detector response function is in the order of 160 eV, a Gaussian function is an sufficient first order approximation. When observing the peak in more detail there is some distinct tailing in the low energy side. This is mainly due to incomplete charge collection in the detector. This distortion as been studied theoretically and various functions have been proposed to model the real peak shape more accurately, being the exponential function one of the most used.

To model the background shape, several different fitting procedures are available and can be chosen according to the type of spectrum. In X-ray fluorescence, the background is mainly due to the coherent and incoherent scattering of the excitation radiation by the sample. The shape can be very complex once it depends both on the excitation spectrum and on the sample composition. Attempts were made to describe empirically the background however no realistic physical model for the background is in use and the analyst chooses the best function that improves the least-square fitting procedure.

The difference between the mathematical function and the spectrum itself is given by the parameter χ^2 [166]. If this parameter is too high (above 10) is probably because there was some element that was not properly identified, or the choice of the function that fits the background was not the best [167].

Once knowing the peak intensity, the fundamental parameter method can be applied. This method consists on assuming an approximate composition of the unknown specimen, calculating the fluorescence intensities from fundamental equations [17], and comparing with the measured intensities that are related to the element concentration. This method is based on the following assumptions: i) all elements are equally distributed in the sample; ii) the intensity of the fluorescence X-ray radiation is proportional to the concentration of the measured element; iii) the effects of other elements present in the sample (called matrix effects) can be calculated using known physical parameters (mass attenuation coefficient, absorption cross sections, etc) and iv) measured intensity is dependent on the experimental configuration and measurement conditions [17, 148, 168].

The intensity I_{P_i} of a characteristic peak of an element *i* is the result of primary fluorescence and inter-elemental effects. Primary fluorescence results from the direct effect of the incident beam or primary radiation on the element considered. Inter-elemental effects are related with secondary radiation produced by other elements in the sample. As characteristic radiation is emitted from the

specimen, it is absorbed by all matrix elements by amounts relative to their mass attenuation coefficients. Depending on the energy of the primary beam and on the elements present in the sample, this radiation can produce additional fluorescence in the element, which gives an increased or enhanced signal from the analyte [102, 148].

The relationship between intensity and concentrations, resulting from primary and secondary fluorescence, can be given by

$$I_{P_i} = I_0 K_i c_i m C_i \ ,$$

(III.12)

where I_0 is the total primary intensity (incident beam), K_i is the calibration factor, c_i is the concentration of the element i, m is the sample thickness (g cm^{-2}) and C_i the self attenuation factor [167]. This last factor is the correction factor for attenuation of primary incoming radiation and outgoing characteristic radiation, and is given by

$$C_i = \frac{1 - e^{-\alpha_i}}{\alpha_i},$$

(III.13)

where α_i is equal to

$$\alpha_i = \sum_j c_j \left[\frac{\mu_m(E_{1,j})}{\sin \varphi_1} + \frac{\mu_m(E_{i,j})}{\sin \varphi_2} \right] m$$

(III.14)

and

$$\sum_j c_j = 1 \, .$$

(III.15)

In Equation (III.14) $\mu_m(E_{1,j})$ corresponds to the mass attenuation coefficient for element j at the incident X-ray energy (cm^2 g^{-1}); $\mu_m(E_{i,j})$ stands for the mass attenuation coefficient for element j at the characteristic X-ray energy for element i (cm^2 g^{-1}), and φ_1 and φ_2 are the angles for incoming and emitted radiation from sample [168].

Because of the attenuation on the detector, the low energy X-ray radiation cannot be detected, and the light elements cannot be determined. In a biological sample, however, these elements constitute the major part of the matrix and will therefore dominate the attenuation coefficient in the C_i factor.

Concerning the calibration factor, it given by

$$K_i = \ \Omega \varepsilon_i C'_i \omega_i \sigma_{X_i} P_{n \to m}$$

(III.16)

where σ_{X_i} is the ionization cross section of an element *i*; ω_i is the fluorescent yield for element *i*; $P_{n\to m}$ the transition probability from level *n* to *m*, in element *i*; C'_i the absorption in air and detector window for element *i*; ε_i the detector efficiency for element *i*; and Ω the detector solid angle [168].

The success of the fundamental parameters method is directly related to the completeness of the characteristic X-radiation model and the correctness of the calculation algorithm. The major errors in the the application of the method accrue because of current uncertainties in certain fundamental data, such as mass absorption coefficients and fluorescence yields.

3.3.1.1.6. Analytical Figures of Merit

To assess the accuracy and to enhance the calculation procedure, reference materials are measured. For calibration it is important to use reference materials with the same matrix of the studied sample. To proceed with the measurements, the measured value must be within the reference material's range.

To check the method precision, each sample should be measured at least 10 times to take into account the oscillations and statistical fluctuations of the measurements. Values of precision below 10% are accepted, and sometimes, if the sample matrix is too complex, these values can go up to 15%.

The detection limits achievable for individual elements are a significant criterion of the usefulness of an analytical technique. It represents the lowest statistically significant concentration level that can be determined from an analytical blank.

To determine the concentration of a certain element the intensity of the characteristic peak must to be known. This intensity is calculated using the average number of total accumulated counts N_T of X-ray photons corresponding to a certain region of interest (ROI). Assuming a Poisson distribution, it has the following standard deviation, σ_T

$$\sigma_T = \sqrt{N_T}\,. \tag{III.17}$$

On the other hand, since the total counts are the sum of the counts referring to the element peak, N_P, and to the background, N_B, it may be written

$$\sigma_T = \sqrt{{\sigma_P}^2 + {\sigma_B}^2}\,, \tag{III.18}$$

where σ_p is the standard deviation of the element peak counts and σ_B is the standard deviation of the background.

For a sufficient large number of occurrences (>10) the Gaussian distribution is a good approximation to the Poisson distribution [166]. To be significantly different from the background,

the signal N_P must be distinguished from the spread in N_B. Thus, according to the properties of the Gaussian distribution, there are 99.7% probability of this happens if [17]

$$N_P > N_B + 3\sigma_B \, .$$

(III.19)

Subtracting the N_B to the Equation (III.19), the detection limit (DL) is given by

$$DL = c_i \frac{3\sigma_B}{I_{P_i}} = c_i \frac{3\sqrt{N_B}}{N_P},$$

(III.20)

where I_{P_i} is the characteristic peak intensity and c_i is the concentration of the known element *i* [169].

The detection limit depends inversely on the counting time (higher count rates) and directly on the intensity on the background radiation.
The detection limit is determined using standard reference materials with known concentrations of the analyte in study.

3.3.1.2. Total Reflection X-ray Fluorescence

The TXRF is a variant of EDXRF. The description of an experimental TXRF setup was first published by Yoneda and Horiuchi [170] in 1971, and it was further enhanced by Aiginger and Wobrauschek [171] since 1974.

The principle of the technique lies in the incidence of a well-collimated beam from an X-ray tube on the sample carrier optically flat surface at a glancing angle less than, or near to, the critical angle.

Ideally, the radiation falling onto the specimen should be monochromatic or it will not be totally reflected, penetrating deeply into the carrier and contributing to scatter and spectral background. Thus, the high energy Bremsstrahlung part must be removed from the radiation deriving out of the X-ray tube. This is solved by using of beam-adapting devices such as a reflecting mirror or multilayer (to either filter or even monochromatize the beam) and slits or diaphragms/edges (to collimate the beam) [172] (*c.f.* Figure 10).

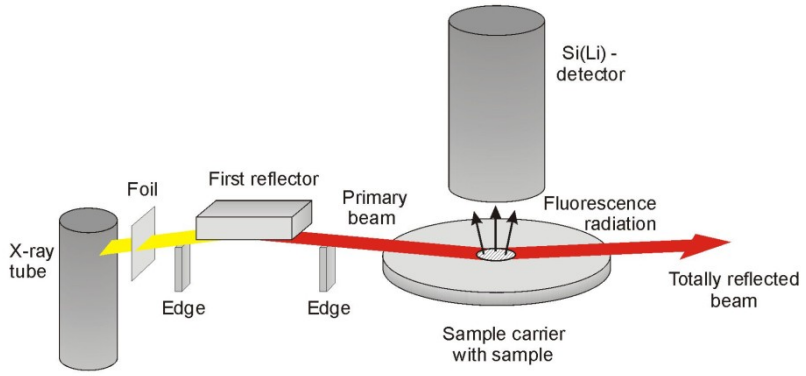

Figure 10: TXRF schematics (by kind permission of Institute for Analytical Sciences, ISAS, Dortmund).

Once scattered, the monochromatic radiation reaches the sample, placed on the carrier, at a very low glancing angle of a few seconds of arc. The sample placed on a carrier is then excited to fluorescence. The sample carrier has to serve not only as a sample support but also as a totally reflecting mirror. Thus, it has to have the following characteristics: roughness should be less than 5 nm within the area of 1 mm^2 and waviness less than 0.001º within the area of about 1 cm^2, it should be resistant to aggressive chemicals and mechanical stresses, it should be highly reflective under operation conditions, free of impurities and fluorescence lines over the energy of interest. The most common materials used are are quartz, silicon, germanium glassy carbon and Perspex acrylic plastic [8, 162].

The emitted X-ray radiation is detected by a semiconductor detector, usually an Si(Li), placed close to (~ 5 mm) and directly above the sample and obtained signal is further processed as in EDXRF. The position of the detector maximizes the intensity of the radiation detected. It is placed very close to the sample what enlarges the solid angle and minimize the radiation absorbed in air. The angle between the detector and the glancing angles is approximately 90º what results in a minimum in the Compton scattering of the incident photons.

Because the primary radiation enters the sample at an angle barely less than the critical angle for total reflection, total reflection occurs and only a small part of the impinging energy penetrates into the substrate, thus the scattering and fluorescence from the substance are minimal. Consequently, the background under the peaks in the fluorescence spectrum is substantially reduced and detection limits are improved. Because the background is so low, pg amounts can be measured in samples with favourable matrices or concentrations in the range of $\mu g\ L^{-1}$ can be obtained without recourse to pre-concentration [8].

Another advantage of this technique, besides background reduction, is the fact that the sample excitation is done twice, by the incoming primary beam and the reflected beam as they both pass

through the sample. Thus, if the glancing angle is less than the critical angle, the fluorescence intensity of the sample will achieve the double value.
The sample is typically presented as a thin film or a few very fine grains on the surface of a quartz plate in order to not disturb total reflection of the carrier. The amount of sample has to be restricted to about 10 µL of a solution or a few µg of a solid material. Liquid samples, as droplets of solutions or suspensions, are normally pipetted on to the carrier and dried by evaporation. To avoid spreading of droplets, the carrier must be hydrophobic, so the quartz-glass carriers are covered by a Si solution prior to use. Solid samples, as pulverized material, can be applied as a few grains, while tissues are applied as thin frozen sections obtained with a microtome. Generally, the sample has to be placed in middle of the carrier within a circular area 6-8 mm in diameter [173].

Total reflection spectrometers are highly effective in micro and trace analyses of various kinds of samples, especially for environmental matrices [174, 175], natural waters [176, 177] and biological samples [9, 178]. It is also used for industrial products analyses, for example high purity reagents and metals [179, 180], determination of trace metals in oils [181, 182] and quantitative surface and thin layer analyses [10, 183]
Although this technique does not allow the detection of low Z elements (*e.g.* Li, Na, Al) and it requires a polished surface for best detection limits**,** the considerable advantages of TXRF have made it a competitor to well established methods such AAS, ICP-AES and ICP-MS.
Once this is a variant of EDXRF, parameters as the X-ray tube, the detection system and the X-ray spectra will not be referred as they were already described in Sections 3.3.1.1.1., 3.3.1.1.3. and 3.3.1.1.4. .

3.3.1.2.1. Quantification

In TXRF, quantification is generally carried out by internal standardization, once matrix absorption and enhancement corrections are not required due to the thin film properties of the samples analyzed. In this technique, only small volumes of liquids, small amounts of powders, thin sections or layers, and individual particles are subject to analysis. Quantification can therefore be carried out after the addition of an element serving as internal standard.
When only one element has to be determined, it is used the addition of an element in a known concentration that gives a wavelength close to that of the analyte. When an appropriate internal standard cannot be found, it is possible to use the analyte itself as the standard element (spiking). When several elements must be determined, which is the case of the present study, any element not present in the sample, generally rare elements as Ga or Y, can be chosen as the standard [8].

For the multi-elemental analysis, the first step required is the determination of the net intensity of the characteristic peaks in the spectrum that can be done following the common practice already described for EDXRF. The sensitivity values for these peaks, however, should be known from preliminary measurements.

Ideally a linear relationship exists between the volume concentration of the analyte i, c_i, and the background corrected net intensity of the principal peak of the analyte, N_i, given in total counts recorded in a preset live time of the detector

$$N_i = B_i c_i \tag{III.21}$$

where B_i is a proportional factor called absolute sensitivity particular of each element [8].

It is common to work with the relative sensitivities, rather than absolute sensitivities, which are the ratios of these sensitivities with respect to a specific element and can be determined by calibration. This specific element is present in a multi-elemental standard solution, and is chosen as a reference element. However, a large number of elements (>5) in one standard solution is not recommended for standardization because of possible spectra overlap [17]. After recorded the spectrum, the net intensity for each element is determined and the relative sensitivities are calculated by

$$S_j = \frac{N_j / c_j}{N_{rf} / c_{rf}} S_{rf} \,, \tag{III.22}$$

where S is the relative sensitivity; N the net intensity; c the concentration of the different elements j and the reference element rf. The quantity S_{rf} is generally set to 1 since only relative sensitivities have to be determined [8].

The relative sensitivities are independent of the sample matrix, and are only applied to special cases with no matrix interference. If the sample analyzed is a saline or gelatinous solution, a mineral or organic matrix (*e.g.* urine), some residues may be formed. Nevertheless, the relative sensitivities of elements determined in these matrices are calculated with a deviation of less than 8% [36] [8]. The relative sensitivities are calculated only once for each particular excitation mode. Any change in the excitation mode leads to a new set of determinations.

For the next step of the quantification it is necessary to use the internal standard. A few µL of the internal standard (w) are mixed with a few mL of the sample (V).The sample can also be deposited on the sample carrier before the addition of the internal standard. However, this may compromise the homogeneity of the distribution.

A small volume (2-10 µL) of the final solution is then pipetted on a clean carrier and dried by evaporation. The sample is measured and the concentration is calculated by (III.22) using for rf the internal standard (is) and for j the analyte of interest (x)

$$c_x = \frac{N_x/S_x}{N_{is}/S_{is}} c_{is} \ .$$

(III.23)

Since c_x is to be determined in the original sample volume, Equation (III.22) must be multiplied with the dilution factor $(1 + w/V)$ [8].

3.3.1.2.2. Analytical figures of merit

The precision and accuracy are verified in the same way as in EDXRF spectrometers (*c.f.* Section 3.3.1.1.6).

The detection limits, however, are normally calculated directly using the absolute sensitivities of the element of interest and according to the International Union of Pure and Applied Chemistry (IUPAC) rules [184], expressed by

$$DL = 3\frac{\sigma_{blank}}{B_i}.$$

(III.24)

Once σ_{blank} is widely influenced by the photon counting of the spectral background (N_B), it is limited by the Poisson statistics and Equation (III.24) can be written as

$$DL = 3\frac{\sqrt{N_B}}{B_i}.$$

(III.25)

This expression is equivalent to the detection limit expression for EDXRF if the absolute sensitivity B_i is replaced by Equation (III.21).

CHAPTER IV - ATOMIC ABSORPTION SPECTROMETRY

4.1. Principles of Atomic Absorption

In 1802, Wollaston observed the phenomenon of atomic absorption by noticing, for the first time, the existence of dark bands in the solar emission spectrum. This observation was only correctly explained in 1859 by Kirchoff and Bunsen as absorption lines due to the presence of various elements in the suns atmosphere. The use of the atomic absorption process as a quantitative analytical tool started in 1953, when Alan Walsh fabricated the first analytical atomic absorption spectrometer [185].

During the absorption process, a photon interacts with the atomic electrons that are promoted to excited states. Radiation is more likely to be absorbed at frequencies that match the energy difference between two quantum states of the atom. Thus, each element will preferentially absorb light at a particular wavelength. The absorption that occurs due to a transition between two electronic states is referred to as an absorption line.

The absorption process can be used to calculate the concentration of the absorbing particles. When a beam of parallel monochromatic radiation passes through a medium having a determined thickness and a certain concentration of absorbing species, the intensity of the beam is attenuated from I_0 to I due to the interactions between photons and the absorbing atoms.

The transmittance, T, of the medium is defined as the fraction of incident radiation transmitted by the medium, and is given by [151]

$$T = \frac{I}{I_0}. \tag{IV.1}$$

The absorbance, A, of a medium is related with the transmittance and is defined by [151]

$$A = -\log T = \log \frac{I_0}{I}. \tag{IV.2}$$

On the other hand, the absorbance is also directly proportional to the path length, b, through the solution and the concentration of absorbing species, c [151],

$$A = abc\,, \tag{IV.3}$$

where a is a constant called absorptivity. Using Equation (IV.2) and (IV.3), it is obtained

$$\log \frac{I_0}{I} = abc = A\,, \tag{IV.4}$$

which expresses the so-called Lambert-Beer law, i.e. that the absorbance (measured as a decrease in transmittance) increases linearly with the concentration of gas-phase atoms.

There are some limitations to the applicability of Lambert-Beer's law. The law is accurate only for dilute solutions, because in high concentrated solutions the average distance between the species responsible for absorption is diminished to the point where each affects the charge distribution of its neighbours, altering the ability to absorb a specific wavelength. Other deviations, called chemical deviations, arise when an analyte reacts with a solvent to produce a product having different absorption spectrum. At last, the Lambert-Beer law is only observed by a truly monochromatic radiation, which is not verified in the presence of stray or scattered radiation.

4.2. Linewidth

The width of a spectral line, such as in the electromagnetic emission spectrum of an atom, is characterized by the spectral linewidth, $\Delta\lambda_{1/2}$. The FWHM, already discussed in Section 3.3.1.1.3., quantifies the spectral linewidth, in terms of wavelength difference, as can be seen in Figure 11.

A particular spectral line can easily be assigned to a specific element. For example, atomic absorption lines from lead and antimony are both near 217 nm, but they are sufficiently narrow to be distinguish since lead is at 217.0 nm and antimony at 217.6 nm [186].

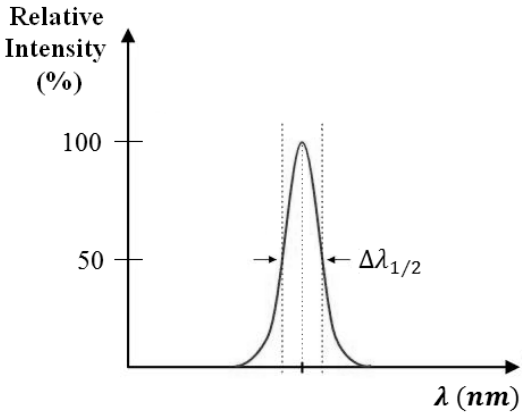

Figure 11: Illustration of the definition of linewidth.

Atomic absorption peaks are much narrower than the bands resulting from absorption by molecules. The spectrum of a molecule is spread out due to the many different transitions which

can occur between the ground and excited states due to the presence of several rotational and vibrational states.
Although atomic spectral lines may be sharp their linewidths are still finite. There are four main factors which influence linewidths: natural linewidth, Doppler effect, pressure effect and self absorption effect.

The natural width is determined by the lifetime of the excited state due to photon absorption. The absorption process is very fast (~10^{-15} s) and the lifetime of the excited state is relatively longer (~ 10^{-9} s), but still sufficiently short to be influenced by the Heisenberg Uncertainty Principle [186]. This principle states that is impossible to know both lifetime and the energy of an excited state with the same exact precision leading to imprecision in the wavelength of the transition. Actually, the observed linewidths are much broader (about 500 times) than the natural linewidths, thus the contribution of this effect to the broadening of the peak is small. The natural width of atomic lines is about 10^{-4} nm [187].

The Doppler broadening is the broadening of spectral lines due to the Doppler effect caused by the distribution of the velocities of atoms. Atoms that are moving toward the source absorb radiation with the effective wavelength shortened, i.e. the photon frequency is shifted to a value higher than the original. The effect is reversed for atoms moving away from the source, i.e. the absorbed radiation will have a frequency shifted to a smaller value than when emitted by the source. Doppler broadening accounts for most of the width of the atomic lines and yield linewidths of 10^{-3} to 10^{-2} nm in atomic spectroscopy [187].

Concerning pressure or Lorentzian broadening, it occurs due to the fact that atoms undergo frequent collisions with other atoms and molecules in the surrounding gas, causing excited atoms to lose their excess energy. As a result, the lifetime of the excited atom is very short leading to line broadening. Depending on the excitation source type, this effect may or not be neglected. For example, since hollow cathode lamps operate at pressures under the atmospheric pressure (about 0.01 atm), the frequency of collisions diminishes and the broadening is negligible, while in flames the broadening can be similar to the Doppler broadening [151].

The self-absorption broadening, also known as self-reversal broadening, is occasionally observed for intense resonance emission lines. It results from the fact that a part of the radiation emitted by the source is absorbed by the source itself. The line profile is changed as a result of the lowering of the maximum intensity accompanied by a corresponding increase in apparent half width [186].

4.3. Atomic absorption spectroscopy instrumentation

The atomic absorption spectroscopy, as it was already referred, is based on the absorption of element-specific source radiation by the atoms of the analyte. It is one of the most valuable and well established techniques with a vast application in biological and environmental analysis, for the elemental and quantitative study of the sample. This sensitive technique enables the detection of small amounts of elements, down to around tenths and hundredths of ppb.

The instrumentation for atomic absorption can be single or double-beam spectrometers [151]. In single beam instruments, one beam of radiation passes from the source through the wavelength selector and to the detector. To obtain the absorbance it is necessary to take a reading through the blank, and then again through the sample, using a source with stable intensity. In the double beam instruments, the light from the source is split in two beams and one passes through the sample and other around it. Although the double beam design removes the fluctuations in the light source the single beam spectrometer (that is the design used in this work) is often preferred because it offers distinct advantages in terms of simplicity and concomitant lower cost. The fact that the radiant energy reaching the detector is generally larger than in the double beam spectrometers, leads to high signal-to-noise ratios.

The main components of an atomic absorption spectrometer are: the emission system, i.e. the radiation source; the absorption system where the sample is going to be atomized; the selection system, which includes the equipment relative to the spectral selection (filters, monochromators); and the detection system, which consists in the photodetection and measurement of absorbance. All these components will be discussed in detail giving emphasis to the components used in this work. However, the importance of the atomizer must be emphasized. It is possible to define several techniques depending on the type of atomizer, such as the FAAS (flame atomic AAS), and also flameless procedures as the ETAAS (electrothermal AAS), also known as graphite furnace AAS (GFAAS), and the vapour generation AAS, namely the hydride generation AAS (HGAAS) and the cold vapour technique (CVAAS), as it will be referred in Section 4.3.2..

4.3.1. Radiation sources

The essential feature of the atomic absorption spectroscopy is the narrowness of the absorbing spectral lines (0.002 to 0.005 nm). In order to apply the Lambert-Beer law it is necessary that the line sources used for excitation are stable and narrower than the linewidth of the analyte absorption peaks. Usually, this condition is met by using line sources, such as the hollow cathode lamp (HCL) or the electrodeless discharge lamps (EDL), instead of continuum sources. However, the HCL is

able to produce even narrower lines than EDL. This is the type of source used in this work and will be described below [185, 186].

A HCL consists of a Pyrex tube containing a quartz or glass window, a cathode and an anode made of tungsten. The cathode has the shape of a hollow cylinder and is fabricated, or the interior is coated, with the element that is being analysed. Thus, the emission line from the lamp is very narrow and at the exactly the same wavelength as that absorbing line of the analyte. The interior of the tube is filled with an inert gas, such as Ne or Ar, with a pressure of a few mbars [186]. The fill gas is selected in a way that no spectral interferences are encountered with the analytical line, and to achieve the highest emission intensity of the analyte spectrum. Applying a voltage of several hundred volts, the gas atoms become ionized at the anode and are accelerated toward the cathode, sputtering atoms from its surface into the gas phase. The metal atoms are then excited by collisions with electrons and ions and then emit the characteristic atomic emission lines.
Because of the lower pressure and lower temperature in a HCL, compared to that in the atomizer, the linewidth of the spectral lines emitted by the radiation source is significantly smaller than that of the absorption lines, approximately 0.0002 nm. Therefore, all of the radiation produced is available for absorption by the atomized sample [185]. The intensity of the atomic line radiation produced increases with increasing current. However, at high lamp currents, an excess of metal atoms is sputtered from the cathode surface. In this situation, may occur self-absorption when the dense cloud of metal atoms absorbs radiation emitted from the nearby excited-state metal atoms, which results in radiation available for absorption by the sample. This can be avoided by running at a low current, which also increases the life of the lamp.
Hollow cathode lamps can be a single element or a multi-element sources [185]. The multi-element HCL operates under the same principles of simple HCL, but with a cathode fabricated from alloys of several elements, instead from just a single element. These lamps are more economic than single element lamps and they have shorter change-over time, if the case of measuring more than one element. However, due to its complexity the multi-element HCL typically has a shorter lifetime than the single-element HCL and also produces lower intensity of the lines emitted for each element, and consequently worse signal-to-noise ratios.

4.3.2. Atomizer

The atomization step can be successfully executed by either flame or flameless. The most commonly used atomizers used nowadays are flames and electrothermal (graphite tube) atomizers. In either of the two methods, thermal energy is used to provide a complete vaporisation of the analyte material and to break the chemical bonds of the component molecules, irrespective of the

sample matrix. In both cases, the sample is in general introduced as an aqueous solution. However, in the graphite furnace it can also be introduced as slurry or a solid. Some elements such as As, Bi, Se and Sn can be easily converted into their volatile hydrides and subsequently introduced in the atomizer, what is the so called hydride generation technique. On the other hand, mercury has enough vapour pressure to be atomized at room temperature without the application of thermal energy, consisting of the cold vapour technique. In this Section the graphite furnace electrothermal atomizer will be described in detail, and compared with the other atomizers, once it is the one used in this work.

Electrothermal atomizers include the graphite furnace, carbon rod, and tungsten ribbon atomizers. The most common commercial electrothermal atomizers are small electrically heated graphite tubular furnaces. The tube, which has about 5 cm long and an internal diameter less than 1 cm, is usually coated with pyrolytic graphite [151]. This substance has a low gas permeability and a good resistance to chemical attack, preventing oxidation and carbide formation. The low permeability reduces the loss of atomic vapour by diffusion through the cuvette wall contributing to an increased analytical sensitivity.

In these atomizers, a 5 to 50 μL aliquot of the sample is injected through a hole in the top of the tube [185]. Care must be taken in the sample injection because if the droplet is injected too high it spreads leading to poor precision, and if the drop adheres to the tip of the injector it can be deposited around its hole affecting the reproducibility of the measurement.

Each end of the furnace tube is connected to a high current, programmable power supply through water-cooled contacts (*c.f.* Figure 12). The furnace is then resistively heated stepwise to the temperatures conducive to gaseous atom formation. First the sample is dried, then ashed and atomized, at the appropriate temperatures. In the drying step, the solvent must be evaporated at a temperature just above its boiling point. In the ashing step, the temperature is raised to remove organic matter and as many volatile components of the matrix as possible; any loss of the analyte must be avoided. Protective internal gas flow efficiently prevents entrance of air. Vapours generated from the matrix during the first and second step are normally excluded by an external inert gas stream that enters the graphite tube (*c.f.* Figure 12). Finally, in the last step analyte atoms are excited and the absorbance is recorded. In this step, the internal gas flow is generally stopped to prevent cooling and removal of the analyte vapour [162, 187]. The optimization of the temperature and duration of these steps are essential parts of the development of analytical methods using AAS, and will be discuss in Section 4.3.6.2.

The normal temperature profile of a graphite furnace can cause heterogeneities in the analyte spreading over the cuvette surface compromising the reproducibility of the measured absorbance. This can be avoided by using transversely heated furnace where the temperature is uniform over

the whole tube. In furnaces with longitudinal heating, the centre of the furnace is hotter than the ends [187].

After measuring, the furnace is cleaned by heating the atomizer to the maximum temperature for a short period. Finally, integrated water cooling and inert gas flows provides rapid cooling of the graphite tube after the operating voltage has been switched off to provide high sampling frequency.

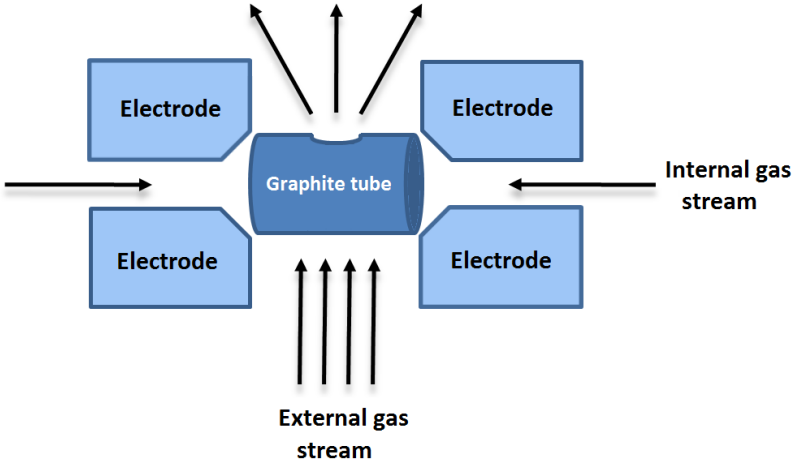

Figure 12: Schematic design of a graphite tube furnace

Electrothermal atomizers can be used to investigate liquid or solid materials that are introduced directly into a graphite tube. These atomizers use small sample volumes, and the entire sample is atomized, whereas in FAAS systems, only a small fraction of the sample enters the flame. In graphite furnace atomizers, the lifetime of an atomized sample in the optical path is typically of the order of several seconds, whereas in FAAS the residence time of the analyte in the optical path is less than 1 s. [185] Thereby, in ETAAS, the signal is averaged over longer time periods, affording higher sensitivity and lower detection limits.

When comparing with the vapour generation techniques (HGAAS and CVAAS), which have analogous, or even better, detection limits and allow speciation analysis, the ETAAS continues offering the advantages of using smaller sample volumes and being suitable to measure elements that do not need to form volatile hydrides [186].

A major limitation of electrothermal atomizers, however, is the reduced precision of the results obtained, compared to FAAS [185]. Replicate results are difficult to obtain because of the reproducibility associated with the furnace operation and temperature control. Also more operator skill is required to find the proper conditions for the thermal program of each type of sample.

4.3.3. Selection System

In AAS it is imperative to isolate the absorption line from background light. This may be achieved by the use of an optical system consisting of: an entrance slit that allow only a narrow beam of light to enter the monochromator; lenses and mirrors, which focus the radiation of the source first in the atomization zone (*e.g.* flame, graphite tube), then on the entrance slit of the monochromator; a prism or a grating that disperses the radiation into its component wavelengths; and an exit slit that isolates the desired spectral band [151]. The narrower the exit slit, the narrower the range of wavelengths which pass through it, i.e. more monochromatic is the light. The monochromator is placed after the sample cell to prevent the detector saturation by the radiation emanating from the atomizer.

A monochromator should be capable of separating two lines 0.1 nm apart, or less, when operating at minimum slit width [186]. In order to separate the analytical line, it is helpful to use a small slit width. However, to obtain a stable measurement signal with a favourable signal-to-noise ratio the slit must be geometrically large to maximize the radiation entering the monochromator. These two apparently contradictory conditions can be mastered using a monochromator with high dispersive power.

Prisms and gratings, are the two different devices used for dispersion of the wavelengths. In a prism the light is refracted when entering and leaving the prism. In this component, the refractive index of the material depends on the wavelength of the light passing through it, the dispersion decreases with increasing wavelength. Prisms have poor resolution (small difference in wavelength which can be separated) in the range beyond 240 nm and are mainly used for elements that have resonance lines which occur in the ultra violet [186].

Diffraction gratings can be transmission or, more usually, reflection gratings. The reflection gratings consist of a series of close, finely ruled lines, produced mechanically or by laser, on a thin metallic layer deposited on optically flat glass. The transmission grating consists in a series of close narrow parallel slits, which will diffract light and originate constructive interference at a specific angle. The dispersion of the gratings is almost constant throughout the spectrum. This means that for the slit varying the wavelength will not alter the bandpass [151].

In practice, monochromators are made using gratings because of the higher resolution, wider spectral range and constant dispersion but they are also more expensive to produce.

The size of an atomic absorption spectrometer is in part also determined by these components. Intelligent selection and design can contribute to a reduction of the overall dimensions of equipment.

4.3.4. Detection System

The detectors used in atomic absorption spectrometers are always photomultipliers.A photomultiplier tube is an electronic tube that is capable of converting a photon current into an electrical signal and of amplifying it. It contains a photosensitive cathode coated with easily ionized material (such as a Cs-Sb alloy) and a collection anode [186]. The cathode and anode are separated by several electrodes, called dynodes. The dynodes have an emissive surface and a positive potential relative to the previous electrode, providing electron multiplication.

When a photon hits the emissive surface an electron is ejected, i.e. the surface acts as a transducer, converting a light beam into an electrical signal. These electrons are accelerated and strike the next dynodes, ejecting several secondary electrons, until a cascade of electrons reach the anode. In this way a single photon striking the emissive surface generates an electron cascade effect and produces a significant electrical signal. At the end, the electrons strike the anode and flow off to the mass. The resulting current is then converted to voltage and measured. The signal is then electronically processed and the data stored in the computer, carrying out the calculations [151].

The amplification factor, typically 10^6-10^7 [151], increases exponentially with the number of dynodes and the interdynode voltage applied. The higher the voltage, the higher the amplification. However, its dark current and noise also increases with the voltage applied. Once thermal emission is the main source of dark current electrons, the photomultiplier should be cooled down to increase its performance.

The detector must be able to cover the spectral range from 190 to 860 nm. The long wavelength limit is determined by the photon energy required to ionise the cathode material. The short wavelength limit is determined by the material used in the light transmitting window (such as quartz) of the photomultiplier.

The main limitations of photomultipliers are the poor response at long wavelengths and measuring low power radiation. Intense light causes irreversible damage to the photoelectric surface and the photomultiplier response (current produced per photon) ceases to be linear. In addition they have extremely fast response times [186].

4.3.5. Interferences

Several types of interferences can be encountered in atomic absorption methods using both flame and electrothermal atomization: spectral, chemical, physical and background interferences. These interferences change the analyte signal while its concentration remains unchanged.

Spectral interference occurs when the absorption of an interfering species either overlaps or lies so close to the analyte absorption that monochromator resolution (or other wavelength selector) becomes impossible. It also happens when the source has overlapping lines (separation less than 0.1 Å [151]), although this is rare because the emission lines of hollow cathode sources very narrow. The solution to overcome these interferences is the use of alternate wavelengths. However, due to the well defined wavelength at which individual elements absorb and to the remote possibility of two elements absorbing exactly the same wavelength, this technique is known to be free of spectral interference.

Chemical interferences are more frequent than spectral ones. They result from several chemical processes occurring during atomization that alter the absorption characteristics of the analyte. The ionization of the analyte contributes for the chemical interferences by decreasing the analytical signal for the free atoms. Ionization suppressors are frequently used in FAAS to provide high concentration of electrons resulting in the suppression of the analyte ionization (*e.g.* Cs and K) [151]. Other processes that contribute for these interferences are the incomplete atomization of the analyte atoms and the analyte atom reaction with anions that form low volatile molecular species, reducing the rate at which the analyte is atomized. However, it can often be moderated by the use of higher temperatures or releasing agents (cations), which react preferentially with the interference and prevent its interaction with the analyte. Other important chemical interference is the reaction of the analyte atom to form molecular species that are stable in the flame conditions (*e.g.* refractory oxides). Protective agents (for example EDTA [186]), prevent this interference by forming stable but volatile species with the analyte.

The physical interferences, together with the chemical interferences, belong to the called matrix effects. These interferences are related to the bulk physical properties of the sample to be analyzed.
In FAAS physical interferences will affect nebulisation efficiencies during the atomization stage, because the amount of sample that reaches the flame depends on physical properties as viscosity, density and surface tension.
In the graphite furnaces these interferences are also originated from differences in viscosity and surface tension. This may originate different droplet sizes and consequently different spreading of the sample solution in the graphite tube, as well as changes in sample solution diffusion into the furnace. To overcome these problems, generally surfactants are added to the sample solution and coated graphite tubes are used to reduce the porosity of the graphite, increasing the tube life at elevated temperatures. Physical properties of sample and standard solutions for calibration curve should match as closely as possible. The most common way to overcome matrix interference in all atomic absorption methods is to use the method of standard additions. This method effectively creates a calibration curve by using incremental additions of only small volumes of standard

solution to a sample, unchanging the bulk physical properties of the sample providing a matched matrix [102, 185].

Background interference is caused by non-specific absorption, arising from light scattering caused by solid particles (for *e.g.* combustion products) and liquid droplets in the atomizing cell, or by broad-band absorption, caused by molecules and radicals from incomplete matrix breakdown during atomization [151]. If part of the radiation is absorbed by molecules or lost due to scattering, a higher gross absorbance is measured. The difference between the net absorption of the analyte atoms and the measured gross absorbance is called background absorbance. The background interference is more serious in graphite tube ETAAS than in FAAS and is one of the major causes of the poorer accuracy encountered with non-flame methods. This interference is easily overcome using background correction methods. Two measurements are made in all background correction systems: the total, or gross, absorbance measured at the resonance line emitted by the source; and the background absorption, which is subtracted from the total absorption to obtain the analyte absorbance [102].

There are several methods for eliminating background absorption. The two lines method requires the presence of a reference line from the source (for *e.g.* an impurity in the lamp cathode [151]), which should be as close as possible to the analyte line but not absorbed by it. This means that two absorbance readings are made with the same source at different wavelengths and sequentially. Any decrease in the power of the reference line is than attributed to absorption or scattering by the matrix of the sample and is used to correct the absorbance of the analyte line. Unfortunately, a suitable reference line is often not available and this method has been disappearing.

A different widely used method is the continuum-source or deuterium lamp background correction, which uses a separate source (deuterium lamp) with broad emission in the ultraviolet region to measure the background absorption. Both radiation from the source and the deuterium lamp pass alternately through the atomizer. The absorbance from the deuterium, which reflects the broad-band absorption or scattering by the sample matrix, is than subtracted from that of the analyte beam. This method cannot be used at wavelengths above about 350 nm [151], because the emission intensity of the deuterium lamp becomes very weak.

Other method employed in background correction is the pulsed lamp or Smith–Hieftje background correction, which uses a single light source, operating in alternatively low and high current. At low current, the lamp emission line is used to measure the absorbance at the maximum of the atomic absorption line of the sample. At high current, there is a broadening of the lamp output due to the temperature gradient, and the measured absorbance is essentially due to the background [186].

The method used in this work, the Zeeman background correction, consists in the application of an external magnetic field to the atomizer, originating a split in the electronic energy levels of the sample. This method will be described in more detail in the below Section.

4.3.5.1. Background correction by Zeeman effect

The instruments based on the Zeeman effect provide a more accurate background correction than the methods described earlier, allowing the direct determination of elements in samples with complex matrix, such as urine and blood. In this method, a magnetic field (from 0.5 to 1 Tesla [151]) is used to broaden either the emission from the lamp, or the absorption spectrum of the sample.

An atomic spectral line may contain several types of transition (depending on the angular momentum and spin of the electron). When applying to the atomizer a magnetic field these transitions will no longer be degenerate in energy, leading to the formation of 3 or more absorption lines for each electronic transition [188]. This shift is due to interaction between the electronic magnetic momentum with the external magnetic field. This phenomenon is called the Zeeman effect and is general for all atomic spectra. If the atom is in a singlet state, the single spectral line is split into three components and the effect is called normal Zeeman effect. If it is not, the electron spin has contribution and the spectral line splits in more than three lines. This is called anomalous Zeeman effect [151, 188]. Although the bulk of elements show the anomalous Zeeman effect, heavy elements like lead, which is the main target of this work, present a normal Zeeman effect, for the magnitude of the applied fields, and so only this will be described.

In the normal Zeeman effect, when the magnetic field is applied to the sample vapour, the single spectral line is divided into three components, generally symmetrical about the original non-field spectral line (*c.f.* Figure 13).

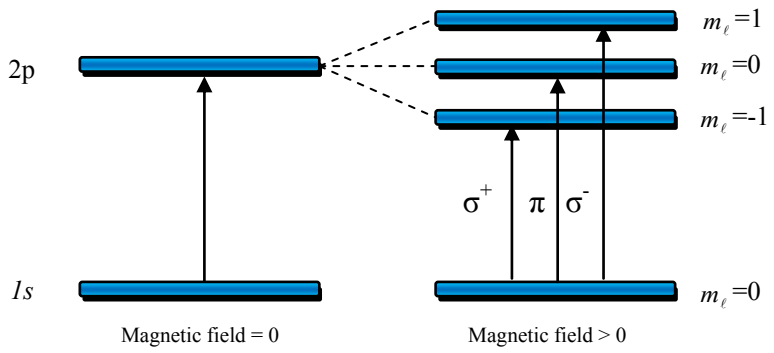

Figure 13: The effect of a strong magnetic field on atomic transitions.

These lines differ from another by about 0.01 nm for the applied magnetic fields. The central line, called π, appears at the same wavelength Thand with half the intensity as the original line. On either side of the π line appears two other lines (the $\sigma^{\pm}$ lines) having one quarter of the intensity of the original line [186].

The $\sigma^{\pm}$ lines ($\Delta m_{\ell} = \pm 1$) are circularly polarized when observed parallel to the magnetic field and linearly polarized perpendicular to the field when viewed perpendicular to the magnetic field.
While the π line ($\Delta m_{\ell} = 0$) is plane polarized with the direction of polarization parallel to the magnetic field [188].
If the magnetic field is applied perpendicular to the light path, the π line is polarized parallel with respect to the magnetic field and the $\sigma^{\pm}$ lines are polarized perpendicular to it. Thus, using a polariser to isolate either the parallel or the perpendicularly polarised light, the incident light becomes alternatively polarised. When the incident light is polarized parallel to the magnetic field, only the π component will absorb radiation, thus it is only attenuated by the analyte. Incident light polarized perpendicular to the magnetic field is only absorbed by the $\sigma^{\pm}$ components so it is only attenuated by the background. In both cycles occurs the matrix scattering, thus there is always some contribution to the background. In the end the background reading is subtracted to the peak absorption, thus giving a background corrected value.
If the magnetic field is parallel to the light path, only the $\sigma^{\pm}$ components appear and the π component is missing completely. Due to the fact that only the $\sigma^{\pm}$ components are present, it is not necessary to use a polarizer in this case, resulting in a better signal to noise ratio compared to the transversal Zeeman method. This is called the longitudinal Zeeman effect, which is recently used in the furnace AAS [151, 186].

The advantages of this technique are that total and background absorption are measured with the same emission profile of the same lamp, allowing the correct background subtraction, and that the technique is not limited to lamps operating in the ultraviolet region. The main disadvantage is the increased complexity of the spectrometer.

4.3.6. Graphite Furnace Atomic Absorption Spectrometry (GFAAS)

The use of graphite furnaces as atomizers for quantitative AAS goes back to the work of L'vov in 1961 [189]. In the L'vov furnace, samples were placed on an electrode and introduced into the aperture of the pre-heated cuvette. The L'vov furnace was simplified by Massmann [190] who omitted the electrode for the introduction of the sample, directly inserting the samples to the graphite tube interior by a hole in the wall. This is still the current geometry used nowadays and the one used in this work. Improvements to the Massmann furnace, as the L'vov platform furnace and the probe atomization, are also used.

The objective of the analyst in GFAAS is to separate the analyte from the matrix before the atomization stage. In addition, it has to be made sure that no analyte is lost in the pyrolysis stage

and that the matrix interferences are minimized. To achieve these goals it is important to pay attention to important parameters of this technique, as the matrix modifier and the thermal program. In this Section it will also be discussed the output signal, quantification method and analytical figures of merit. Relevance will be given to the use of microwave digestion (MWD) and ultrasound solid-liquid extraction (USLE) as sample preparation method.

4.3.6.1. Matrix modifiers

Everything in a sample other than analyte is called the matrix. Ideally the matrix decomposes and vaporizes during the ashing step, also called pyrolysis (meaning decomposing with heat). To enable a more efficient thermal separation between analyte and concomitants, during the pyrolysis stage, a chemical modifier must be added to the sample. Chemical modifiers are substances that decrease the loss of analyte during the ashing, making the matrix more volatile or the analyte less volatile (raising its boiling temperature) and stabilizing the analyte while the matrix is removed by volatilization.

The choice of the optimal chemical modifier mostly determines the potential of the method for the analysis of complex samples. However, the selection of an unsuitable chemical modifier can create more matrix effects rather than eliminate them. The number of compounds that are used as modifiers is very large, for example, the oxalic and nitric acids (NH_4NO_3 modifier), the metal nitrates ($Mg(NO_3)_2$ modifier), the ammonium phosphates ($NH_4H_2PO_4$ modifier) and the organic compounds as ascorbic acid and Pd/Mg modifiers [191]. For the determination of lead there are several different modifiers that have been particularly used to attenuate interferences and improving the atomization process [192]. One of the most common and also used in this work is $Pd(NO_3)_2$, which is known as a universal modifier [105, 193, 194].

Chemical modifiers are separated into two classes, conventional or permanent, according their application procedure. The conventional chemical modifiers are introduced into the atomizer along with the test sample. The permanent modifiers are introduced into the atomizer at the beginning of its operation or applied to the to the surface of the atomizer (*e.g.* by electrolysis), obtaining a coating of the chemical modifier thermally deposited onto the surface [195]. Permanent modifiers have the advantage of reducing contamination because, during thermal treatment, the volatile impurities in these modifiers are eliminated, increasing the atomizer lifetime. W, Ir and Rh are some single chemical compounds that are normally used as permanent modifiers [13].

4.3.6.2. Thermal Program

The furnace thermal programming is used to decrease, as much as possible, the matrix elements before the atomization is carried out. A temperature program usually consists of the following steps: drying, pyrolysis or ashing, atomization and cleaning. All these steps must be optimized for each analyte and each type of matrix. For each stage it is necessary to select the heating rate and the holding time at the selected temperature, which depends on the temperature and the sample volume [186].

The purpose of the drying step is to evaporate the solvent at a temperature just above its boiling point. For *e.g.*, in aqueous solutions the temperature should be above 100 ºC, about 110ºC [162]. Components with a higher boiling point might require more drying steps for safe removal. The drying process also should be fast but not too much to avoid spattering of the solvent.

In the ashing step, the temperature is raised to remove organic matter and to reduce, or eliminate, interferences due to, for *e.g.*, nonspecific absorption. At these temperatures, most the organic molecules of the matrix break into small volatile molecules that are flushed from the furnace. The choice of the ashing temperature requires a compromise between removing potentially interfering sample matrix (high temperatures and high hold times) and avoiding the lost of the analyte (short hold time and low temperatures). The use of a chemical modifier, as mentioned above, helps to solve this duality.

In the atomization stage, there is the generation of analyte atoms in the ground state. These atoms are then excited by the source radiation and finally the absorption is measured.

The atomization temperature must be high enough to give rapid and complete atomization of the element of interest. A high heating rate should be selected in order to obtain the highest density of atoms in the ground state. However, the lifetime of graphite tubes is quickly deteriorating at temperatures above 2700 °C, and the temperature must be selected accurately [187]. It is also important that the analyte signal returns to the baseline during the atomization cycle in order to avoid memory effects (interference from previous runs).

In the cleaning step, the graphite furnace is heated to the maximum temperature, for a short period of time, in order to volatilize potential residues from the matrix and the analyte.

The optimization of these operating conditions is essential, as well as, the study of the absorbance variation with temperature in ashing and atomization steps (ashing/atomization curves) for the selection of the optimum temperatures.

4.3.6.3. Data Analysis: output signal

Under optimum conditions, the atomization peaks should be relatively symmetric. A typical output signal from the atomic absorption spectrometer used in this work (Analytik Jena AG, Jena, Germany, model 650) is present in Figure 14. The image shows the absorbance at the wavelength of a lead peak when a 20 µL of sample plus 5 µL of matrix ($Pd(NO_3)_2$ sample of aqueous solution added with 18 ppb Pb was atomized.

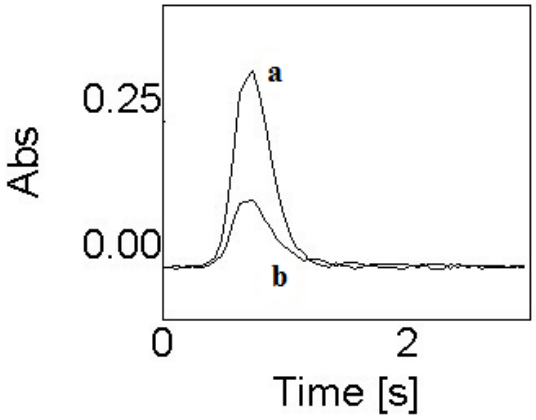

Figure 14: Pb Absorption profiles for aqueous calibration standard (18 µg L^{-1} Pb). a) atomic absorbance profile; b) background absorbance profile.

Irregular peaks indicate problems that might result in wrong interpretations and results. For example, the degradation of the peak shape, or a large change in the slope of calibration curve, indicates that is time to change the furnace. Relatively broad peaks can indicate the formation of stable carbides, the use of too low atomization temperature, insufficient external gas flow, or uncorrected non-specific absorption. Multiple peaks might originate from memory effects, spattering of the sample solution during stages prior to atomization (once part of the analyte might be atomized from the platform and other part from the tube wall, for *e.g.*), wrong background correction, or from the analyte itself (more than one compound).

Also the measurement of furnace blanks, i.e. solutions containing all the reagents/solvents used in the analysis, but with no analyte present, is very important. If an atomization signal appears during a blank it might indicates a insufficient cleaning temperature or time. It may be necessary to repeat the cleaning step, or even exchange the graphite tube [151, 187].

Once the matrix can influence the atomization behaviour of the analyte and thus the shape of the peak, signal peak area evaluation should be used in GFAAS. Peak area evaluation increases the reproducibility and the linearity of the calibration curve once the absorbance is not measured only at the moment of greatest atom density.

4.3.6.4. Quantification

In GFAAS the quantification is made by the standard calibration method that consists in the calibration against known standards, i.e. solutions containing known concentrations of analyte, to obtain accurate quantitative results. An atomic absorption spectrometer measures the absorbance of the analyte which is proportional to the analyte quantity present in the sample (*c.f.* Lambert-Beer law, Section 4.1.). A calibration curve is obtained by measuring the absorbance peak area of a number of standards with increasing analyte concentration and plotting these values against the respective known concentrations [162].

The standard solutions should be prepared using high purity metals dissolved in high purity reagents, or even commercially available standard solutions, which have low levels of contaminating species. In order to obtain a good precision, they should be measured at least three times. A blank should be measured before the standards, to assess the contamination by impurities during the analytical procedure and the existence of interfering species in the reagents [187].
When a calibration line is plotted usually is used a linear regression analysis to find the best straight line through the experimental points. Subsequently, sample concentrations can be interpolated from the calibration curve. It is also very important to subtract the blank from every standard and sample signal to remove possible interferences due to impurities.

Aqueous standards are used when matrix components in the sample do not interfere with the analytical signal. When the matrix of the sample is too complex, to compensate for the chemical and spectral interferences, it is also used the so called standard addition method, or spiking. This method consists in adding known quantities of analyte to the sample. From the signal difference between the spiked and unspiked samples, it is deduced how much analyte was in the original sample. This method requires a linear response to the analyte [187].

4.3.6.5. Analytical figures of merit

The precision and accuracy are verified in the same way as in EDXRF spectrometers (*c.f.* Section 3.3.1.1.6). However, in GFAAS it is usual to test the precision within bath, one vessel of the same sample several times, and between baths, several vessels of the same sample.

In GFAAS it is normal to use not only the detection limit usually represented by the limit of detection (LOD), but also the limit of quantification (LOQ) that represents the lowest analyte concentration that can be determined quantitatively. In the concentration range between the LOD and the LOQ the analyte may be detected, but not quantitatively determined.

The detection limits are normally calculated with the criterion of $[X]+3SD$ for LOD and $[X]+10SD$ for LOQ, $[X]$ being the mean absorbance signal of 10 blanks measurements and SD the corresponding standard deviation of ten measurements [196].

4.3.6.6. Sample Preparation

There are several preparation methods for organic and inorganic sample materials, in order to transform a sample for analysis. One of the classical methods, and still the most frequently used, is the microwave digestion [197, 198], which is a wet decomposition method in a closed system that uses a combination of high temperature and pressure to enable digestion. In general, this method consists in microwave digestion with acid, and sometimes H_2O_2, in a teflon bomb. Lead, for *e.g.*, is an analyte that is generally measured in soft tissues by solubilising them using microwave pressurized acid digestion [125, 199]. This methodology involves a complicate and time consuming sample handling and consequently a low throughput. In addition, the solutions volumes used in the treatment tend to increase the limit of detection. In this work, this method will be only used as a tool to assess the results obtained with another technique that is the ultrasonic solid-liquid extraction and that will be discussed in more detail in the next Section.

4.3.6.6.1. Ultrasonic solid-liquid extraction

The use of ultrasonic energy - ultrasonication - can greatly enhance analytical chemistry and represents a growing area of research [200, 201]. Recent advances in technology have improved so much the sample treatment that for many metals, total digestion of samples may be overcome by a simple ultrasound solid–liquid extraction procedure [202].

Ultrasound frequencies range roughly from 15 kHz to 1 GHz [203]. Once acoustic wavelengths are much larger than molecular dimensions, the interaction of ultrasonic energy with matter do not arises from a direct interaction with molecular species. Instead, when ultrasonic waves cross through a liquid media, interaction occurs due to a phenomenon called cavitation. This process is described by the generation of bubbles due to the acoustic wave's oscillating pressure. These bubbles grow, oscillate, split and finally implode, releasing the concentrated energy stored in a very short time. Localized hot-spots with temperatures near to 5000 ºC and pressures of 1000 atm are originated, thus these bubbles can be considered as micro-reactors [16]. Cavitation causes physical phenomena, such as pitting and mechanical erosion of solids, due to the microjets of solvent with velocities greater than 100 m s^{-1} [204], which can lead to particles of smaller size. Cavitation also causes radicals formation, which induces the oxidation of chemical species. As an example, when ultrasonic power is applied to water it results in the formation of hydroxyl radical and hydrogen

peroxide. Due to this phenomena, the analyte present in the solid may be extracted into the liquid media, when submitted to ultrasonic energy [205].

The most common ultrasonic devices commercially available to use in analytical chemistry are ultrasonic baths, sonoreactors and ultrasonic probes. Ultrasonic baths provide indirect ultrasonication and have some disadvantages compared to the other devices. Their lack of reproducibility and their low ultrasonic power are restricting for the majority of the ultrasound applications required in chemical analysis. Sonoreactor devices also provide indirect ultrasonication but with 50 times more intense ultrasonic energy than the later. However, the cavitation produced is lower than the one provided with the ultrasonic probe. The ultrasonic probe is the most powerful system available for the solid–liquid extraction of analytes and was used in this work. It can supply an ultrasound intensity in the order of 100 $W.cm^{-2}$, at least, 100 times greater than the ultrasonic bath [16].

The ultrasonic probe (*c.f.* Figure 15) provides a direct ultrasonication of the sample once it is immersed directly into the solution, having no power loss due to the transfer through the vessel walls. Probes are usually made of titanium, which is resistant to cavitation, have low acoustic loss, and is chemically inert. However, tip erosion may lead to contamination by metallic particles.
There are several parameters that should be paid attention during the use of ultrasonication probe. The intensity of ultrasonication (the vibrational amplitude of the tip) can be set to any desired level by the amplitude control of the probes. The higher the amplitude, the more intense is the sonication. However, very high amplitude levels lead to probe deterioration and, typically, this parameter is set to 50% [206].

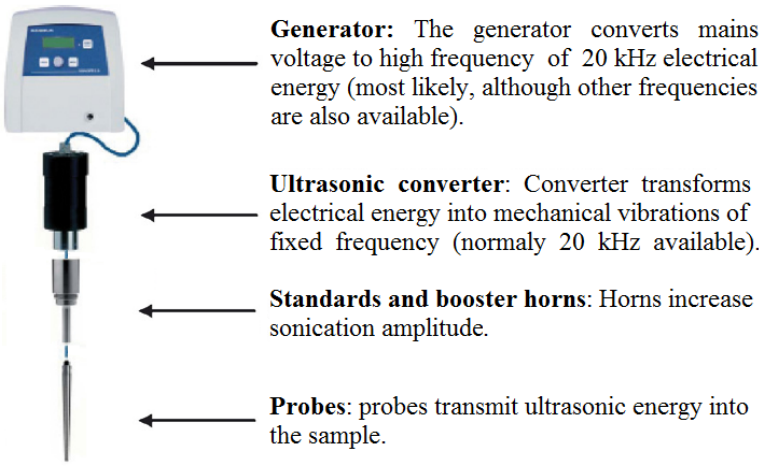

Figure 15: Comprehensive scheme of an ultrasonic probe (adapted from [16] with kind permission of J.L. Capelo)

Temperature must also be controlled. During sonication a slow, but constant, increase in the bulk temperature is achieved, which changes physical characteristics of the liquid media and affects cavitation. This problem is normally overcome by cooling down the sample in an ice bath or, if long sonication times are needed, using pulse mode that avoids the temperature increase [16]. The reaction vessel shape is also important and must be conical in order to allow the probe to be inserted more deeply into the sample, thus avoiding aerosoling [207]. The contact between the probe and the sides of the vessel must be always avoided.
The sample volume is also important and there are different probes for different range of volumes. This information is usually given by the manufacturer, but higher volumes lead to higher diameter probes. Typically, solid liquid extraction by ultrasound probes is operated at about 20 kHz frequency, with sonication times of 5 min or less [206, 208], sample mass ranging between 10 and 50 mg [209-211] and with the particle size of the solids as small as possible [16].

The USLE of metals from solid biological samples to liquid media offers some advantages. In this process only the supernatant is injected into the furnace, which results in a drastic background decrease and diminishes the build-up of carbonaceous residues inside the furnace. Under this procedure, volumetric and sedimentation errors that occur when pipeting particles are avoided. The USLE allows high sample throughput as the sample treatment is typically completed in 1 minute. Furthermore, the amounts of sample required are regularly of tens of milligrams. In addition, the final sample volume is made up to some hundreds of μL, typically 500, which renders low limits of detection. On the overall, USLE match many of the concepts of analytical minimalism as outlined by Halls [212]: low sample mass and low reagent volume consumption, low solvent extraction volumes, low waste generation, easy of handling, high throughput and short treatment time.
The ultrasonic probe is very efficient in the solid-liquid extraction of elements and has been used as a sample preparation technique for elemental analysis by ETAAS [208, 213]. It has been described as a powerful tool to extract lead from solids [202, 206, 214]. The technique is effective when the lead is softly bounded to the solid, as it is in the case of a co-precipitation. However there are some contradictory results reported to date in literature regarding ultrasonic elemental extraction. The reasons for these facts may be explained on the basis of an incorrect application of the ultrasonic procedure rather than to a lack in ultrasonic extraction efficiency [16]. In many papers there is a lack of experimental details that should be reported, what difficult to find an explanation for controversial data.

CHAPTER V - EXPERIMENTAL PROCEDURE

5.1. Animals and Experimental design

Rats are similar to humans from the biological point of view. Their genetic, basic physiology and behaviour characteristics are closely resembled, thus many human diseases can be replicated in mice and rats [215]. Rats short life-cycles, the ease of handling these animals, the simplicity in controlling the surrounding environment (diet, temperature, lighting, etc.), their low cost, and avoiding to expose humans to health risks, are responsible for the suitability of rats in intoxication studies, always observing the ethics in animal use. Keeping this in mind, a major study of the mechanisms underlying lead concentration in biological samples of exposed rats was developed.

In this study, it was used Wistar rats, a strain of albino rats that belongs to the species *Rattus Norvegicus*. Animals were assigned to one of the following two experimental groups: the exposed group fed with 0.2% w/v of lead acetate in drinking water since the foetal period (n=30); and the control group, which got normal drinking water (n=20 by collection). The lead exposure regimen was based on the previous validated study of Bielarczyk *et al.* [216], and prepared by dissolving lead acetate (Panreac Quimica SA - Lead (II) Acetate 3-hydrate DIDATIC) in distilled water.
Wistar rats, aged from 1 to 11 months, were used in this study, in a total of 10 collections with 5 rats each, 3 exposed rats and 2 control rats, giving a total of 50 rats. The experimental chronogram was designed to show the dynamicity of lead exposure within several tissues and excretions of animals during different stages of their development, from newborns to adults in a later stage in life. In order to achieve this purpose, a monthly evaluation of lead exposure was performed in animals belonging to both the control and contaminated groups.
Animals were housed in standard cages placed in their usual room in the Instituto de Medicina Molecular – Instituto de Fisiologia (Faculdade de Medicina de Lisboa) laboratory, in accordance with EU legislation on animal experimentation. Animals were placed in cages with commercial pellet food (Panlab A04) and water *ad libitum*, kept at 18±1 ºC and relative humidity of 60±10%, on a 12:12-h dark–light cycle.

Several tissues and excretions were analysed in each collection: urine and faeces, kidney and liver and four different bones, namely, iliac bone, femur, tibia-fibula, and skull (frontal, parietal and occipital bone).
For urine and faeces collection, rats were individually placed in metabolic cages for a 24 hour collection. Due to the number of metabolic cages available for each collection, only urine and faeces of 2 exposed rats and 2 control rats were analysed. Samples were stored in separate plastic vessels with no chemicals addition, and stored at 2 ºC.
After the excretions collection, at the end of each month of exposure, the animals were sacrificed by an overdose of sodium pentobarbital (100 mg mL^{-1} per kg body weight), and the soft tissues and

bones were collected. Soft tissues and bones were kept in different plastic vessels, containing a 10% para-formaldehyde solution with 7.4 pH (37-38% w/w, Panreac) and stored at 2 ºC to avoid deterioration. The skull samples were stored in separate receptacles from the rest of the bones, because of their small size.
All procedures involving animals were in accordance to EU law on animal experimentation. and a total of 380 samples were collected.

Brain samples from rats with different periods of lead-exposition were also analysed, but with a different purpose. The presence of lead in brain has been linked to neurotoxicity, mild mental retardation and low IQ scores in children [48, 54]. Therefore, lead determination in brain is a key feature in the study of these health problems. However, two main reasons make lead determination in rat brain difficult, especially if the targets are specific brain areas. One is the low sample mass available, typically 10 to 20 mg of wet tissue that hinders the sample replication. The second reason is the low lead concentration usually found in rat brain. To overcome these problems it was developed a sample preparation method based in the use of ultrasound solid-liquid extraction. With that purpose, two different areas of the brain were studied: the Hypothalamic Defence Area (HDA) and the Nucleus Tractus Solitarius (NTS). A total of 24 tissues from control rats, 12 HDA and 12 NTS, as well as 24 tissues from exposed rats, 12 HDA and 12 NTS, were analysed. The brain samples were collected using the same procedure mentioned above for the soft tissues. After sampling, they were placed in four different vessels, depending on type of tissue and if it belongs to an exposed or to a control rat, preserved in formaldehyde and stored in the refrigerator at 2 ºC. Thus, it was not possible to do an age dependent study in these samples.
The sample preparation method applied to the brain samples was also used to study the urine samples, in order to overcome problem of urine precipitates. In fact, a precipitate tend to be formed in non preserved or long-term preserved urine [12]. Consequently, the concentration of lead in urine lowers with time as it co-precipitates with the solid. As result, accurate lead quantification in urine is achieved only if the solid phase and the liquid phase are both interrogated for lead content.

Analysis of formaldehyde containing the soft tissues and bones were also performed using ETAAS in order to assess the presence of lead diffusion from the samples to the formaldehyde.

Some preliminary studies were also done in the hair of the rats, because, due to its regular growth, hair is seen as an important time dependent biomarker. However, after some analysis made with the EDXRF and the μ-PIXE techniques, it was shown that the hair of the rats was externally contaminated and the study was discontinued. This was probably due to the contamination of the rat's snout, while drinking water, and consequently contaminating the paws and hair during their

cleaning processes. These results will not be presented in this dissertation, once they will not contribute for an accurate excretion study over age.

5.2. Sample preparation

This Section is divided in 3 subsections according to the measurement technique. First, it will be discussed the sample treatment for the samples analysed by EDXRF, namely faeces, kidney, liver and bones. Next, it will be explained the treatment method for samples that were analysed by TXRF, namely urine. Finally, the sample preparation for samples measured by ETAAS, namely urine, brain and formaldehyde will be presented.

5.2.1. Sample treatment for EDXRF

For the EDXRF analysis it is necessary to convert the sample into pellets. For that purpose soft tissues were sliced and lyophilized using a Modulyo Freeze Dryer System, from Edwards (UK), for 4 days at -60 ºC and 20 Pa. The faeces were also lyophilized, but since they have less water than soft tissues, 3.5 days at -60 ºC and 20 Pa was enough to dry the samples. The bones were dried in a Memmert oven for 4 days at 60 ºC to make them easily breakable, enhancing the powdering process.
After these processes all samples were, without any further chemical treatment or additive, powdered with a pestle in a porcelain mortar and pressed into circular pellets, with 20 mm in diameter, by a 13 ton manual hydraulic press from Specac.

To reduce contamination, it was used a different mortar and a different pestle for control and exposed rats, and all the material was carefully washed with ethanol and Milli-Q ultrapure water (18 MΩ cm resistivity).

Each pellet, weighing about 0.2 g, was glued (heptane mixture) on a Mylar film, fixed into a slide mount and placed on the sample holder (50 mm x 50 mm) in front of the X-ray beam for the element determination (*c.f.* Figure 16). Two pellets of each sample were made. If there was not enough tissue amount, the same pellet was measured two times in different positions.
These procedures were held in Centro de Física Atómica da Universidade de Lisboa.

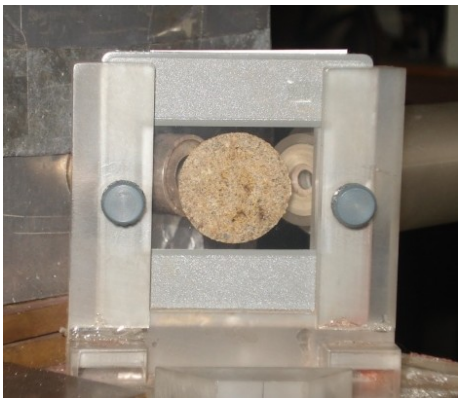

Figure 16: Bone pellet placed on the sample holder before EDXRF measurement.

5.2.2. Sample treatment for TXRF

The TXRF analysis was carried out using quartz discs, with a diameter of 30 mm and a thickness of 3 mm, as sample holders. In order to obtain low sensitivity, the cleaning process of these carriers is critical. First, sample residues (from previous measurements) were removed using a soft brush. Secondly, the quartz discs were rinsed with acetone and gently placed in a PTFE (Polytetrafluoroethylen, Teflon) support inside a beaker with detergent bath (RBS 50, Carl Roth GmbH, Karlsruhe, Germany) for boiling during 2 h. After cooled down, the support with the carriers was rinsed with distilled water and placed in another beaker with Milli-Q ultrapure water (18 MΩ cm resistivity). This water was boiled again, cooled down and dried up with fluff -free scientific cleaning wipes (Kimwipes, Kimberly-Clark Corporation, UK) . The support was then placed in a third beaker with concentrated ultrapure HNO_3 (Merck, Suprapur 65%) and boiled during 1 h. Finally, quartz carriers were rinsed with ultrapure water and subsequently dried. Boiling must be done in a clean fume cupboard in order to prevent any contamination.

After this cleaning process, the quartz carriers must be rinsed with a silicon solution and, subsequently, dried at 100 ºC for about 1 h to keep aqueous samples in position in the carriers. Thus, before adding the sample, an alcoholic silicone solution from Serva, (SERVA Electrophoresis Heidelberg, Germany) was added to the pre-cleaned quartz carrier. This avoids the tear up of the samples, and keeps the droplets small and in the middle of the quartz discs.
Afterwards, an aliquot of 2 µL of urine was pipetted on the quartz-glass carrier and thoroughly dried under infrared light (Philips, 150 W) for about 15 min. Without adding any chemicals, a first run of the spectrum was done to determine the best suitable internal standard. To be used as internal standard, the element should not be present in the original sample, should not interfere with

the target element (Pb), and must have an adequate XRF response. In the present work it was chosen Ga (1000 µg mL^{-1}, Aldrich, Milwaukee, USA).

Subsequently, a volume of 2 µl of urine, followed by 10 ng of Ga (diluted solution), were both pipetted onto different quartz-glasses. After this, the samples were dried for about 15 min under infrared light to adhere evenly to the surface of the quartz carrier (*c.f.* Figure 17). It was verified that the whole sample and the internal standard were in the field of view of the detector (8 mm in diameter), otherwise the quantification via internal standard might fail. Milli-Q ultrapure water was used to dilute the samples whenever necessary. Finally, the samples were directly measured by the TXRF spectrometer.

Since these urine samples were measured soon after their collection, no significant precipitate was visible. These processes were held in ISAS, Dortmund, Germany.

Figure 17: Quartz carriers with urine samples being dried before TXRF analysis.

5.2.1. Sample treatment for ETAAS

The sample treatment for the formaldehyde is very different from the sample treatment for the urine and the brain. The analysis of formaldehyde was straightforward, while for urine and brain a new methodology had to be developed and validated. Thus, concerning brain and urine samples, two methodologies were used: USLE as a main methodology to measure all the samples, and MWD to validate the suitability of USLE. The two methodologies will be described below. Later in Section 5.4, the validation study for the USLE method will be presented.

During the sample treatment special attention has been given to the cleaning process that occurs previously before material usage. All material was carefully cleaned using HNO_3 (10% v/v, Merck (Suprapur 65%) and left to stand for 24 h. Afterwards, it was rinsed with Milli-Q ultrapure water (18 MΩ cm resistivity) and left to dry. These processes were held in REQUIMTE facilities in the Chemistry Department of the FCT-UNL.

5.2.1.1. Formaldehyde

In order to detect eventual lead diffusion in the formaldehyde used to preserve the tissues, samples of this liquid were collected from the receptacles containing the kidneys, liver, bones (each receptacle containing iliac bone, tibia and fibula and femur), skull, NTS and HDA from exposed rats. Original formaldehyde (containing no tissue) was also collected. The formaldehyde samples were centrifuged in a *Sky Line minicentrifuge-vortex* (*ELMI*, Riga, Latvia) at 2500 rpm for 10 min to avoid solid particles. From each formaldehyde sample a 0.5 mL aliquot was withdrawn, placed in the autosampler cups (*c.f.* Figure 18), and its lead concentration determined in triplicate by ETAAS. When necessary dilutions were made with Milli-Q ultrapure water (18 MΩ cm resistivity).

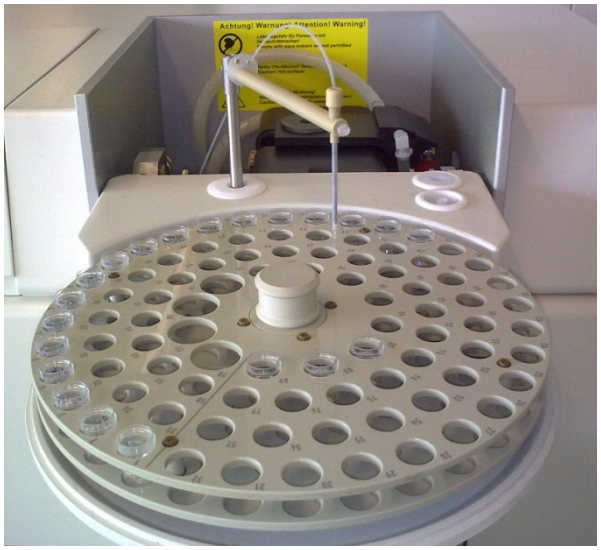

Figure 18: Autosampler detail.

5.2.1.2. Urine

The urine samples were taken and left with no further treatment in closed vessels. After some weeks, the formation of a precipitate was observed. Afterwards, samples (volume 5 to 25 mL) were acidified with nitric acid (Merck, Suprapur 65%) up to 10% v/v, shaked for 10 minutes and then left to stand for at least 48 h before analysis. After, they were sonicated using an ultrasonic probe UPS200s (dr. Hielscher - Ultrasound Technology, Teltow, Germany) in steps of 2 min (x3, 200 W, 24 kHz, 50% ultrasonic amplitude, 14 mm diameter titanium probe tip), being allowed to cool in an ice bath for 1 min between sonication steps. The supernatant part of all samples was pipetted to the autosampler cups (*c.f.* Figure 18) and measured in triplicate using the ETAAS technique. Whenever needed, samples were diluted with 10% HNO_3 blank solution to fit the calibration curve. The blank samples (10% HNO_3) were submitted to the same procedure.

To validate this procedure, some samples were analysed before and after ultrasonic treatment.

The precipitate formed in the urine samples was dissolved using microwave-assisted acid digestion. Once the urine samples were acidified and sonicated as explained above in this Section, 1 mL was withdrawn and centrifuged at 7000 rpm for 3 min using a centrifuge Tehtnica Centric 150 (Železniki, Slovenia). The supernatant was carefully removed and the precipitate was allowed to dry at 50ºC, in a JP Selecta Sa oven, until constant weight was observed (24 h).

After, the precipitate was weighted (from 2 mg up to 6 mg) using a a digital balance, *Mettler Toledo - AT21 Comparator (max 22g; d = 1μg*) and transferred to a PTFE capped digestion bomb (45 mL capacity Parr reactors). It was added 50 μL of H_2O_2 (30% m/v, Panreac, Barcelona, Spain) to the precipitate and the mixture was left to stand for 15 min. Afterwards, 2 mL of HNO_3 conc. (65% m/m, Merk, Darmstadt, Germany) was added and the mixture was left to stand for 15 min. Finally, the microwave-assisted acid digestion was done in a De Longui microwave oven model Perfecto Easy Microwave MW314 (350 W, 2.5 min).

When the digestion was finished, the sample was made up to 5 mL with 10% v/v HNO_3, pipetted to the autosampler cups, and measured in triplicate using the ETAAS technique. Blanks were treated in the same way. It is important to emphasize that this methodology duration is about 4 h, mainly due to the large amount of time that is needed for the digestion bomb to cool down after the digestion process.

5.2.1.3. Brain

The brain samples were removed from the formaldehyde solutions and allowed to dry until constant weigh at 50 ºC (24 h) in a JP Selecta Sa oven. The dry samples (from 2 mg up to 4 mg, weighted using the same digital balance, Mettler Toledo) were transferred to 1.5 mL cups and 1 mL of 10% v/v HNO_3 (Merck, Suprapur 65%) was added. After, the samples were sonicated using the same ultrasonic probe, UPS200s, in steps of 1 min (x3, 200 W, 24 kHz, 50% ultrasonic amplitude, 1 mm diameter titanium probe tip). Between sonication steps the samples were allowed to cool in an ice bath (1 min). The supernatant part was pipetted to the autosampler cups (*c.f.* Figure 18) and measured in triplicate using the ETAAS technique.

Whenever needed, the samples were diluted with 10% HNO_3 blank solution to fit the calibration curve. The blank samples (10% HNO_3) were submitted to the same procedure.

After the brain samples were sonicated, they were removed from the 10% v/v HNO_3 solutions and allowed to dry until constant weigh at 50 ºC (24 h) in a JP Selecta Sa oven. The dry samples were weighted again in the same digital balance (2 mg to 4 mg) and transferred to the PTFE digestion bomb. The following procedure is identical to the one described in the microwave digestion of urine samples.

5.3. Spectrometers used

5.3.1. EDXRF Spectrometer

In this work it was used a home-made spectrometer (*c.f.* Figure 19). This spectrometer consisted of a commercial X-ray tube (PHILIPS PW 2184/00) with a tungsten (W) anode supplied by high voltage power supply (PW 1140, 100 kV, 80 mA maximum) and equipped with a molybdenum (Mo) changeable secondary target. The X-ray generator was operated at 50 kV and 20 mA, and a typical acquisition live time of 1000 s was used.

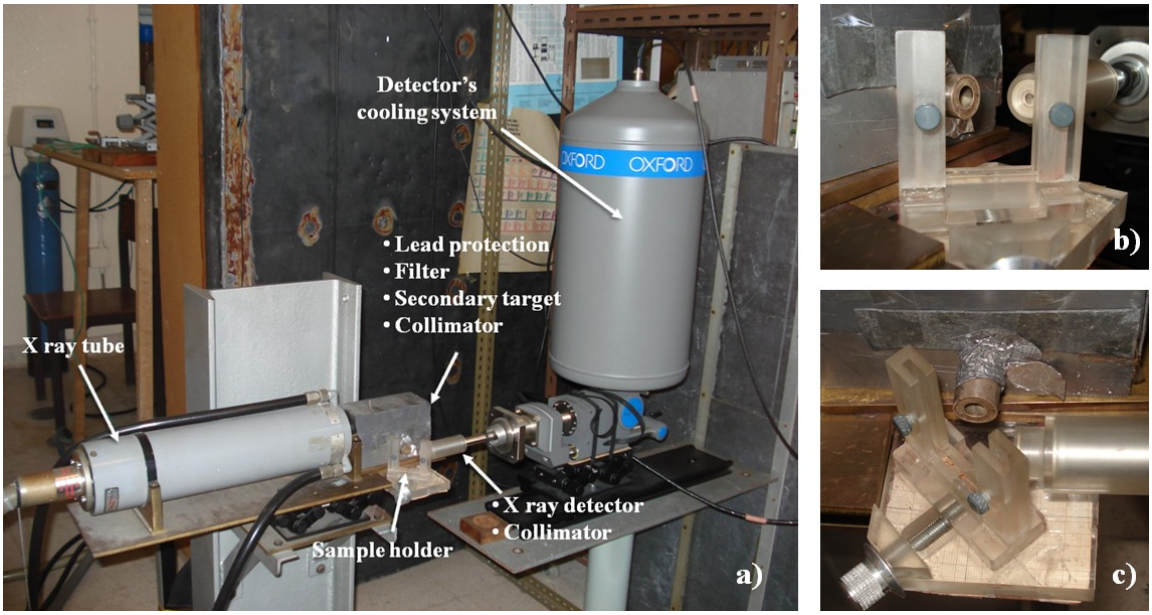

Figure 19 a) EDXRF spectrometer; b) sample holder seen from the front; c) sample holder seen from above

The binding energy of the *K* shell of the W anode is 69.52 keV [217], what means that an operation tension of 50 kV, corresponding to an electron beam with 50 keV energy, is not enough to excite the characteristic lines of the anode. Thus, the radiation that is going to excite the secondary target of Mo, consists in the Bremsstrahlung originated from the anode. According to what was described in Section 3.3.1.1.1., the maximum intensity occurs at 33 keV. This energy is close to the binding energy of Mo, 20.00 keV [217], and enough to excite the secondary target in order to obtain its characteristic radiation with the values of 17.44 keV for K_α and 19.60 keV for K_β. The *L* lines, due to their low energy (about 2 keV), are not of interest in the excitation of the sample. With this configuration it is possible to obtain a quasi-monochromatic source and to excite not only the *K* spectrum of elements up to $Z = 41$ (binding energies less than 19.60 keV), but also the *L* spectrum of elements with atomic number higher than the atomic number of Mo.

The X-ray tube, the secondary target and the sample were positioned in a triaxial geometry with 90º angles to decrease the background radiation as mentioned before (Section 3.3.1.1.2.) [18, 218]. The use of an Ag filter in front of the X-ray tube and two silver collimators (between secondary target-sample and sample-detector) also contribute to reduce the scattered radiation and improve the detection limits. The collimators used have been made using a series of thin apertures. The diameter and length of the collimators, and the material used have been carefully tested in order to find an optimal design.

The focus of the beam in the sample is an ellipse with a major axis of about 2 cm and a minor axis of about 1.5 cm. The sample holder must be made from light elements and it should have the less material possible (besides the sample itself) in order to avoid the spectrum contamination and increase of background. The sample holder used was made of perspex and the sample was glued on a mylar fixed in a slide holder, allowing a direct exposition of the sample to the X-ray beam.

The characteristic radiation emitted by the elements present in the sample is detected by an *Oxford* Si(Li) detector, with a 30 mm^2 x 5 mm active area, energy resolution of 135 eV at 5.9 keV and a 8 μm beryllium window which is at 27 mm from the sample. The beryllium window is highly robust and absorbs strongly the low energy X-ray radiation. Due to the absorption of radiation in the Be window and to the absorption of radiation in air, only elements with atomic number higher than Al can be detected. The acquisition system is a Nucleus PCA card and the signal treatment and corrections to dead time are automatically adjusted by a Oxford 2040 commercial processor. Finally, the spectrum is obtained through the Quantum MCA v. 3.00 software and, as referred in Section 3.3.1.1.5., quantitative evaluation is made using the fundamental parameters method [167, 219].

In this work, the concentrations were derived using the code XRFAES (X-ray Fluorescence Automatic Evaluation System) developed at the Department of Physics, Chalmers University of Technology.

As an intermediate step between spectrum analysis and calculation of concentration using Equation (III.12), a separate calculation is made to quantify the attenuation coefficient for elements that are specified to occur in the sample. A set of equations corresponding to the intensity of the coherent and incoherent scattered radiation [167] and the normalization condition (Equation III.15) are then solved until the convergence condition is reached (relative difference in concentration between two successive iterations is less than 1% or a maximum of 100 iterations is used). In addition to all those elements that have their characteristic lines in the spectra, a number of virtual elements can be selected by the operator to represent all of the undetermined light elements that belong to the matrix of the sample [167, 168].

For biological soft tissues, this matrix is essentially H, C and O, which are the main constituents of biological tissues [220].

When studying hard tissues, the sample matrix is different. For example, bones are mainly consisted by hydroxyapatite. In this case, once the matrix of the sample is composed of elements that are visible in the spectrum, such as Ca, the final concentrations calculated have errors of about 10%.

Often, in the experimental spectrum some lines of different elements overlap. In this work, special attention was given to the overlap between the Kr(K_α) and Pb(L_β), and between the As(K_α) and Pb(L_α). The Kr(K_α) peak area was calculated from the Ar(K_α) peak area, supposing a steady air composition. After, this Kr(K_α) peak area was subtracted from the total Kr(K_α)+Pb(L_β) peak area. The obtained Pb(L_β) peak area was then used to calculate the Pb concentration. The ratio between the Pb(L_β) and Pb(L_α) lines was used to obtain the Pb(L_α) peak area. Subtracting this peak area to the As(K_α)+Pb(L_α) area, it is possible to obtain the As(K_α) peak area.

5.3.1.1. Dection limits and accuracy

The detection limit of the EDXRF technique was calculated by using the Equation (III.20) for different standard reference materials.

When measuring soft tissues and faeces the detection limit for lead was calculated using the standard reference material Orchard leaves 1571, from National Bureau of Standards (NBS), prepared in pellets according to the sample preparation method described in Section 5.2.1. This standard has the same light element matrix as faeces and soft tissues, i.e. its composition is mainly H, C and O. The detection limit calculated for Pb was 2 μg g^{-1}.

The detection limit of this spectrometer for the bones measurements was obtained using the standard reference pattern of Bone Ash 1400 from NBS. This standard was also prepared according to Section 5.2.1., and it was calculated the value 5 μg g^{-1} for Pb.

The accuracy was also checked by analysing the reference materials present in Table 1. All the measurements showed a good agreement with the certified value assuring the accuracy of the method.

A relative standard deviation (RSD) less than 10% was obtained for the different pellets of the same organ.

Reference Material	Certified Pb concentration	Measured Pb concentration
Orchard leaves NBS 1571	45±3	42±3
Bovine Bone 05-02 Wadsworth Center	16.1 ± 0.3	17±2
Caprine Bone 05-04 Wadsworth Center	31.5 ± 0.7	29± 3

Table 1: Comparison of the lead concentration (μg g^{-1}) in the standard reference materials obtained in this work with the respective certified values. Results presented as $\bar{X}$±SD.

5.3.2. TXRF Spectrometer

The spectrometer used for TXRF measurements is a commercial spectrometer, Extra II, R. Seifert & Co., Ahrensburg, Germany, located in the Institute for Analytical Sciences (ISAS) in Dortmund, Germany. It is equipped with a Mo X-ray fine focus tube with a line focus of 0.04 mm height and 8 mm width, a Mo filter with a 50 μm width and a low-pass reflection module made of quartz crystals (Seifert & Co., Ahrensburg), which acts together with two edges (diaphragms) as a cut-off filter. It is combined with an Oxford Pentafet Si(Li) detector with 80 mm^2 active area, energy resolution of 165 eV at 5.9 keV and a 8 μm beryllium window, which is at 1 mm from the sample and a computer-controlled analyzer, Link System QX 2000 (Oxford Instruments, High Wycombe, UK).

The glancing angle is 0.09º and the operating conditions for the Mo X-ray tube were adjusted to 50 kV and a varying current that assured a dead time less than 50% (up to 38 mA). The acquisition live time for all spectra was set to 250 s. The quantification was achieved by using the internal standard of Ga (Gallium, standard solution 1000 μg mL^{-1}, Aldrich, Milwaukee, USA) [221].

5.3.2.1. Detection limits and accuracy

The Pb detection limit for the urine samples was determined using Equation (III.24), and it was obtained the value 0.1 μg mL^{-1}.

The accuracy evaluation was carried out by spiking a control urine sample with a standard stock solution of Pb (1000 μg mL^{-1}, Merck, Germany). The recovery rates of lead in the urine samples spiked with 0.5, 1, 2, 3 and 5 μg mL^{-1} Pb, ranged between 90% and 100%, showing a good response of the spectrometer for urine. The RSD was less than 10% for all the three replicates made.

5.3.3. ETAAS Spectrometer

The ETAAS measurements were carried out using with an Analytik Jena AG atomic absorption spectrometer model AASZeenit 650 equipped with a transversely heated graphite furnace, a MPE 60 autosampler and a Zeeman-effect background correction system (transverse magnetic field).

The light source used was a HCL (Analytik Jena AG) operating at 4.0 mA current at 217.0 nm resonance line. The electrothermal program used is given in Table 2.

A spectral band pass of 0.5 nm was selected and high purity argon was used as purge gas.

The atomic signals were measured by a wide range 9 stage photomultiplier in the peak area mode.

A volume of 20 µL of sample and 5 µL of matrix modifier, $Pd(NO_3)_2$ 10 µg mL^{-1} (Fluka, Buchs, Switzerland), were introduced in the graphite furnace.

The graphite tube used was an AAS Z-standard tube. The chemical modifier was kept at 2º C and protected from light.

Stage	Temperature/time (ºC/s)	Argon flow rate (L min^{-1})
Dry 1	90/35	2
Dry 2	105/25	2
Dry 3	110/13	2
Pyrolysis	900/13	2
AZ (auto zero)	900/4	0
Atomize	1800/4	0
Cleanout	2300/5	2

Table 2: Heating program for determination of Pb in urine.

5.3.3.1. Detection limits and accuracy

The atomic signals were measured in the peak area mode and it was obtained the following equation of standard calibration line:

$$Y = (0.0047 \pm 0.0002)\, X + (0.001 \pm 0.003),\ (R^2 > 0.995,\ n=18), \quad \text{(V.1)}$$

where Y is the integrated absorbance (peak area) and X is the Pb concentration in µg L^{-1}.The stock standard solution of lead (1000 µg mL^{-1}) was obtained from Fluka (Buchs, Switzerland) and the standard solutions were prepared by appropriate dilution of the stock standard solution using Milli-Q ultrapure water (18 MΩ cm resistivity) and HNO_3, purchased from Merck (Suprapur 65%), to

acidify the standards. The calibration curve was linear from 0 to 30 µg L^{-1} and was made with six calibration points.

Concerning the detection limits of the spectrometer, calculated according the criterion described in Section 4.3.6.5, the limit of detection (LOD) obtained was 0.7 µg L^{-1} and the limit of quantification (LOQ) obtained was 2.1 µg L^{-1}. These are also the detection limits for the formaldehyde measurement once it has no previous sample treatment.
Taking into consideration these instrumental limits, the limits of detection and the limits of quantification of the sample treatments described in Section 5.2.1. are presented in Table 3. It is important to notice that in the digestion protocol (for the urine precipitate and brain tissue) the method limits were calculated taking into account the mass of sample placed in the digestion vial and the dilution made through the process, i.e. the final volume. For the USLE protocol, in the case of the brain samples, the method limits were calculated taking into account the mass of sample used in the extraction process and the extracting volume solution.

The accuracy of the measurements was assessed by the measurement of an urine control material, from Clinical RECIPE (Munich, Germany), with a Pb concentration of (64.2±3.7) µg L^{-1}. It was supplied in lyophilized form and it was reconstituted by dissolving the total content with high purity distilled water. The calibrator originally closed was stored at 4 ºC and after reconstitution at -20º C. This control was prepared in triplicate with the same protocol as the samples, including the ultrasonication, to validate not only the measurements but also the method. The measured value was (62.0±6.0) µg L^{-1}, i.e. the lead was totally recovered in the listed confidence interval.
Formaldehyde samples were spiked in order to test the accuracy of the spectrometer in this type of matrix. Known amounts of lead up to 6 µg L^{-1}, 15 µg L^{-1} and 24 µg L^{-1}, were spiked and the samples analyzed. The recoveries obtained were 98±7%, 102±4% and 101± 2% respectively ($\overline{X}$±RSD, n=3).
For the brain samples, it was not tested the accuracy once the matrix is the same as solutions used for the standard calibration points.

For urine, within bath and between baths precision was calculated using the Calibrator Material. The values obtained were 5% (n=9) and 7% (n=3), respectively.
For formaldehyde and brain samples three injections of each sample were made and a RSD less than 10% was obtained.

		Urine-solid phase (µg g^{-1})	Urine-liquid phase (µg L^{-1})	Brain (µg g^{-1})
USLE	LOD	-	0.7	0.35
	LOQ	-	2.1	1.05
MWD	LOD	1.75	-	1.75
	LOQ	5.25	-	5.25

Table 3: Limits of detection and limits of quantification for the different sample treatment methods assessed.

5.4. Validation of the USLE methodology developed for urine and brain samples[1]

5.4.1. Ash/Atomization curves

When ETAAS is used for the direct determination of lead in organic samples, such as formaldehyde and urine, some problems must be carefully addressed in the method of analysis. Thus, volatilization of the organic phase leads to an increase in the actual concentration of the analyte. In addition, the auto sampler dispensing becomes complicated as the formation of the drop is hindered by the superficial tension of the liquid, which makes the drop become adhered to the dispenser´s tip. Furthermore, in some cases aqueous standard cannot be used for calibration [222]. To complicate things further, Volynsky *et al.* [223] emphasized that the spreading of organic samples over the graphite furnace surface distorts the atomic absorption profiles, renders the analytical curve non-linear and decreases the sensitivity. Furthermore, according to Tserovsky and Arpadjan [224], the removal of organic liquids after their penetration into the graphite requires long pre-treatment at high temperature. Hence, the volatile compounds would be lost at this stage. Taking into consideration the above mentioned problems that can hinder the analysis, first it was made an ash/atomization study to find out the best temperature for the ashing and atomization stages. The ash/atomization curves are presented in Figure 20.

The matrix modifier used was palladium nitrate, which was selected as it was used with success in previous studies dealing with lead determination in complex samples [14, 206]. As may be seen in Figure 20, nitrate palladium stabilizes the lead inside the graphite tube up to 1100 ºC for both

[1] The work presented in this Section has been published in: D. Guimarães, J.P. Santos, M.L. Carvalho, G. Vale, H. M.Santos, V. Geraldes, I. Rocha, J.L. Capelo, Ultrasonic energy as a tool to overcome some drawbacks in the determination of lead in brain tissue and urine of rats., *Talanta* 86 (2011) 442-446. Reproduced with permission from *Talanta.* Copyright © 2011 Elsevier.

aqueous standard and urine sample. To extend the life of the graphite tubes, it was selected a lower ashing temperature as optimum, 900 ºC. As far as the temperature of atomization concerns it was selected 1800 ºC as optimum.

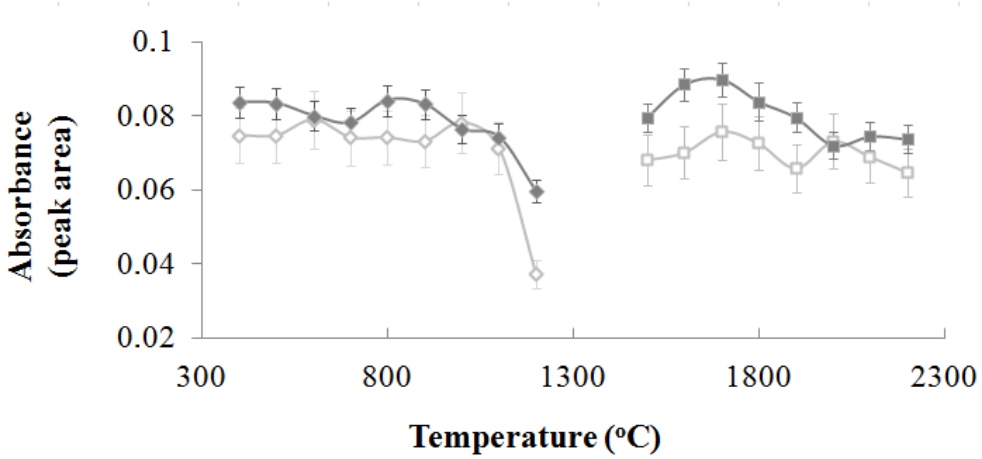

Figure 20: Ashing and atomisation curves for Pb in (i) an aqueous standard solution (♦ , ashing curve; ■, atomization curve) (15 µg L^{-1}); and (ii) urine liquid fraction (◊ , ashing curve; □ , atomization curve) (15 µg L^{-1}).

The Figure 21 shows the absorption profiles of the samples studied in this work. Similar atomic absorption profiles are observed for aqueous standard, formaldehyde, urine liquid phase, and brain extract. This similarity facilitates calibration with aqueous standards.

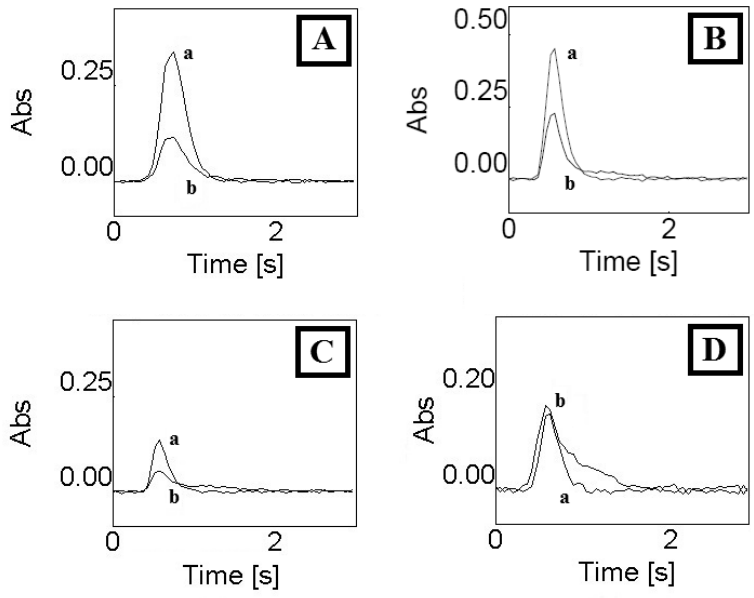

Figure 21: Pb Absorption profiles for: (A) Aqueous calibration Standard (18 µg L^{-1} Pb); (B) formaldehyde containing NTS control brain sample (24 µg L^{-1}, Pb was spiked); (C) HDA exposed rat brain sample after USLE (5.4 µg L^{-1} Pb); (D) Urine of exposed rat after USLE (6.7 µg L^{-1} Pb;). a, atomic absorbance profile; b, background absorbance profile.

Further to these results, the formation of carbonaceous residues inside the graphite tube was not observed throughout the experiments. Formation of carbonaceous residues is a common problem when samples with high organic content are introduced into the graphite tube, leading to a number of problems that have been described elsewhere [225].

5.4.2. Analysis of urine sample from rats: overcoming the formation of precipitate

It is well known that when a solid in a solution is formed, metals can be absorbed on its surface, leading to a variation in the actual content on these metals in the liquid fraction as the solid precipitation takes place [226, 227].

To demonstrate this fact it was analyzed the liquid fraction of four urines with solid fraction. The liquid fraction was analysed before and after the USLE sample treatment as described in Section 5.2.1.2. The solid fraction was observed by naked eye. The amount of lead found in the liquid phase was increased after treatment in all cases studied, as may be seen in Table 4. In some of them, the lead concentration increases dramatically. This result confirmed that the acidification of the sample was not enough to extract the lead associated to the solid phase, being necessary the aid of the ultrasonic energy to make the lead extraction feasible.

Finally, to assess the complete solid-liquid lead extraction, the solid phase was analysed to detect any non-extracted lead. The sediments were separated from the liquid phase, dried, weighed and solubilised with a microwave assisted acid pressurized digestion protocol, as explained in the sample treatment Section 5.2.1.2. From the eight solid fractions analysed, lead was detected only in four samples, being the amount of lead found in the precipitate less than 2% of the total lead contained in the sample (lead in the liquid phase and also lead in the solid phase). These results confirmed that the solid-liquid ultrasonic extraction was successfully achieved.

Sample	Found Content	
	Before USLE	After USLE
Urine A	432 ± 26	752 ± 56
Urine B	109 ± 4	833 ± 62
Urine C*	53.3 ± 0.3	60.9 ± 1.2
Urine D	5 ± 2	110 ± 26

Table 4: Lead concentration found in the liquid fraction of the urine of rats before and after treatment with ultrasonic energy ($\overline{X}$±SD, n=3, µg L^{-1}). Urine A, B and C correspond to rats exposed to lead. Urine D corresponds to control rat.*(mg L^{-1}).

5.4.3. Analysis of lead in brain rats tissue

The brain samples of exposed and control rats were preserved in formaldehyde, with different brains collected and preserved in the same receptacles, concerning the type of the tissue and the exposure regimen. Therefore, it was investigated if lead from the contaminated brains was diffused to the formaldehyde.

Lead from brain tissue was extracted using ultrasonic energy as described in Section 5.2.1.2.. Data presented in Table 5 show that the lead found in the formaldehyde was negligible in comparison with the one found in the brain tissue of rats exposed to lead. When non-exposed rats were studied, the lead content of both, formaldehyde and brain was below the limit of detection of the method.

To assess the complete ultrasonic lead extraction from the brain tissue, after sonication some samples were solubilised with the aid of a microwave assisted acid pressurized digestion protocol described in 5.2.1.2. The concentration of lead obtained for all the samples studied was below the limit of detection of the method.

To further confirm the completeness of the lead extraction, the multi-injection technique was used. This technique makes possible to reach lower limits of detection [228], because after the drying step, samples are re-injected several times on the graphite tube. Hence, the amount of metal in the tube is increased by a factor of two or three or more, depending on the number of re-injections used. In despite of being 3 times re-injected, the levels of lead found were below the limit of detection of the method.

To assess the correct performance of the re-injection method, the same samples were spiked with lead up to 8 µg L^{-1}. Samples were analysed with two and three re-injections. The lead recoveries obtained were ($\overline{X}$±RSD, *n*=3) 105±4% and 97±4%, respectively. These results further confirms that ultrasonic energy do works and is a powerful tool in the extraction of lead from soft tissue, confirming previous literature on this topic [14, 205, 206].

Sample	Formaldehyde	Total Brain
HDA Exposed	0.007 ± 0.001	0.211± 0.014
NTS Exposed	0.007 ± 0.001	0.173 ± 0.010
HDA Control	BDL	BDL
NTS Control	BDL	BDL

Table 5: Lead content in the formaldehyde and in the total mass of brains in each vessel containing formaldehyde, for exposed and non-exposed rats ($\overline{X}$±SD, *n*=3, µg). BDL indicates below detection limit of the respective methods.

5.4.4. Analytical results and conclusions

The sample treatment developed was applied to a number of rats under study, with no distinction in age, as shown in Table 6. When brains of exposed and non exposed rats are compared, lead accumulation is clearly observed in the brain tissue. Histological examination and histochemical analysis (Rhodozinate method) were also done to study the distribution of lead in brain tissues, but once it is a little out of the scope of this dissertation the results are only going to be presented in Annex 3.

The levels of lead in urine of exposed rats are also high in comparison with no exposed rats.

However, these results are only preliminary and the main propose was to show the suitability and validation of the USLE sample preparation method to the urine samples. The age dependency study is only going to be discussed in Chapter VI.

It was developed a rapid and simple ultrasonic-based methodology to determine lead in brain and urine from rats. The new methodology allows handling mg of brain sample in a few minutes. The volume required to extract the lead from the brain was 1 mL, and can potentially be reduced to 250 µL by just changing the ultrasonic tip used. Furthermore, the lead concentration in urine that had developed a precipitate can be easily determined by acidification (nitric acid, 10% v/v) and ultrasonication (6 minutes) of the sample.

	Urine	NTS	HDA	Formaldehyde NTS	Formaldehyde HDA
Exposed rats	752 ± 56 **	2.3 ± 0.2	3.1 ± 0.2	4.4 ± 0.6	4.8 ± 0.3
	833 ± 62 **	2.4 ± 0.1	3.2 ± 0.3		
	60.9 ± 1.2	2.1 ± 0.2	3.4 ± 0.3		
	27.4 ± 2.0	2.4 ± 0.1	3.5 ± 0.2		
	5.5 ± 0.1	2.7 ± 0.1	3.0 ± 0.2		
	4.3 ± 0.4	1.9 ± 0.2	3.2 ± 0.3		
Control rats	BQL	BDL	BDL	BDL	BDL
	BDL	BDL	BDL		
	BDL	BDL	BDL		
	225 ± 23 **	BDL	BQL		
	110 ± 26 **	BDL	BQL		
	BDL	BDL	BQL		

Table 6: Concentration of lead found in random urine ($\bar{X}$±SD, mg L^{-1}; *n*=3) and brain ($\bar{X}$±SD, µg g^{-1}; *n*=3) samples treated with the USLE protocol. Formaldehyde ($\bar{X}$±SD, µg L^{-1}; *n*=3) was measured directly by ETAAS. **(µg L^{-1}; *n*=3). BDL - below detection limits; BQL - below quantification limits (*c.f.* Table 3).

5.5. Statistical Analysis

Earlier studies have shown that concentration levels of trace elements, such as lead, do not usually follow a normal distribution [229, 230]. In this study, once the measured data was not normally distributed and the number of samples was less than 30, the measurements were statistically analyzed using nonparametric tests such as Mann-Whitney for 2 independent variables, Kruskall-Wallis for *K* independent variables, Wilcoxon Rank test for 2 dependent variables and Spearman rank correlation coefficient for correlations. The statistical analysis was carried out using the Statistical Package for Social Sciences (SPSS) software, version 17.0 and a value of *p* lower than 5% ($p<0.05$) was considered statistically significant [231, 232].

The Spearman rank correlation coefficient, r_s, is a non-parametric measure of statistical dependence between two variables, i.e. it determines if the relationship between two measures taken on a single group is significant.

A Spearman correlation is mostly used when one or both of the variables are not assumed to be normally distributed, or to correlate data that is ordinal. It can also be used for interval or ratio data and the values of the variables are first converted in ranks. As it uses ranks rather than the actual scores the Spearman correlation can still be used even when the relationship between the two variables is non-linear.

The values of r_s range from -1 to +1. If the ranks agree perfectly with each other, r_s is equal to 1, indicating a perfect positive association between two variables. If the two series of ranking were in exactly reverse order, the value of r_s is equal to -1, indicating a perfect negative association.

Another important parameter, besides the intensity of the correlation, is its significance that depends on the *p*-value. The *p*-level represents the probability of error that is involved in accepting the observed result as valid. As mentioned above, the correlation would be statistically significant if $p < 0.05$ [233, 234].

When there was a need to compare mean lead concentrations between different rats, the Mann-Whitney U test was used. This test is a nonparametric hypothesis test used to compare the two means of two independent populations. It is used when the populations are not normally distributed, or if the data are only ordinal in measurement. The observations from both groups are combined and ranked.

A test of a statistical hypothesis consists in two different hypotheses: the null hypothesis denoted by H_0, is the hypothesis that is going to be tested and the alternative hypothesis, H_1, that corresponds to the sample observations being influenced by some non-random cause.

The test can be one or two tailed. In the one tailed test the null hypothesis is less or equal to a certain value, and the alternative hypothesis is greater than that value. In the case of two tailed

tests, used in this work, the null hypothesis state is equal to a determined value and the alternative hypothesis is to be different than that value. The two tailed hypothesis being tested with the Mann-Whitney U consist in H_0 - the two populations are identical and H_1 - the two populations are not identical.

Applying the hypothesis test if the *p*-value is less than the significance level, reject the null hypothesis, and conclude instead that the populations have different medians. If the *p*- value is higher than the significance level, the null hypothesis is not rejected and there is no evidence that the medians differ [231, 235].

The Kruskal Wallis test is a generalized form of the Mann-Whitney test method, which permits to test more than two groups to see if several populations have the same continuous distribution, at least as far as their medians are concerned.

When the aim was to compare the means of different organs for the same rat, the Wilcoxon signed rank test was used. This test is also a non-parametric hypothesis test that follows the same assumptions of Mann-Whitney, i.e. it can be used when the population cannot be assumed to be normally distributed or the data is on the ordinal scale with the purpose to verify if the population means are the same. However, it is used when the samples are related and are not independent. This test also combine and rank the observations, but ranking a variable that involves paired differences of observations [235].

CHAPTER VI - RESULTS AND CONCLUSIONS

6.1. Results and discussion

In this Chapter the measurements of the different tissues are presented, analysed and discussed. The results are separated by excretions and organs: firstly urine and faeces, then soft tissues, namely kidney and liver, and finally the bones. All results are going to be expressed as mean value ± standard deviation ($\overline{X}$±SD).

6.1.1 Urine and faeces[2]

6.1.1.1. Urine lead analysis

The urine samples were measured using the ETAAS and TXRF techniques. It should be referred that the urine samples analyzed by TXRF were measured 1-2 weeks after their collection and no significant precipitate was visible. The results obtained by both techniques for the same samples are listed in Table 7. The values obtained from the two methods overlap within the error bars.

Sample	TXRF (µg L^{-1})	ETAAS (µg L^{-1})
11 month old - exposed rat 1	550±70	490±50
11 month old - exposed rat 2	650±60	720±30
10 month old - exposed rat 1	750±30	800±30
9 month old - exposed rat 1	700±70	690 ±40
10 month old - control rat 1	BDL	BDL
9 month old - control rat 1	BDL	BQL

Table 7: Comparison of Pb concentration values for urine samples measured by TXRF and ETAAS techniques. BDL and BQL refers to below detection limit and below quantification limit, being BDL < 100 µg L^{-1} for TXRF and BQL < 80 µg L^{-1} and BDL < 30 µg L^{-1} for ETAAS (both including dilution factor).

The Figure 22 shows the average values of lead concentration measurements with both techniques in urine samples collected in rats with ages ranging from 1 to 11 months. The represented results are displayed in Table 18 of Annex 4. As can been seen, the highest average concentration was found in the youngest contaminated rats, 5 460±115 µg L^{-1}, and the lowest was found in the oldest contaminated rats, 600±140 µg L^{-1}. These values are about the same order of magnitude, or one

[2] The work presented in this Section has been published in: D. Guimarães, M. L. Carvalho, M. Becker, A. von Bohlen, V. Geraldes, I. Rocha and J. P. Santos, Lead concentration in feces and urine of exposed rats by X-ray Fluorescence and Electrothermal Atomic Absorption Spectrometry., *X-ray Spectrometry* (2011), doi: 10.1002/xrs.2361. Reproduced with permission from, *X-ray Spectrometry* Copyright © 2011 John Wiley & Sons, Ltd.

order higher, than lead concentration values reported in other studies [68, 236, 237].

Concerning the control group, apart from the collections of 1, 4 and 5 months old, all the collections have values below detection or quantification limits. In the three exceptions, the mean lead concentrations range from 120±40 to 225±20 µg L^{-1}. However, the lead concentration in control rats is always lower 7 to 88 times than the respective contaminated group.

Analysis of the urine samples, using the Mann-Whitney U test, revealed significant differences (p <0.01) for the lead concentration in the samples from the contaminated group when compared to the control group.

The standard deviation affecting the lead concentration values is relatively high in a few cases, which might be attributed to the individual variability in urinary excretion capacity of the different analysed rats.

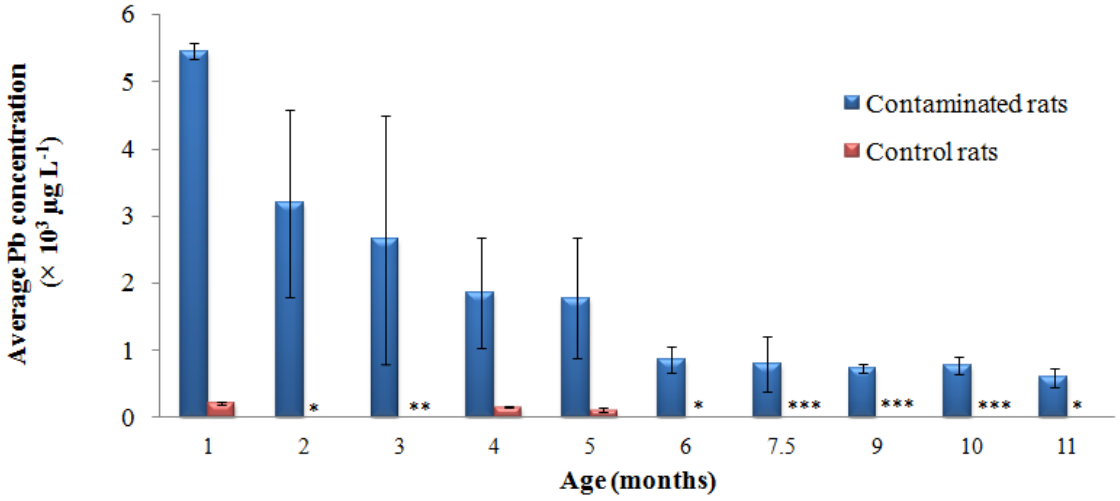

Figure 22: Comparison of Pb concentration obtained in urine for exposed and non-exposed rats. All samples were measured by ETAAS except for 7.5; 9 and 10 months which were measured by TXRF. In the control rats *, ** and *** corresponds to BQL < 80 µg L^{-1}; BDL < 30 µg L^{-1} (including diluting factors) and BDL < 100 µg L^{-1}, respectively.

From Figure 22, it is evident that the lead concentration decreases with age in exposed rats. Applying the Kruskal-Wallis test between the different age samples it is possible to divide the measured data in the following 3 plateaus with no statistically significant concentration relation: plateau 1 (P1) contains only the youngest rats; plateau 2 (P2) contains the 2, 3, 4, and 5 month old rats (p = 0.478) and plateau 3 (P3) contains rats with ages between 6 and 11 months (p = 0.221). The Kruskal-Wallis test revealed statistically significant differences between these three groups (p <0.001), with following average concentration values: P1 - 5 460±115 µg L^{-1}, P2 - 2 400±1 310 µg L^{-1} and P3 - 760±190 µg L^{-1}.

The high lead excretion in plateau 1, containing only 1 month old rats, may be explained by the fact that these newborn rats were delivered by contaminated dams. As seen in humans [48], the rapid

skeleton turnover that causes a large mobilization of the bone lead stored during pregnancy in the first months of newborns life may also explain the high lead concentration in youngest rats urine. The low glomerular filtration rate and a not fully developed tubular secretion in newborns may also explain the differences in excretion [5].

The decrease of the urine lead concentration with age may suggest a decrease in the lead uptake. This was corroborated by Quarterman *et al.* [238] and Smith *et al.* [37], which also observed a decrease in the rate of uptake as a consequence of increasing age. On the other hand, it should be considered that chronic renal insufficiency, which may result from irreversible loss of nephrons and the progressive deterioration of kidney, can also inhibit the removal of lead [239].

6.1.1.2. Faeces lead analysis

The average values of lead concentration in faeces samples collected from rats with ages ranging from 1 to 11 months are displayed in Figure 23. These results are presented in Table 19 of Annex 4. Some of the samples were also measured by PIXE in order to double check the results. The obtained results are displayed in Table 23 of Annex 5.

Concerning Figure 23, the highest average concentration value in the two different groups was found in the 4 months rats, being 11 370±3 280 μg g^{-1} for contaminated rats and 54±3 μg g^{-1} for control ones. The lowest average concentration value for contaminated rats corresponds to the 9 months collection (4 470±300 μg g^{-1}), and for the control rats to the 7.5 months collection (6±1 μg g^{-1}).

The fecal average lead concentration values measured in this work are approximately one order of magnitude higher than the concentration values reported in some studies [68, 236, 240], and about 4 orders of magnitude higher than others studies [113]. However, it should be taken into account that these studies were made on exposed workers and other animals (otters, minks and pigs) with a different exposure regime. It is important to stress that the rats analyzed in the present work were delivered by contaminated females, which may originate higher lead accumulation level.

In general, the results obtained in control rats differ from the corresponding contaminated group by about 2 orders of magnitude. The error bars associated to the average lead concentration values are within the biological variability of the samples, being 37% the highest value for the 1 month old rats.

The differences in the lead concentration between the exposed and control groups, for each collection, were tested using the Mann-Whitney U test, which revealed that these groups are statistically different (p <0.01).

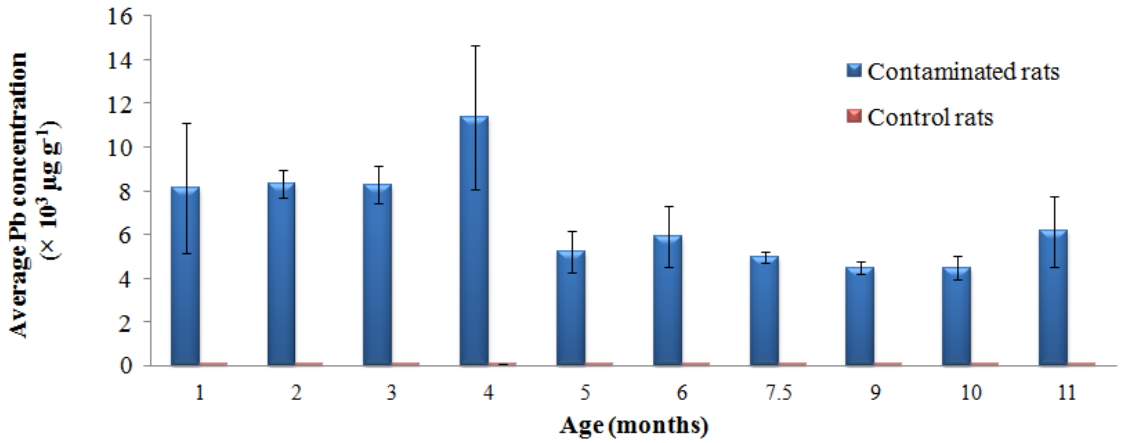

Figure 23: Comparison of Pb concentration obtained by EDXRF in rat faeces from exposed and non-exposed group.

In Figure 23 it can be noticed the existence of two levels of lead excretion: plateau 1 that contains rats with ages ranging from 1 to 4 months, and plateau 2 containing rats from 5 to 11 months. The application of the Kruskal-Wallis test to the plateaus 1 and 2 indicates that there is no statistically significant difference between the different collections that form each group (p = 0.105 for group 1 and p = 0.371 for group 2). The subsequent application of the Mann-Whitney test to these two plateau reveals that they are statistically different (p <0.001), with average values of 9 160±2 740 µg g^{-1} and 5 320±1 200 µg g^{-1}, for plateau 1 and 2 respectively.

Since the bulk of lead ingested passes through the alimentary tract unabsorbed, these results support the hypothesis that the decrease with age of lead excreted is due to the decrease in lead intake.

6.1.1.3. Correlation between lead concentration in urine and faeces

The lead content in faeces and urine was compared.

The ratio faeces/urine varies by a factor of 3 to 4 depending on the animals' age as it is shown in Figure 24. A linear tendency (R^2=0.6906 for a linear correlation) between the Pb faeces/urine ratio and the animals age can be identified. The ratio increases with the animals' age, meaning that the rate of excretion by urine is more accentuated with age than the rate of excretion by faeces. Spearman correlation test showed a strong positive correlation of r_s=0.782 with a p=0.008.

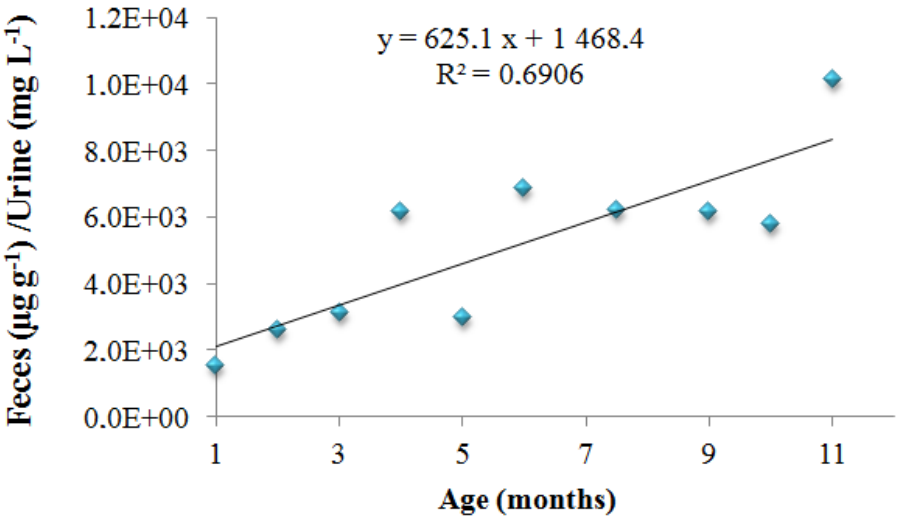

Figure 24: Fecal/urinary lead concentration ratio values as function of age of rats from 10 different collections (n= 20).

A Spearman's correlation matrix was also calculated (Table 8) to study the correlation between the elemental concentrations and the dependence of these concentrations on age. According to this test, the closer $|r_s|$ are to 1, the stronger is the correlation for a significance level p, which expresses the probability of error that is involved in accepting the results as valid.

As can be observed in Table 8, there is a negative correlation with age for both Pb concentration in faeces and in urine, being very strong for urine samples and strong for faeces samples. A strong statistically significant correlation between the lead concentration in urine and in faeces can also be observed.

Variable	Age	Pb in urine	Pb in faeces
Age	-	**- 0.988[b]**	**- 0.685[a]**
Pb in urine	-	-	**0.697[a]**
Pb in faeces	-	-	-

Table 8: Spearman correlation matrix for the average Pb concentrations in urine and faeces for the 10 collections. The correlations are significant at p<0.03 if marked with [a], and significant at p<0.001 if marked with [b].

6.1.2. Liver and kidneys[3]

6.1.2.1. Liver lead analysis

The average values of lead concentration in liver samples collected from rats with ages ranging from 1 to 11 months are displayed in Figure 25. These corresponding results are listed in Table 20 of Annex 4.

Some of the samples were also measured by PIXE in order to double check the obtained results and are presented in Table 23 of Annex 5.

Concerning Figure 25, the highest average lead concentration value in liver of the exposed group rats (22±6 μg g^{-1}) occurs in the 1 month old collection, and the lowest (6±1 μg g^{-1}) in the two older collections.

The results obtained in this work for lead concentration in liver of contaminated rats are of the same order of magnitude of the values reported in the work by Mykkanen [241], and are, in general, one order of magnitude higher than the values reported in the works by Schroeder [242] and Smith [37]. However, in both later works the rats were not delivered from contaminated dams and were submitted to lower doses of lead (namely 5 and 150 μg g^{-1} lead, respectively). In the former work, the newborn rats were exposed to lead from foetal period with a concentration of 0.5% lead acetate.

In the control group, all values were found to be below detection limit, with exception of the 2nd and 3rd collections' results. Nevertheless, the mean lead concentration in those collections (4±1 μg g^{-1}) is close to the detection limit of 2 μg g^{-1}, and below the acceptable value to have intoxication repercussions in animals [84].

In general, considering the value of the detection limit for the BDL cases, the results obtained in control rats, are about 2- to 11- fold lower than the corresponding contaminated group.

The differences of the lead concentration between the exposed and control groups, for each collection, were tested using the Mann-Whitney U test. It revealed that these groups are statistically different with $p < 0.01$.

The error bars associated to the average lead concentration values are quite acceptable within the biological variability of the samples, being 38% the highest value for the rats with 7.5 month old.

[3] The work presented in this Section is in revisions phase in: D. Guimarães, M.L. Carvalho, V. Geraldes, I. Rocha, L.C. Alves, J.P. Santos, Lead in liver and kidney of exposed rats: aging accumulation study., *Journal of Trace Elements in Medicine and Biology* (2011). Reproduced with permission from *Journal of Trace Elements in Medicine and Biology* Copyright © 2011 Elsevier.

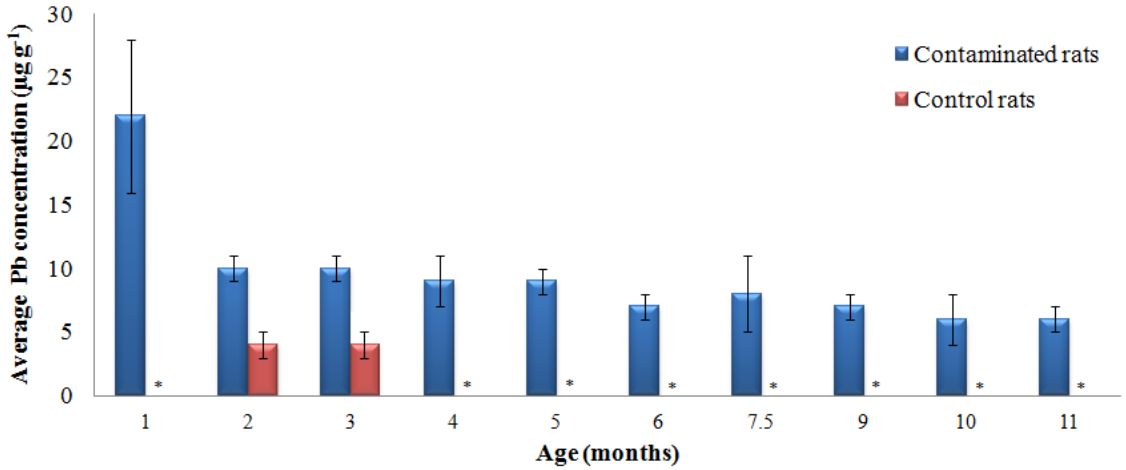

Figure 25: Comparison of Pb concentration obtained by EDXRF in rat livers from exposed and non-exposed group. In the control rats * corresponds to BDL < 2 µg g^{-1}.

There is a decrease in the lead concentration accumulated in liver with the time of exposure (Figure 25). The application of the Kruskal-Wallis test to all the collections shows that there are three different plateaus statistically different: plateau 1 (P1) with the youngest rats; plateau 2 (P2) with rats aging from 2 to 5 month old, and the plateau 3 (P3) containing the collections of rats with ages between 6 to 11 months old. There is no clear evidence that the different collections forming each plateau are statistically different: P2 has p= 0.116 and P3 has p= 0.120. The subsequent application of the Mann-Whitney test to these two plateaus reveals that they are statistically different (p<0.001), with average values of 22±6 µg g^{-1}, 10±1 µg g^{-1} and 7±1 µg g^{-1} for P1, P2 and P3 respectively.

The liver lead concentration decreasing over time was also observed in other studies [37, 241, 242]. This decrease with age is due to several significant age-related differences in the physiological handling of lead, including the greater absorption from gastrointestinal tract and the higher percent lead retention in tissues in the younger, the greater reactivity of organs and the nutritional deficiencies of the young animals and children [81]. The elevated levels of lead ingestion with a higher intake of lead on a body weight basis [37] also contribute to the existence of these differences between young and older rats.

The very high concentration value on P1 liver (22±6 µg g^{-1}) is, probably, due to the fact that these rats are born from dams already contaminated with lead. In general, mother and foetus can be considered an unique system that remains in equilibrium through pregnancy. So, in the end of pregnancy an identity exists between the blood lead concentrations in the mother and the child, between their bone lead concentration and, as a consequence, in their soft tissues [48, 243]. This fact, together with all the features mentioned above, may contribute to the remarked high lead level

in the first month, once that at 3 weeks of age rats start to feed themselves from the same concentration of lead as the dam, and not from maternal milk that contains roughly 1/1000 of the concentration of lead present in maternal diet as showed by Mikkanen [241].

6.1.2.2. Kidney lead analysis

The measurements of lead concentration in kidney samples collected from rats with ages ranging from 1 to 11 months are displayed in Figure 26. These results are listed in Table 21 of Annex 4. Some of the samples were also measured by PIXE in order to double check the results and the obtained results are listed in Table 23 of Annex 5.

Regarding Figure 26, the mean concentration values in exposed rats do not present great variability, ranging from 44 ± 6 μg g^{-1} to 79 ± 26 μg g^{-1}. These results are higher than the lead concentration values reported in other studies made by Schroeder [242] (1.10 μg g^{-1} to 1.54 μg g^{-1}), Rader[81] (10.78 μg g^{-1} to 6.50 μg g^{-1}), and Mahaffey [244] (13 μg g^{-1}). However, these studies were made in different exposure regimens, namely 5 μg g^{-1} lead in the first mentioned study, and 200 μg g^{-1} lead in the last two, and the rats were not delivered from contaminated dams. Still the values obtained in this work are similar to those obtained by Victery [245] for rats fed with a 1000 ppm lead acetate diet, and by Mykkanen [241] for rats exposed to lead from foetal period with a concentration of 0.5% lead acetate. The high levels of lead found in kidney may be due to the disruption of the normal excretory function of the kidney [246], causing disproportionate accumulation of lead in the rats.

Concerning the control group, all the values are below detection limits, i.e. 2 μg g^{-1}, and consequently are below the value of 5 μg g^{-1} considered to be the threshold for acute intoxication in animals [84]. These values are at least one order of magnitude lower than the ones obtained in the exposed rat groups.

Analysis of the kidney samples, using the Mann-Whitney U test, revealed significant differences (p <0.01) for the lead concentration between the contaminated collection and the respective control.

The concentration values are not affected by great variability, with a maximum value of 33% for the 4 month old collection. This shows that there is a high consistency in the results, not only among the 3 rats of the same collection, but also among measurements in different pellets of the same rat.

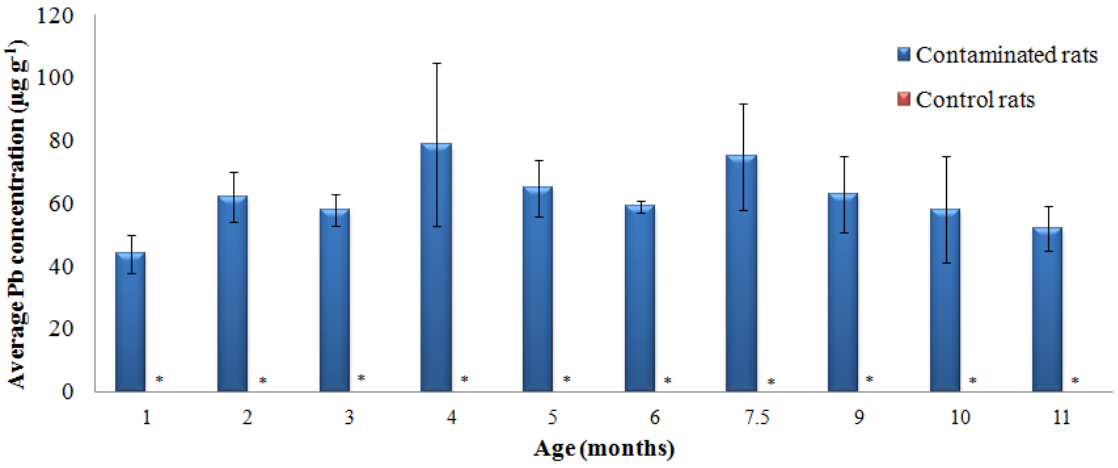

Figure 26: Comparison of Pb concentration obtained by EDXRF in rat kidneys from exposed and non-exposed group. In the control rats * corresponds to BDL < 2 µg g^{-1}.

From Figure 26 it is not clear if there is any age dependency of lead concentration in kidney tissues. Applying the Kruskal-Wallis test between the different age samples it is possible to divide the measured data in the following 2 plateaus: plateau 1 (P1) contains only the youngest rats and plateau 2 (P2) contains rats from 2 to 11 month old, showing no evidence of statistically significant differences between these different collections (p = 0.128). The application of the Mann-Whitney test reveals statistically significant differences between these two plateaus (p = 0.001), with mean concentration values of respectively 44±6 µg g^{-1} and 63±9 µg g^{-1}.

These results emphasize that kidneys have a different behaviour from liver concerning lead accumulation. Kidney, as stated by Victery [245], seems to have a finite capacity to absorb lead and are not affected by the extent of exposure but mostly by the lead dose. It is also remarkable that the mean concentration value for the two groups is very close. However, the strange behaviour of the kidneys during the first month has already been noticed by Mykkanen [241] in the first week-old-pups, who found that kidney showed a very low lead concentration compared to their dams suggesting the different role of kidney in the young animal compared to adult. He also pointed out that kidney concentrations decreased over time, although the study was only done during 7 weeks.

6.1.2.3. Correlation between lead concentration in kidney and liver

The relationship between the kidney (y-axis) and the liver (x-axis) is presented in Figure 27. It is observed that the 1 month old pups have a different behaviour concerning the other ages, with a drastic increase in the liver mean lead concentration and a decrease in the kidney mean lead concentration. The fact that kidney presents higher lead concentration than liver is in agreement with the work of other authors [241, 242].

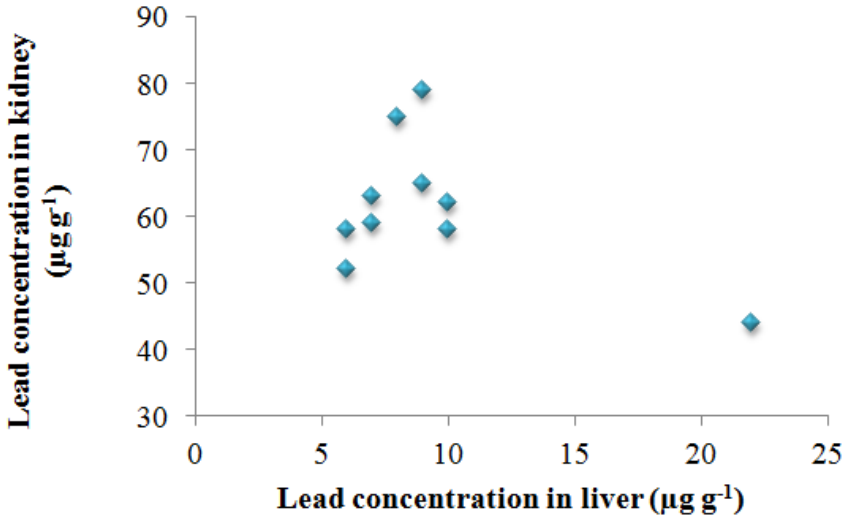

Figure 27: Relationship between median kidney and liver lead concentrations for contaminated rats over time (◆ ; *n*=3).

Although these two variables are not linearly related, if the ratio between kidney and liver lead concentrations (Figure 28) is studied, it can be identified a linear tendency (R^2=0.6245) between the lead ratio and the animals age. This ratio varies from 2 to 10 depending on the age. Applying the Spearman to these two variables a strong positive correlation of r_s=0.794 with a p=0.006 was verified.

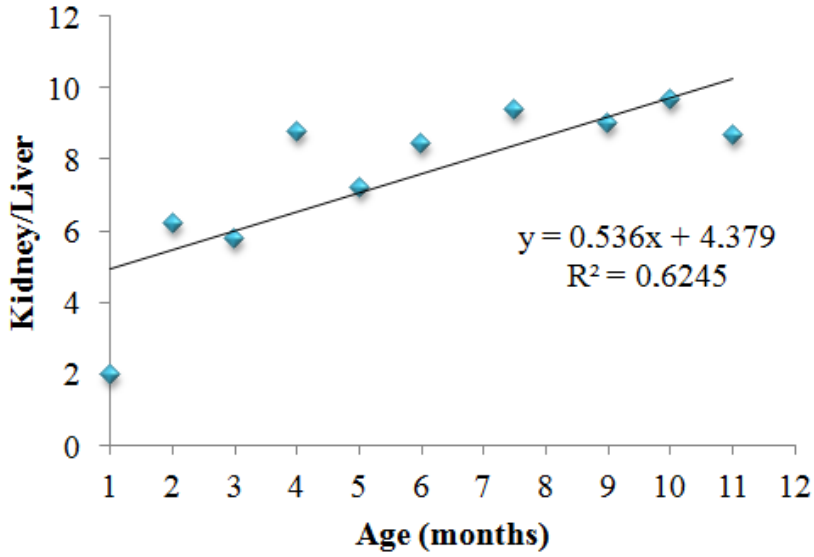

Figure 28: Kidney/liver lead concentration ratio values as function of age of exposed rats from 10 different collections (◆ ; *n*=3).

A Spearman's correlation matrix was also calculated (Table 9) to study the correlation between elemental concentrations and the dependence of these concentrations on age. A negative strong correlation with age for lead concentration in liver was verified. It can also be observed that lead concentration in kidney does not have a statistically significant correlation neither with liver lead concentration nor with age.

This test showed that liver and kidneys lead concentrations don't correlate. This means that there is no dependency between the accumulations of lead in these soft tissues. It was also showed that kidney doesn't correlate with age, which means that kidney doesn't seem to be affected by the exposure duration unlike the liver. This behaviour was also observed in rats in the work of Victery et al [245] and in pigs in the work of Gyori et al [113].

Variable	Age	Pb in kidney	Pb in liver
Age	-	0.018[b]	**- 0.890[a]**
Pb in kidney	-	-	0.055[b]
Pb in liver	-	-	-

Table 9: Spearman correlation matrix for the average lead concentrations in kidney and faeces for the 10 collections. [a] p=0.001; [b] p> 0.800.

6.1.3. Bones: iliac, femur, tibia-fibula and skull[4]

6.1.3.1. Bones lead analysis

In Figures 29, 30, 31 and 32 are presented the lead concentrations measured in the bones for non exposed Wistar rats and exposed since foetal period. The measured results are listed in Table 22 of Annex 4.

For the exposed rats, the values are very similar between iliac, femur and tibia-fibula, ranging from approximately 300 µg g^{-1} to near 100 µg g^{-1}. The skull, has also a lower limit about 100 µg g^{-1}, but an upper limit of about 250 µg g^{-1}. The highest average lead concentration in all types of bones occurs in the 1 month old collection, and the lowest is found in the two last collections.

The lack of information in the works about the lead concentration in bones concerning the diversity of bone (in many cases comparing only similar types of bone), if the published data refer either to

[4] The work presented in this Section has been accepted in D. Guimarães, M.L. Carvalho, V. Geraldes, I. Rocha, J.P. Santos, Study of lead accumulation in bone of Wistar rats by X-ray fluorescence analysis: aging effect., *Metallomics* (2011), doi: 10.1039/C1MT00149C**.** Reproduced with permission from *Metallomics* Copyright © 2011 RSC Publishing.

dry, wet or ash weight, and the exposure doses and time, makes the comparison between works difficult. Nevertheless, these results are about the same order of magnitude, or one order higher that values found in other works, such as, the work of Denton *et al.* [46], Mahaffey *et al.* [244] and Rader *et al.* [81]. However, in these works the exposure regimen was lower than the one used in the present work and the rats were not exposed since foetal period.

In the control rats, along all age groups, the values are lower than the reference value reported by ATSDR [5], 10 µg g^{-1}, above which there are descriptions of adverse health effects. Values similar to the ones measured in this present work have also been reported for femur of control rats [81].
Using the Mann-Whitney U test to compare exposed and non-exposed rats of the same age, significant differences (p<0.001) were revealed for the lead concentration in the four type of bone samples. Assuming, conservatively, the detection limit value for the cases with BDL values, the measured lead concentration values in all bones of control rats are about 18 to 43 times less than the respective contaminated group.

Despite the 1st month collection, with coefficients of variation ranging from 40 to 31% for the several bones, the measured lead concentrations don't show a high standard deviation, however, the coefficient of variation is never inferior to 10%.

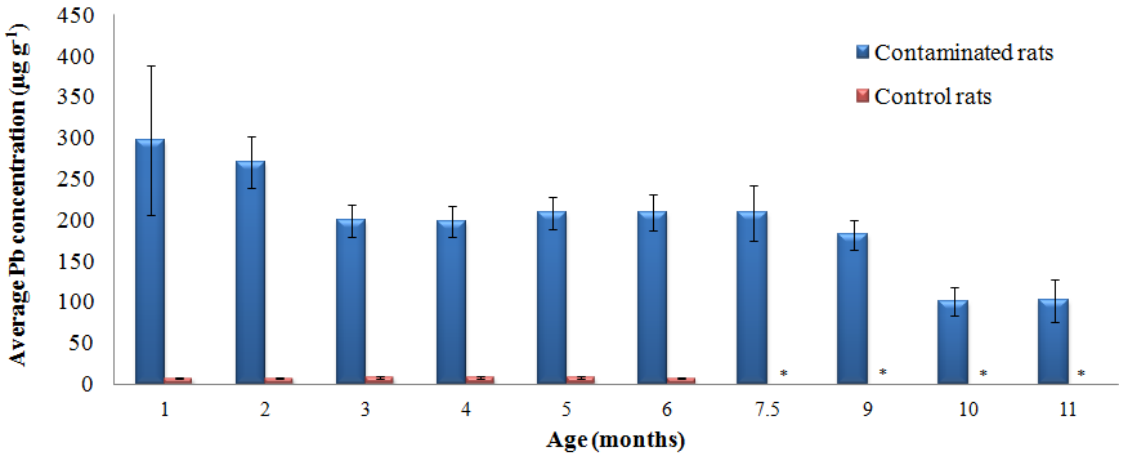

Figure 29: Comparison of Pb concentration obtained by EDXRF in rat iliac bones from exposed and non-exposed group. In the control rats * corresponds to BDL < 5 µg g^{-1}.

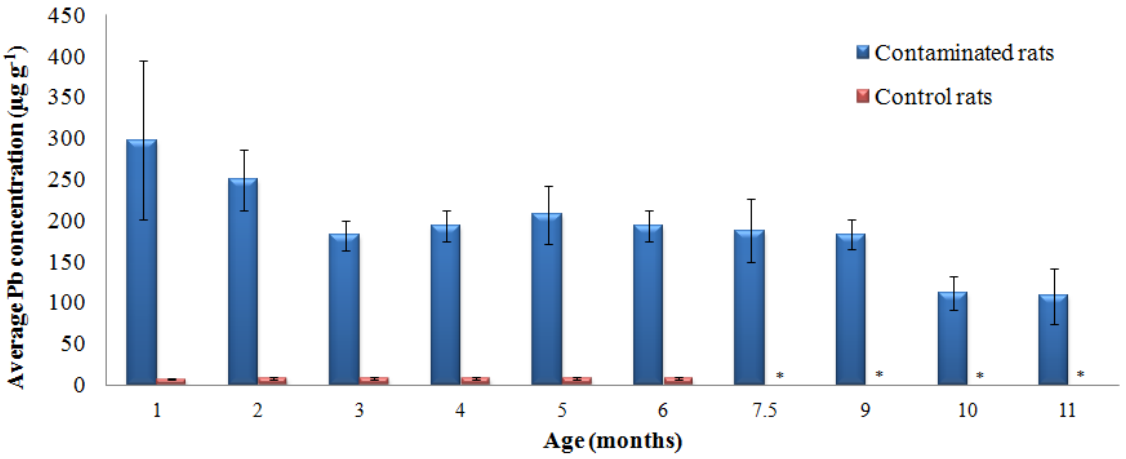

Figure 30: Comparison of Pb concentration obtained by EDXRF in rat femurs from exposed and non-exposed group. In the control rats * corresponds to BDL < 5 µg g^{-1}.

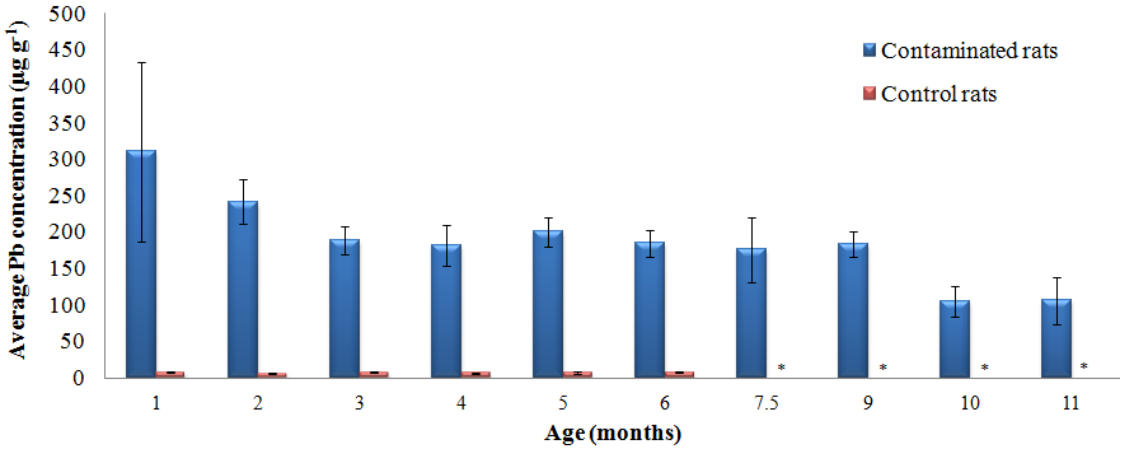

Figure 31: Comparison of Pb concentration obtained by EDXRF in rat tibia and fibulas from exposed and non-exposed group. In the control rats * corresponds to BDL < 5 µg g^{-1}.

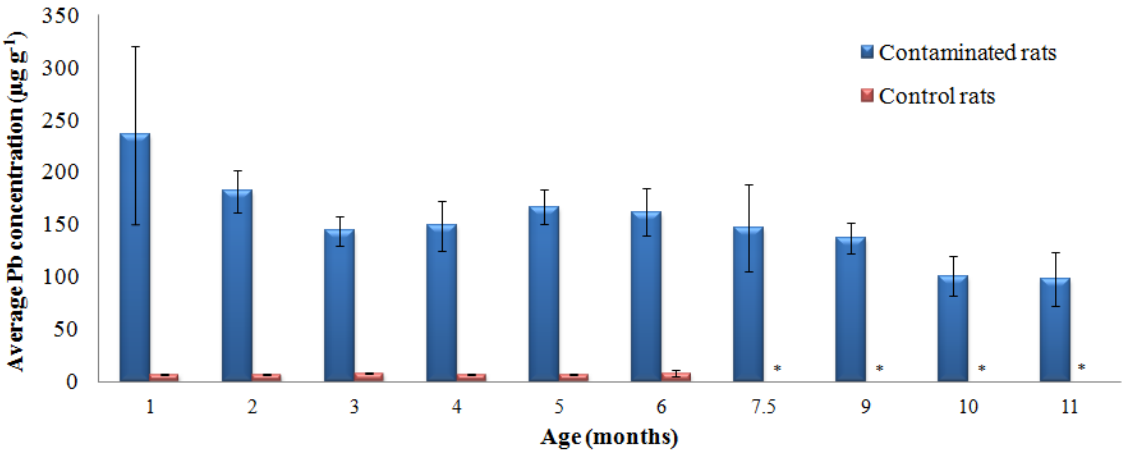

Figure 32: Comparison of Pb concentration obtained by EDXRF in rat skulls from exposed and non-exposed group. In the control rats * corresponds to BDL < 5 µg g^{-1}.

It can be observed in Figures 29, 30, 31 and 32 that there is a decrease of the mean lead concentration accumulated in all bones with age, and that these decrease maybe done by steps. To test this hypothesis, it was applied the Kruskal-Wallis test to the different bones between all the collections. Results show there are three different plateaus of accumulation for all bones: plateau 1 (P1) containing the youngest rats of the 1st and 2nd collection; plateau 2 (P2) containing rats aging from 3 to 9 months old; and the plateau 3 (P3) containing the two older collections. In Table 10 are listed the mean values of each plateau, as well as the *p*-values obtained with the Kruskal-Wallis test between the collections that form each plateau, which are not statistically different. Subsequent application of the Mann-Whitney test between the different plateaus for each bone, with *p*-values of $p \leq 0.001$ for all cases also corroborates the statistical difference and individuality of each plateau.

	P1	**P2**	**P3**
Iliac bone	284±62* *p*=0.749	202±20* *p*=0.257	101±21* *p*=0.873
Femur	274±68* *p*=0.337	191±21* *p*=0.362	110±27* *p*=0.749
Tibia-fibula	277±85* *p*=0.624	186±20* *p*=0.542	105±26* *p*=0.337
Skull	211±59* *p*=0.394	149±19* *p*=0.214	99±22* *p*=0.749

Table 10: Mean lead concentration of the plateaus of accumulation for the several bones. Kruskal Wallis test *p*-values between the collections that form each plateau of lead accumulation for the four types of bone. * values are in $\mu g\ g^{-1}$.

The decrease of mean lead concentration in bones over time, and the youngest high skeletal retention, has also been observed in other studies [47, 81, 115]. The rapid formation of bone in young animals and inclusion of lead into the new bone, contribute to this increased retention [47, 81, 247]. Important age dependent factors also contribute to the lead concentration decrease with age, namely the gastrointestinal absorption [36, 248], the skeletal uptake [249], and the lead intake [37, 238]. All these factors are considerably greater in younger animals than in adults. However, other studies made in human bones showed that lead concentration increased with age due to the decrease in the bone turnover rate [43, 250]. The present work may be indicative that besides the decrease in bone turnover rate with age, lead concentration in bones continues to diminish, which may reflect the more significant contribution of decreasing ingestion, absorption and retention of lead in the rats organism.

As in the liver and urine samples, it was found a high mean lead concentration in the first month, which seems to be a consequence of the exposure to lead since foetal period.

6.1.3.2. Correlations between lead concentration in bones

The mean lead concentrations values between the different types of bone are displayed in Figure 33. As can be seen, the concentration of lead in iliac bone is in general higher than in the femur, tibia-fibula and skull bones. While the concentration in femur and tibia-fibula bones are similar, skull presents a considerable tendency to have a lower mean lead concentration.

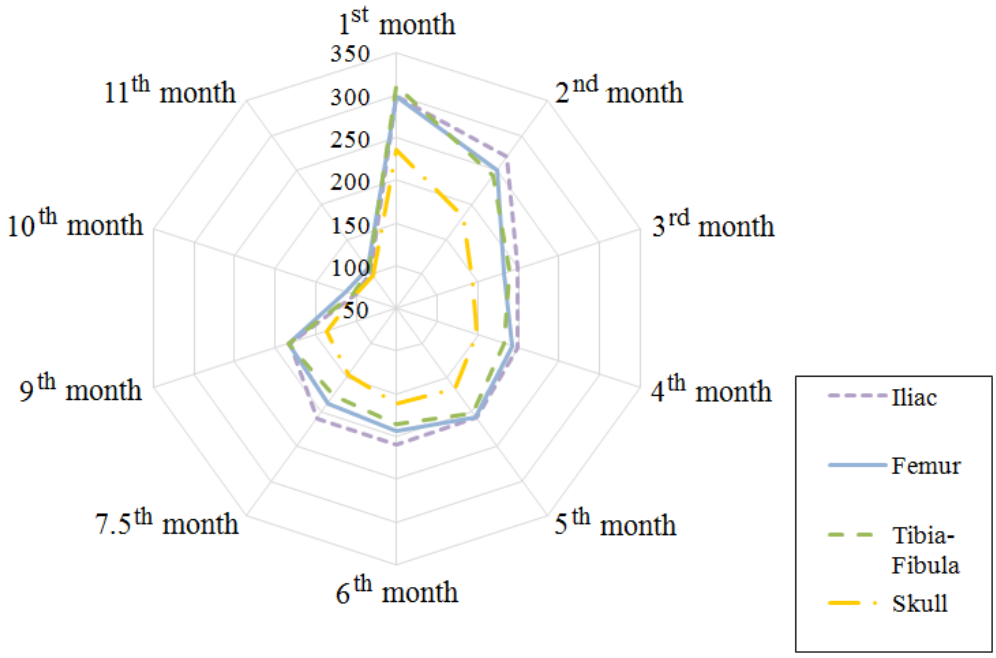

Figure 33: Distribution of mean lead concentrations (μg g^{-1}) over age on iliac bone, femur, tibia-fibula and skull.

These tendencies, however, tend to disappear in all types of bone as the rats become older. This result corroborates the suggestion of Aufderheide and Wittmers [88] that accumulation takes place predominantly in trabecular bone during childhood and in both cortical and trabecular bone in adulthood. This happens because in childhood the bone calcification is most dynamic in the trabecular bones, whilst in adulthood, calcification takes place at sites of remodelling in both cortical and trabecular bones.

To assess whether these differences are statistically significant, it was applied a Wilcoxon test between the different types of bones during the time of exposure. The test showed *p*-values $p<0.05$ only when comparing the skull with the other types of bone.

The differences between lead accumulation in skull and other bones were also reported in other works. Denton *et al.* [46] results showed a higher lead concentration in femur than in skull,

independently the amount of lead ingested. Holtzman *et al.* [251] and Smith *et al.* [252] also found the same tendency, while works made in humans, for *e.g.* by Barry and Mossman [41], Khandekar and Anand [253], and Drasch *et al.*[115], found the highest lead concentration in skull. The disparity between works made in humans and rats may be explained by an existing difference between the human bone structure and the rat bone structure (compact, spongy).

Whilst femur, tibia and fibula (long bones) are composed of trabecular (or spongy) bone tissue covered by compact bone, skull is primarily composed of dense compact tissue, and iliac bone is composed mainly by trabecular bone. Since the spongy bones are more vascular than the compact bones, it is expected that iliac bone presents a higher mean lead concentration. Due to the higher blood affluence, it is expected the iliac bone to have the higher mean lead concentrations followed by femur and tibia and fibula and then skull, as it was observed in this work. However, in some works such as Drasch *et al.* [115], pelvic bone showed a lower lead concentration than femur.

To study the correlation between elemental concentrations and their dependence on age, a Spearman correlation matrix was carried out (Table 11). It was found a very strong statistically significant positive correlation between the lead concentration in femur and iliac, skull and iliac and skull and femur. Strong positive correlations between the other types of bones can also be observed. According to this test, there is a strong negative correlation with age for all bone lead concentrations. This correlation tends to be very strong in tibia-fibula and skull.

Variable	Age	Iliac	Femur	Tibia-Fibula	Skull
Age	-	**-0.788[a]**	**-0.782[a]**	**-0.867[a]**	**-0.842[a]**
Iliac	-	-	**0.923[a]**	**0.825[a]**	**0.942[a]**
Femur	-	-	-	**0.830[a]**	**0.988[a]**
Tibia-Fibula	-	-	-	-	**0.855[a]**
Skull	-	-	-	-	-

Table 11: Spearman correlation matrix for the mean lead concentrations in bones for the 10 collections. The correlations are significant at $p<0.01$ if marked with [a].

6.1.4. Correlations between all excretions and organs

A Spearman's correlation matrix was calculated (Table 12) to study the correlation between elemental concentrations of the organs and excretions that haven't been correlated yet.

This correlation test showed that faeces and kidneys don't correlate with the other organs. It was also observed that lead concentration in urine does not have a statistically significant correlation with kidneys, but it has a strong correlation with all the other organs. A strong correlation was found between liver and all the bones. This means that when there is a decrease in the lead concentration accumulated in liver and bones there is also a decrease in lead concentration excreted through urine. Despite the evidence of this correlation, urine mean lead concentration measurements should still not to be used as a marker for body lead burden due to the high coefficient of variation associated to the urine samples.

Variable	Pb in urine	Pb in faeces	Pb in liver	Pb in kidney	Pb in iliac bone	Pb in femur	Pb in tibia-fibula	Pb in skull
Pb in urine	-	-	**0.865** ***p*=0.001**	-0.061 *p*= 0.868	**0.763** ***p*=0.010**	**0.758** ***p*=0.011**	**0.818** ***p*=0.004**	**0.830** ***p*=0.003**
Pb in faeces	-	-	0.503 *p*=0.138	-0.043 *p*=0.907	0.375 *p*=0.285	0.345 *p*=0.328	0.418 *p*=0.229	0.430 *p*=0.214
Pb in liver	-	-	-	-	**0.841** ***p*=0.002**	**0.718** ***p*=0.019**	**0.767** ***p*=0.010**	**0.767** ***p*=0.010**
Pb in kidney	-	-	-	-	0.059 *p*=0.872	0.158 *p*=0.663	-0,128 *p*=0.725	0.116 *p*=0.751

Table 12: Spearman r_s correlation values for the average lead concentrations in all the organs and excretions studied, and the corresponding *p*-values.

6.1.5. Formaldehyde lead measurements

To investigate if there was diffusion of lead into the formaldehyde used as preservative it was analysed 5 samples of formaldehyde containing contaminated kidneys, 5 samples of formaldehyde containing contaminated liver, 5 samples of formaldehyde containing contaminated bones (iliac bone, femur and tibia-fibula) and 5 samples of formaldehyde containing contaminated skull.
The formaldehyde measured values and the respective soft tissues and bone tissues concentrations are listed in Table 13.

The results show that the concentration of lead in formaldehyde is about 3 orders of magnitude lower than the concentration of lead in the soft tissues and, at least, about 5 orders of magnitude lower than the concentration of lead in the bone tissues. Based on the total mass of the biological tissues (minimum mass: kidneys -2 g, liver - 8 g, bones ~ 4 g and skull - 2 g) and the total volume

of the formaldehyde in which they were contained (20 mL for kidney and skull, and 50 mL for liver and other bones), it was concluded that the amount of lead in formaldehyde is less than 2% than the existing in the corresponding tissue and it can be neglected. The concentration value measured (n=3) in a formaldehyde original sample was BQL.

Samples of contaminated rats		Tissue ($\mu g\ g^{-1}$) n=2	Formaldehyde ($\mu g\ L^{-1}$) n=3
Kidney	11 month old - rat 1	34±2	50.0±0.6
	9 month old - rat 3	61±2	90.9±1.3
	6 month old - rat 2	42±4	83.1±1.0
	5 month old - rat 1	66±5	68.9±1.0
	3 month old rat 3	62±2	55.3±2.7
Liver	10 month old - rat 3	6±1	BDL
	9 month old - rat 1	7±1	BQL
	7.5 month old - rat 3	6±1	BQL
	4 month old - rat 3	8±1	BDL
	1 month old - rat 3	16±2	4.2±0.3
Lowest lead concentration bone tissue	10 month old - rat 1	106±20	BDL
	6 month old - rat 2	166±16	BQL
	4 month old - rat 3	197±19	3.7±0.3
	2 month old - rat 2	268±26	8.4±0.2
	1 month old - rat 3	248±24	BDL
Skull	6 month old - rat 1	180±17	BDL
	5 month old - rat 1	186±19	BDL
	4 month old - rat 2	129±13	BDL
	3 month old - rat 2	135±14	BDL
	1 month old - rat 1	331±33	BDL

Table 13: Concentration values of lead in soft tissues, bones and in the formaldehyde used to preserve the samples, measured by EDXRF and ETAAS, respectively. BDL and BQL refers to below detection limit and below quantification limit, being BDL < 0.7 $\mu g\ L^{-1}$ and BQL < 2.1 $\mu g\ L^{-1}$

6.2. Conclusions

Although the use of animal model systems is a common procedure, few data are available that correlate the differences in tissue lead levels for different exposure times in animals born from contaminated progenitors. With this in mind, the use of X-ray fluorescence and atomic absorption techniques aim to increase the understanding of distribution of heavy elements in the organism.

This study showed the suitability of the TXRF and ETAAS techniques to study lead contamination in urine samples, despite the complex matrix of this sample. The use of ultra-sound sonication in preparation of urine (and also brain) samples, within the ETAAS study framework, is stated in this work as a necessary procedure when urine presents precipitation to guarantee that all the significant lead accumulated in the precipitates is removed for the liquid and taken into account during the measurements.

It was also demonstrated that EDXRF technique can be successfully used for the analysis of lead contamination in faeces, kidney, liver and bones providing a fast, easy and non destructible analysis. This technique requires no chemical preparation what reduces the odds of contamination.

The obtained results were validated by certified materials and by double checking the measurement of some samples with the PIXE technique. Formaldehyde used to preserve the samples was also measured using the ETAAS technique to assure there was no significant diffusion of the lead content from the samples to the preservative. The results show that the diffusion can be neglected once it is < 2%.

In the present work, were determined urine and faeces lead contents with maximum values of about 5 500 μg L^{-1} and 11 000 μg g^{-1} respectively. The ratio between all the faeces and urine concentrations measured is about 3 to 4 orders of magnitude, and application of the Spearman correlation test showed a positive correlation between the fecal/urinary ratio and the time of exposition. It was also verified that the lead concentration in the urine and faeces of the control rats are, in general, near or below the upper limit values for no accumulation of lead in the organism (100 μg L^{-1} and 50 μg g^{-1}, respectively).

Regarding the contaminated rats, lead concentration values ranging from 6 to 22 μg g^{-1} were determined in liver, and from 44 to 79 μg g^{-1} were determined in kidney. This shows that kidney has a greater capacity to retain lead than liver. The ratio kidney/liver varies from 2 to 10 over time and is strongly positively correlated with the age of the animals.

Relating to the control animals, all values are below EDXRF detection limits of the technique, except the rats of two collections with values of 4 μg g^{-1}.

The bones mean lead concentration of exposed rats range from 100 to 300 μg g^{-1}, while in control rats it does not exceed 10 μg g^{-1}.

Differences between the mean lead concentrations in all bones during time were statistically tested. Despite the iliac bone presents higher mean lead concentrations than the other bone tissues, the differences were only statistically significant for skull, which presented the lower mean lead concentration. Analysis of a radar chart allowed to infer that these differences tend to be attenuated with age.

Application of non-parametric statistics to elemental concentrations pointed out a positive correlation between urine and faeces lead content. A negative correlation with age was also found, very strong for urine lead concentration and strong for faeces lead concentration.
A strong positive correlation with time of exposure was also verified in the liver concentrations, but not in the kidney. The correlation between these two soft tissues was also analysed using the Spearman correlation test and no significant relation was found.
Spearman correlation test applied to mean lead concentration in all different types of bones showed strong and very strong positive correlations. This test also demonstrated that the mean lead concentrations in bones are negatively correlated with the age of the animals. This correlation is strong in iliac and femur and very strong in tibia-fibula and skull.
It was also observed that mean lead concentration in faeces and kidneys do not correlate with the mean lead concentration in other organs, and that mean lead concentration in urine does not have a statistically significant correlation with kidneys. However, a strong correlation was found between mean lead concentrations in urine and all the other organs, as well as between mean lead concentrations in liver and all the bones.

Results suggest that the removal of lead through the faeces and urine decreases with the age and is made in different levels of excretion (Table 14). The three different groups existing in the urine excretion coincide more or less with different stages of growing of the rats: when rats become sexual active (1.5 months) [254, 255] and become social adults (~ 6 months) [254, 255]. In faeces, the step corresponding to the sexual activity of the animal is not evident. However, the gap from the first to the second group also occurs, practically when the animals reach the adult age.
Concerning the kidney time dependency, the kidney mean lead concentration is practically not affected by the exposure time (except for the 1st month). On the other hand, the lead accumulation in liver decreases with the age of the rats and is made at different levels of retention. These different plateaus also coincide with the age when rats became sexually active and become social adults (*c.f.* Table 14). It is known that at various stages of growth and development the levels of enzymes vary, and unique enzymes may exist at particular developmental stages [5, 256]. These differences might explain these levels of susceptibility to lead intoxication, once enzymes are involved in activation of the processes during the metabolism of lead.

These plateaus of accumulation are also present in the bones, but more late in time (Table 14). This fact maybe due to the longer half-life time of lead in bones when compared to soft tissue.
Thus, the decrease of the mean lead concentrations with age by plateaus was observed in all the excretions and organs (except for kidney).

In all the organs(except kidney) and in urine it was noticed that the highest mean lead concentration values occur in rats with 1 month-old, which is probably a result of the prenatal exposure once is not detected in other works made in exposed rats, but not from foetal period.

Sample	Plateaus of excretion/accumulation (months range)		
	P1	P2	P3
Pb in faeces	1^{st}-4^{th}	5^{th}-11^{th}	-
Pb in urine	1^{st}	2^{th}-5^{th}	6^{th}-11^{th}
Pb in liver	1^{st}	2^{th}-5^{th}	6^{th}-11^{th}
Pb in iliac bone	1^{st}-2^{nd}	3^{rd}-9^{th}	10^{th}-11^{th}
Pb in femur	1^{st}-2^{nd}	3^{rd}-9^{th}	10^{th}-11^{th}
Pb in tibia-fibula	1^{st}-2^{nd}	3^{rd}-9^{th}	10^{th}-11^{th}
Pb in skull	1^{st}-2^{nd}	3^{rd}-9^{th}	10^{th}-11^{th}

Table 14: Different temporal range of the plateaus of accumulation of lead concentration in the several organs measured.

It is known that about 90% of the amount of lead taken into the human body are expelled within a couple of weeks in the waste [5], which, assuming a similar lead kinetic for the rats, explains the high concentration values measured in the rats faeces.
This fact, together with the decrease of lead content in faeces and urine with animals' age seems to support the works of Kehoe *et al.* [1], Quarterman *et al.*[238], Smith *et al.* [37]. According to these authors, there is a decrease in absorption of lead with time that is primarily due to a decrease in the rate of uptake of lead as a factor of age, and not as adaptive consequence of the continuous ingestion of this toxic element.
This decrease in lead intake and gastrointestinal absorption and the decrease in lead skeletal retention, seem to be the most suitable explanations for this decrease of mean lead concentrations in bones and soft tissues. Assuming that there is a decrease in lead ingested and absorbed, the mean

lead concentration distributed by blood throughout the body, making it available to other tissues and for excretion, also diminishes.

Although most of these statements are obviously exploratory, the results obtained in this work increase the understanding of the lead concentration in several tissues and excretions, their relations and its dependency on age. However, it also introduces the need of more studies in the domain of lead toxicokinetics and metabolism.

ANNEX

Annex 1 – Quantum numbers

Symbol	Designation	Description	Range of values	Conventional nomenclature
n	Principal quantum number	Has the greatest contribution on the energy of the orbital, and describes the size of the orbital, once it is related with the distance of the electron from the nucleus (higher n higher distance).	n = 1,2,3,4 ….	$n = 1 \rightarrow K$; $n = 2 \rightarrow L$; $n = 3 \rightarrow M$; $n = 4 \rightarrow N$; etc.. A group of orbitals with the same principal quantum number is called a shell
ℓ	Azimuthal or angular quantum number	It is a measure of the orbital angular momentum and describes the shape of the orbital (spherical $\ell = 0$; polar $\ell = 1$; clover-leaf shaped $\ell = 2$, etc).	$\ell = 0, 1, 2, \ldots, (n-1)$	$\ell = 0 \rightarrow s$ $\ell = 1 \rightarrow p$ $\ell = 2 \rightarrow d$ $\ell = 3 \rightarrow f$; etc. . A group of orbitals with the same angular quantum number is called a subshell
m_ℓ	Magnetic quantum number	Describes the orbital's orientation in space, and is related with the quantization of the z component of the angular momentum.	$m_\ell = -\ell, (-\ell+1), \ldots, 0, \ldots, (-\ell+1), \ell$.	-
s	Spin quantum number	Describes the spin or direction (clockwise or counter-clockwise) in which an electron spins and quantifies the intrinsic angular momentum of the electron.	$s = +½$, $s = -½$.	-
j	Total angular momentum quantum number	Represents the coupling between ℓ and s . Can't be negative.	$j = \ell \pm ½$	-

Table 15: Quantum numbers description

Annex 2 – X-ray spectra nomenclature

The nomenclature used to identify the X-ray emission spectra was introduced by M. Siegbahn in the 1920's [257] and is based upon the relative intensity of lines (characteristic radiation) from different transitions (Table 16).

According to this nomenclature, the X-ray spectra are classified in series, K, L, M, ..., as the X-ray photons emitted correspond, respectively, to the radiative transitions to the atomic levels K, L, M, respectively (see Annex 1). Each series has several groups of transitions and the more intense transition is called α, followed in decreasing intensities by the $\beta, \gamma, \delta,$ etc transitions. This also identifies the X-ray as originating from an electron transition between a specific energy level within the initial state and a specific energy level within the final shell. The electron transitions follow a set of selection rules based on the quantum numbers (see Annex 1).

Siegbahn Nomenclature	Transition	Spectroscopic Nomenclature $n\ell_j$
$\boldsymbol{K_{\alpha 1}}$	$L_{III} \rightarrow K$	$2p_{3/2} - 1s_{1/2}$
$\boldsymbol{K_{\alpha 2}}$	$L_{II} \rightarrow K$	$2p_{1/2} - 1s_{1/2}$
$\boldsymbol{K_{\beta 3}}$	$M_{II} \rightarrow K$	$3p_{1/2} - 1s_{1/2}$
$\boldsymbol{K_{\beta 1}}$	$M_{III} \rightarrow K$	$3p_{3/2} - 1s_{1/2}$
$\boldsymbol{K_{\beta 2}}$	$N_{II,III} \rightarrow K$	$4p_{1/2} - 1s_{1/2}$ $4p_{3/2} - 1s_{1/2}$
$\boldsymbol{L_{\alpha 1}}$	$M_V \rightarrow L_{III}$	$3d_{5/2} - 2p_{3/2}$
$\boldsymbol{L_{\alpha 2}}$	$M_{IV} \rightarrow L_{III}$	$3d_{3/2} - 2p_{3/2}$
$\boldsymbol{L_{\beta 1}}$	$M_{IV} \rightarrow L_{II}$	$3d_{3/2} - 2p_{1/2}$
$\boldsymbol{L_{\beta 2}}$	$N_V \rightarrow L_{III}$	$4d_{5/2} - 2p_{3/2}$
…		

Table 16 - Some of the transitions of series ***K*** and ***L***.

Annex 3 – Histological examination and histochemical analysis of lead in NTS and HDA

i) Sample treatment

The histologycal and histochemical analysis samples were processed following the usual procedures described by Martoja and Martoja [258].

The histochemistry was performed according to the rhodizonate method for lead salts [259] to reveal lead granules. In brief, brain samples preserved in formaldehyde (10% v/v) were washed for 3 h with Milli-Q water for formaldehyde removal. Afterwards, they were dehydrated in a progressive series of ethanol dilutions and finally placed in xylene used for intermediate impregnation. Subsequently, the samples were embedded in paraffin and placed in the oven at 50º C over night. After paraffin inclusion, sections with 5 to 7 μm thickness were stained with sodium rhodizonate solution for 1 hour. Then, counterstained with aqueous fast green (0.05%) in acetic acid (0.2%) for 1 minute. Finally, the sample was rinsed in distilled water, dehydrated, clear and mounted in DPX resin. Additional sections were stained with haematoxylin and eosin for structural analysis.

Slides were prepared in duplicate for each tissue with 5 sections per slide, and examined through optical microscope observation. Pictures from tissue sections were acquired using the image analysis software Irfan View v. 4.0.

ii) Experimental Instrumentation

The histochemical and histological examinations were accomplished using a Leica Jung-RM-2035 microtome and a Leica-ATC2000 (Wetzal, Germany) optical microscope, with a DFC digital camera.

Absolute ethanol (Merck, Germany), prepared to different grades, and xylene (Carlo Erba RPE, Italy) were used during the dehydration and impregnation in histology processing.

For the revelation of the lead granules within tissues it was used sodium rhodizonate, glacial acetic acid and aqueous fast green FCF as counterstain, all purchased from Sigma-Aldrich (USA). Hematoxyline and eosine were from Riedel de Haen (Seelze, Germany). DPX resin from BDH (Poole, England) was used as mounting medium for slides.

iii) Results

The results from the rhodizonate method revealed the presence of lead granules within both tissues (*c.f.* Figure 34). The hematoxylin and eosin staining show the target brain tissues where some nervous cells can be observed (Figure 35).

The histochemistry results were obtained with an Optical microscopy (1000x). It can be observed that lead granules are present in great amounts in tissues from exposed rats and undetectable or in residual amounts in control tissues. Concerning the exposed tissues, the microscopy observations suggest that lead granules have a tendency to accumulate in some specific sites of HDA tissues (*c.f.* Figure 34A), which were identified as the cellular bodies of nervous cells (*c.f.* Figure 35A). In the NTS tissues, the lead granules seem to be scattered unevenly.

The histological and histochemical results confirm the presence of lead in the brain of exposed rats and add complementary information on the distribution of lead in brain tissues.

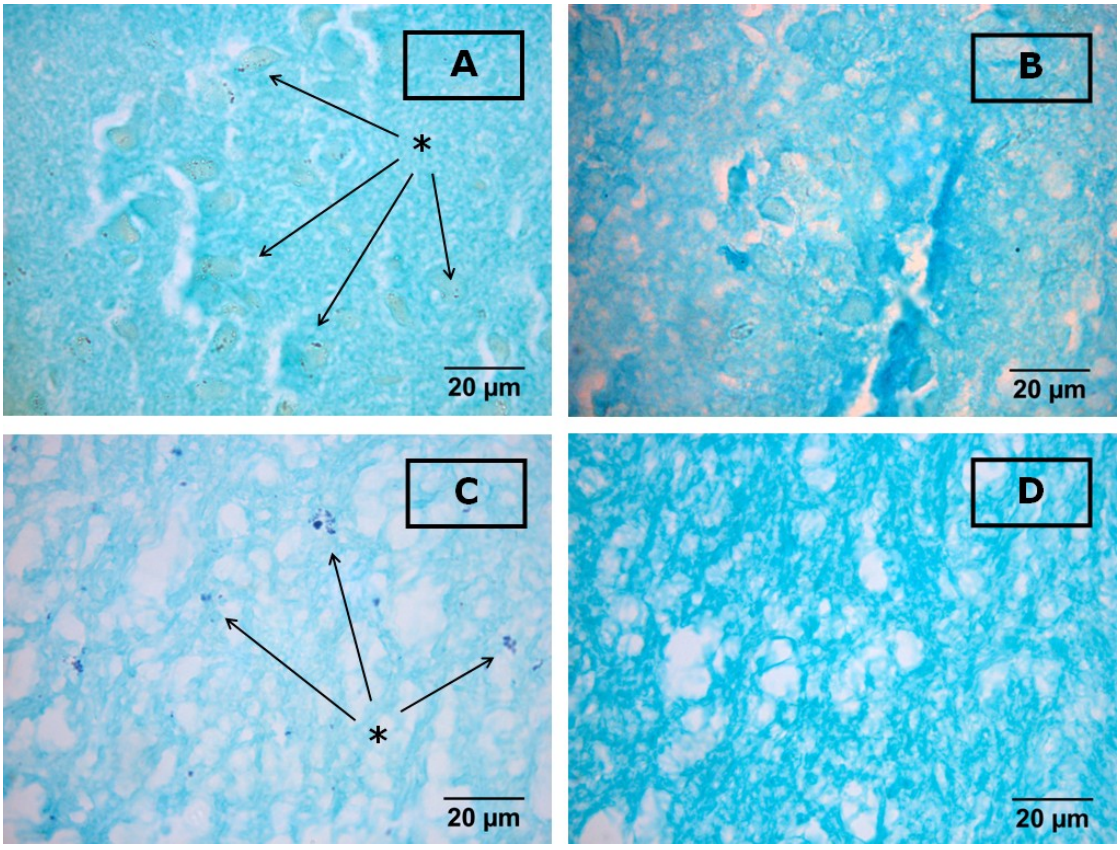

Figure 34: Histochemical detection of Pb granules in Wistar rat brain tissues. Legend: A – HDA from exposed group; B – HDA Control; C - NTS from exposed group; D - NTS Control. * Pb granules (arrowhead).

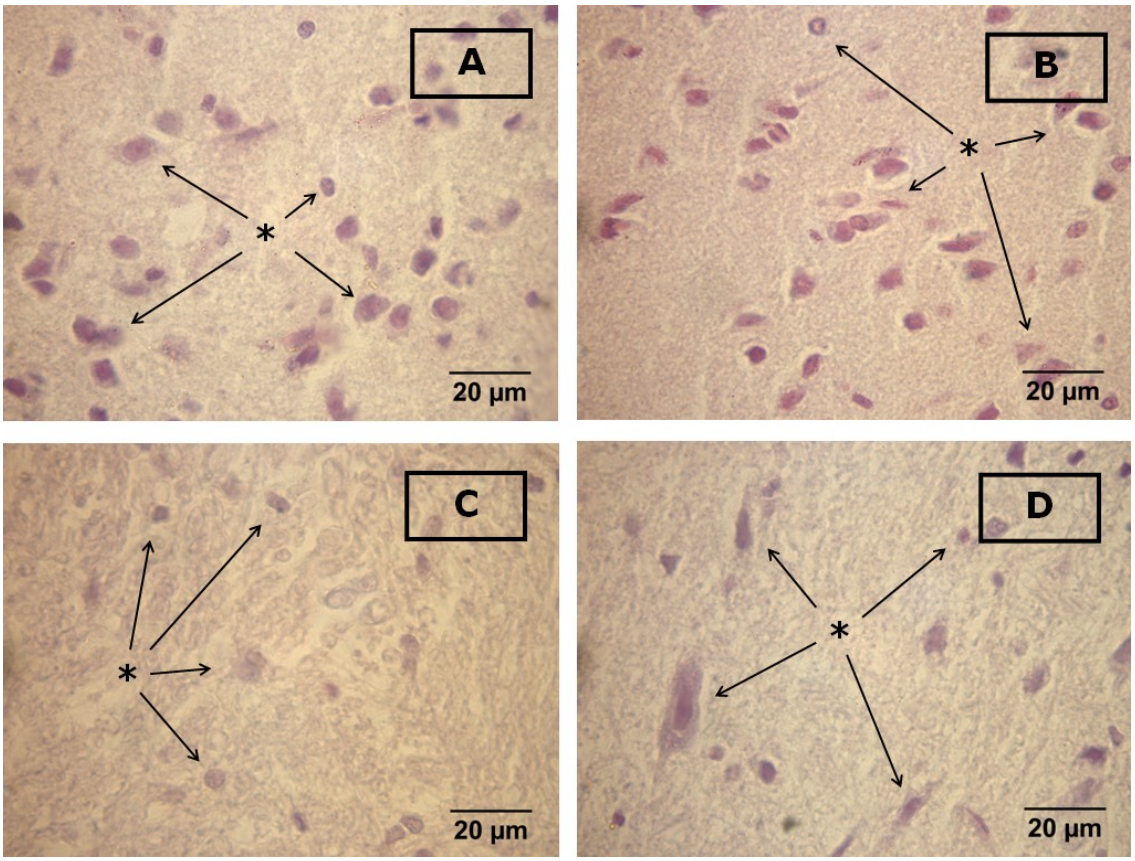

Figure 35: Wistar rat brain tissues stained by Hematoxilin and eosin. A – HDA exposed group; B – HDA Control; C - NTS exposed group; D - NTS Control. * Cellular bodies (arrowhead)

The histological examination and histochemistry confirmed the presence of lead in tissues from exposed animals and the absence of this element in control tissues. It was also possible to observe that the distribution and accumulation of lead granules is different depending on the region of the brain analyzed. In the HDA tissue, the lead tends to accumulate in cellular bodies of cells in this tissue area [260]. On the other hand, in the NTS tissues the lead seems to be distributed randomly and no preferential sites for accumulation were observed as in the previous case.

The histological studies also corroborate the higher lead accumulation in HDA. To conclude, it must be emphasize the fact that there was a preferred lead accumulation in the two brain areas that control hypertension. Further studies are being carried out to investigate the influence of lead accumulation in the inhibition of the pressure control pathways.

Annex 4 – Mean lead concentrations values measured in the several organs and excretions

	Exposed Rats[a]				Non exposed Rats[b]			
	Concentration min-max	Mean Value	SD[c]	CV[d] %	Concentration min-max	Mean Value	SD[c]	CV[d] %
1 month	5 300-5 560	5 460	115	2	210-250	220	20	9
2 months	2 020-4 570	3 190	1 400	44	BQL*[e]	-	-	-
3 months	915-4 715	2 650	1 850	70	BDL*[e]	-	-	-
4 months	950-2 655	1 860	820	44	140-170	160	15	9
5 months	950-3 050	1 780	900	51	80-160	120	40	34
6 months	555-1 130	870	190	22	BQL*[e]	-	-	-
7.5 months	500-1 100	800	420	53	BDL**[e]	-	-	-
9 months	670-800	730	70	10	BDL**[e]	-	-	-
10 months	600-900	770	130	17	BDL**[e]	-	-	-
11 months	450-740	600	140	23	BQL*[e]	-	-	-

Table 17: Concentration of lead (µg L^{-1}) in the urine of Wistar rats. All samples were measured by ETAAS except for 7.5; 9 and 10 months which were measured by TXRF. [a] Exposed rats: a total of 6 measurements by collection (2 rats, 3 different measurements each). [b] Control rats: a total of 6 measurements by collection (2 rats, 3 different measurements each). [c] SD: standard deviation. [d] CV: coefficient of variation. [e] BQL*: Below quantification limit for ETAAS < 80 µg L^{-1} (including diluting factors); BDL*: Below detection limit for ETAAS < 30 µg L^{-1}(including diluting factors); BDL**: Below detection limit for TXRF < 100 µg L^{-1}.

	Exposed Rats[a]				Non exposed Rats[b]			
	Concentration min-max	Mean Value	SD[c]	CV[d] %	Concentration min-max	Mean Value	SD[c]	CV[d] %
1 month	4 150-10 330	8 120	2 980	37	11-15	13	2	15
2 months	7 880-9 300	8 320	660	8	8-9	9	2	22
3 months	7 280-9 030	8 280	840	10	10-13	11	2	18
4 months	7 340-14 820	11 370	3 280	29	50-56	54	3	6
5 months	3 970-6 150	5 230	950	18	7-10	9	2	22
6 months	4 510-7 290	5 910	1 420	24	12-21	17	5	29
7.5 months	4 680-5 200	4 960	260	5	6-7	6	1	17
9 months	4 030-4 680	4 470	300	7	7-11	9	3	33
10 months	3 880-4 980	4 480	550	12	6-12	9	3	33
11 months	5 200-8 000	6 140	1 610	26	8-11	10	2	20

Table 18: Concentration of lead (µg g^{-1}) in the faeces of Wistar rats measured by EDXRF. [a] Exposed rats: a total of 6 measurements by collection (3 rats, 2 different pellets each). [b] Control rats: a total of 4 measurements by collection (2 rats, 2 different pellets each).[c] SD: standard deviation. [d] CV: coefficient of variation.

	Exposed Rats[a]				Non exposed Rats[b]			
	Concentration min-max	Mean Value	SD[c]	CV[d] %	Concentration min-max	Mean Value	SD[c]	CV[d] %
1 month	15-29	22	6	27	BDL[e]	-	-	-
2 months	9-11	10	1	10	3-4	4	1	25
3 months	9-10	10	1	10	3-4	4	1	25
4 months	7-11	9	2	22	BDL[e]	-	-	-
5 months	7-10	9	1	11	BDL[e]	-	-	-
6 months	6-8	7	1	14	BDL[e]	-	-	-
7.5 months	5-10	8	3	38	BDL[e]	-	-	-
9 months	6-8	7	1	14	BDL[e]	-	-	-
10 months	5-7	6	2	33	BDL[e]	-	-	-
11 months	5-7	6	1	17	BDL[e]	-	-	-

Table 19: Concentration of lead (µg g^{-1}) in the liver of Wistar rats measured by EDXRF. [a] Exposed rats: a total of 6 measurements by collection (3 rats, 2 different pellets each). [b] Control rats: a total of 4 measurements by collection (2 rats, 2 different pellets each). [c] SD: standard deviation. [d] CV: coefficient of variation. [e] BDL: Below detection limits < 2 µg g^{-1}.

	Exposed Rats[a]				Non exposed Rats[b]			
	Concentration min-max	Mean Value	SD[c]	CV[d] %	Concentration min-max	Mean Value	SD[c]	CV[d] %
1 month	37-49	44	6	14	BDL[e]	-	-	-
2 months	55-72	62	8	13	BDL[e]	-	-	-
3 months	52-64	58	5	9	BDL[e]	-	-	-
4 months	44-102	79	26	33	BDL[e]	-	-	-
5 months	57-73	65	9	14	BDL[e]	-	-	-
6 months	57-60	59	2	3	BDL[e]	-	-	-
7.5 months	57-89	75	17	23	BDL[e]	-	-	-
9 months	47-79	63	12	19	BDL[e]	-	-	-
10 months	36-71	58	17	29	BDL[e]	-	-	-
11 months	48-60	52	7	13	BDL[e]	-	-	-

Table 20: Concentration of lead (µg g^{-1}) in the kidney of Wistar rats measured by EDXRF. [a] Exposed rats: a total of 6 measurements by collection (3 rats, 2 different pellets each). [b] Control rats: a total of 4 measurements by collection (2 rats, 2 different pellets each). [c] SD: standard deviation. [d] CV: coefficient of variation. [e] BDL: Below detection limits< 2 µg g^{-1}.

	Bone lead concentration (µg g^{-1})							
Age (months)	Iliac		Femur		Tibia and Fibula		Skull	
	Exposed	Control	Exposed	Control	Exposed	Control	Exposed	Control
1	298±91	7±1	298±97	7±1	311±123	8±1	236±85	7±1
2	271±32	7±1	250±37	8±2	242±31	6±1	182±20	7±1
3	199±19	8±1	182±18	8±1	189±19	8±1	144±14	8±1
4	199±19	8±1	193±19	8±1	182±28	7±1	149±24	7±1
5	209±20	8±1	207±36	8±1	201±20	7±2	167±17	7±1
6	209±22	7±1	194±19	8±1	185±18	8±1	162±23	8±3
7.5	209±34	BDL	188±38	BDL	176±45	BDL	147±42	BDL
9	182±18	BDL	183±18	BDL	184±18	BDL	137±15	BDL
10	101±17	BDL	112±20	BDL	105±21	BDL	101±19	BDL
11	102±26	BDL	108±34	BDL	106±32	BDL	98±26	BDL

Table 21: Lead concentration (µg g^{-1}, dry weight) in the bones of Wistar rats measured by EDXRF. For the exposed rats each age group contains 3 animals, 2 different pellets each what resumes to a total of 6 measurements by collection. For control rats each group has 2 animals, 2 different pellets each what resumes to a total of 4 measurements by collection. Values are presented as mean± SD (Standard deviation). Values below detection limits (BDL) have concentrations < 5 µg g^{-1}).

Annex 5 - PIXE measurements

The PIXE is a powerful multi-elemental analytical technique that has detection limits for thick targets of the order of 1-10 μg g^{-1} [261]. However, when focusing the beam to a small areal dimension, typically a few microns, the detection limits can be improved by a factor of 100, and it is possible to provide concentration data in function of position [262]. Although being considered a non-destructive technique, when analysing materials sensitive to heat, such as organic compounds (*e.g.* soft tissues and bones), it is necessary to have some extra care to control the intensity of the beam. One of the biggest disadvantages of this method is the use of a complicated and expensive particle accelerator for the injection of the protons that act as excitation source [152].

i) Sample treatment

For the PIXE analysis, the material already powdered was compressed into pellets (15 mm diameter, 1 mm thick) on a boric acid substrate, Alfa Aesar 99.8% (Spain), by a 10 ton manual hydraulic press from Specac. A perspex device was used to avoid the contact of the powdered material with the steel pressure vessel case, improving the cleaning and decontamination between different samples.

ii) Experimental setup

From the whole set, 9 samples (3 of faeces, 3 of kidney and 3 of liver) were also measured using the PIXE set-up installed at the 2.5 MV Van de Graaff accelerator of Instituto Tecnológico e Nuclear (ITN), Sacavém Portugal. The system, described in Reis *et al.* [263, 264], includes a Sirius Si(Li) detector with 150 eV resolution positioned at 110º with the beam direction. The samples were placed in an Al sample holder and were irradiated with a proton beam passing through a 5 mm collimator using different energy and beam current values according to the atomic number of the sample elements to be quantified. A total acquisition live time of 40 minutes was used. The obtained spectra were deconvoluted with the AXIL computer program based on a non-linear least squares fitting and the concentration calculations performed with the DATTPIXE software code [265, 266].

Elemental detection limits using the same approach as in Custódio [169], are calculated to be of 2 μg g^{-1} for lead.

The accuracy evaluation was carried out by measuring the certified reference material BCR®482 Lichen, with a lead concentration of 40.9±1.4 μg g^{-1}. Using the same protocol as for the PIXE samples determination, a value 48.3±9.0 μg g^{-1} was measured. It should then be considered that the used PIXE setup and methodology employed presents an uncertainty of about 20% in the measurement of lead in biological samples.

iii) Results

The results obtained with the PIXE and the EDXRF techniques agree within the uncertainties of the measurements (Table 22). Small deviations can be explained by the used PIXE protocol when correcting sample concentration for the beam irradiation damage induced in biological samples.

Samples of contaminated rats		PIXE (µg g^{-1}) *n*=3	EDXRF (µg g^{-1}) *n*=3
Faeces	3 month old - rat 1	10 190±910	8 980±420
	3 month old - rat 3	7 980±620	7 580±230
	5 month old - rat 1	5 060±610	6 030±410
Kidney	5 month old - rat 3	85±14	66±6
	4 month old - rat 3	47±7	47±4
	6 month old - rat 3	80±16	60±6
Liver	4 month old - rat 2	11±2	8±1
	1 month old - rat 2	20±3	23±2
	3 month old - rat 1	8±1	9±1

Table 22: Comparative study of faeces, kidney and liver samples measured using the PIXE and EDXRF techniques.

References

[1] R. Kehoe, F. Thamann, J. Cholak, Normal absorption and excretion of lead, Journal of the American Medical Association, 104 (1935) 90-92.

[2] W.N. Rom, Environmental and occupational medicine, 2nd ed. ed., Little, Brown, 1992.

[3] V. Thomas, R. Socolow, J. Fanelli, T. Spiro, Effects of reducing lead in gasoline: An analysis of the international experience, Environmental Science & Technology, 33 (1999) 3942-3948.

[4] E.K. Silbergeld, The International Dimensions of Lead Exposure., Int J Occup Environ Health, 1 (1995) 336-348.

[5] ATSDR, Toxicological Profile for Lead, Atlanta, Georgia, 2005.

[6] H. Needleman, Low Level Lead Exposure: History and Discovery, Annals of Epidemiology, 19 (2009) 235-238.

[7] M. West, A. Ellis, P. Potts, C. Streli, C. Vanhoof, D. Wegrzynek, P. Wobrauschek, Atomic spectrometry update-X-ray fluorescence spectrometry, Journal of Analytical Atomic Spectrometry, 25 (2010) 1503-1545.

[8] R. Klockenkämper, Total reflection X-ray fluorescence analysis, Wiley, New York ; Chichester, 1997.

[9] R. Klockenkämper, A. von Bohlen, Determination of the critical thickness and the sensitivity for thin-film analysis by total reflection X-ray fluorescence spectrometry, Spectrochimica Acta Part B-Atomic Spectroscopy, 44 (1989) 461-469.

[10] A. von Bohlen, Total reflection X-ray fluorescence and grazing incidence X-ray spectrometry - Tools for micro- and surface analysis. A review, Spectrochimica Acta Part B - Atomic Spectroscopy, 64 (2009) 821-832.

[11] P. Legotte, W. Rosa, D. Sutton, Determination of cadmium and lead in urine and other biological samples by graphite-furnace atomic-absorption spectrometry, Talanta, 27 (1980) 39-44.

[12] P. Parsons, W. Slavin, Electrothermal atomization atomic absorption spectrometry for the determination of lead in urine: results of an interlaboratory study, Spectrochimica Acta Part B-Atomic Spectroscopy, 54 (1999) 853-864.

[13] J. Sardans, F. Montes, J. Penuelas, Determination of As, Cd, Cu, Hg and Pb in biological samples by modern electrothermal atomic absorption spectrometry, Spectrochimica Acta Part B-Atomic Spectroscopy, 65 (2010) 97-112.

[14] C. Maduro, G. Vale, S. Alves, M. Galesio, M. da Silva, C. Fernandez, S. Catarino, M. Rivas, A. Mota, J. Capelo, Determination of Cd and Pb in biological reference materials by electrothermal atomic absorption spectrometry: A comparison of three ultrasonic-based sample treatment procedures., Talanta, 68 (2006) 1156-1161.

[15] I. Lavilla, J. Capelo, C. Bendicho, Determination of cadmium and lead in mussels by electrothermal atomic absorption spectrometry using an ultrasound-assisted extraction method optimized by factorial design, Fresenius Journal of Analytical Chemistry, (1999) 283-288.

[16] H. Santos, J. Capelo, Trends in ultrasonic-based equipment for analytical sample treatment., Talanta, 73 (2007) 795-802.

[17] R.v. Grieken, A. Markowicz, Handbook of X-ray spectrometry : methods and techniques, Marcel Dekker, New York, NY, 1992.

[18] R.W. Ryon, J.D. Zahrt, Polarized Beam X-ray Fluorescence, in: R.v. Grieken, A. Markowicz (Eds.) Handbook of X-ray spectrometry : methods and techniques, Marcel Dekker, New York, NY, 1992.

[19] J.S. Casas Fernández, J. Sordo, Lead : chemistry, analytical aspects, environmental impact and health effects, 1st ed. ed., Elsevier, Amsterdam ; London, 2006.

[20] S. Hernberg, Lead poisoning in a historical perspective, American Journal of Industrial Medicine, 38 (2000) 244-254.

[21] R.H. Major, Some landmarks in the history of lead poisoning, Annals of Medical History, 3 (1931) 218-227.

[22] J. Santiago, Goya, Fortuny, Van Gogh, Portinari: lead poisoning in painters across three centuries, Revista Clinica Espanola, 206 (2006) 30-32.

[23] F. Luque, A. Gonzalez, Role of lead poisoning in the psychopathology of Vincent van Gogh, Actas Luso-Espanolas De Neurologia Psiquiatria Y Ciencias Afines, 25 (1997) 309-326.

[24] M. Markowitz, Lead poisoning: a disease for the next millennium., Curr Probl Pediatr, 30 (2000) 62-70.

[25] E.E.E. Agency, State and outlook 2005 - Part A: Integrated assessment, in, OPOCE - Office for Official Publications of the European Communities, 2005.

[26] A.T.E.C.L. Poisoning, The Global Dimensions of Lead Poisoning: An Initial Analysis, in, Alliance To End Childhood Lead Poisoning and EDF, 1994.

[27] Preventing lead poisoning in China, Environmental Health Perspectives, 104 (1996) 1024-1026.

[28] J. Nriagu, M. Blankson, K. Ocran, Childhood lead poisoning in Africa: A growing public health problem, Science of the Total Environment, 181 (1996) 93-100.

[29] B. Lanphear, D. Burgoon, S. Rust, S. Eberly, W. Galke, Environmental exposures to lead and urban children's blood lead levels, Environmental Research, 76 (1998) 120-130.

[30] E.P. Laug, F.M. Kunze, The penetration of lead through the skin, Journal of Industrial Hygiene and Toxicology, 30 (1948) 256-259.

[31] A.C. James, W. Stahlhofen, C. Rudolf, R. Kobrich, J.K. Briant, M.J. Egan, W. Nixon, A. Birchall, Deposition of inhaled particles, in: E.S. Ltd (Ed.) Human respiratory tract model for

radiological protection: a report of a task group of the International Commission on Radiological Protection, Ann. ICRP, Missouri, 1994, pp. 231–299.

[32] G. Nordberg, Handbook on the toxicology of metals, 3rd ed. ed., Academic, Oxford, 2007.

[33] J. Brito, Fluorescência de Raios X in vivo aplicada ao estudo da concentração de chumbo ósseo - contributo para modelos da toxicocinética do chumbo, in: BioPhysics, Faculdade de Ciências da Universidade de Lisboa, Lisboa, 2000, pp. 232.

[34] R. Kehoe, Metabolism of lead in man in health and disease, Archives of Environmental Health, 2 (1961) 418-422.

[35] L. Gerhardsson, V. Englyst, N. Lundstrom, G. Nordberg, S. Sandberg, F. Steinvall, Lead in tissues of deceased lead smelter workers, Journal of Trace Elements in Medicine and Biology, 9 (1995) 136-143.

[36] E. McCabe, Age and sensitivity to lead toxicity - Review, Environmental Health Perspectives, 29 (1979) 29-33.

[37] D. Smith, H. Mielke, J. Heneghan, Subchronic lead feeding study in male rats, Archives of environmental contamination and toxicology, 55 (2008) 518-528.

[38] J.A.A.d. Brito, Fluorescência de Raios X in vivo aplicada ao estudo da concentração de chumbo ósseo - contributo para modelos da toxicocinética do chumbo, in: Physics, Faculdade de Ciências da Universidade de Lisboa, Lisboa, 2000, pp. 232.

[39] A. Schutz, S. Skerfving, J. Ranstam, J. Christoffersson, Kinetics of lead in blood after the end of occupational exposure, Scandinavian Journal of Work Environment & Health, 13 (1987) 221-231.

[40] H. Hu, M. Rabinowitz, D. Smith, Bone lead as a biological marker in epidemiologic studies of chronic toxicity: Conceptual paradigms, Environmental Health Perspectives, 106 (1998) 1-8.

[41] P.S.I. Barry, D.B. Mossman, Lead concentrations in human tissues, British Journal of Industrial Medicine, 27 (1970) 339-351.

[42] P.S.I. Barry, Distribution and storage of lead in human tissues, in: J.O. Niagru (Ed.) The biogeochemistry of lead in the environment, Elsevier/North Holland Biomedical Press, Amsterdam, 1978, pp. 97-150.

[43] P.S.I. Barry, Comparison of concentrations of lead in human tissues, British Journal of Industrial Medicine, 32 (1975) 119-139.

[44] J. McGowan, Bone: Target and source of environmental pollutant exposure, Otolaryngology-Head and Neck Surgery, 114 (1996) 220-223.

[45] K. Staudinger, V. Roth, Occupational lead poisoning, American Family Physician, 57 (1998) 719-726.

[46] J. Denton, G. Potter, J. Santolucito, A comparison of skull and femur lead levels in adult-rats, Environmental Research, 23 (1980) 264-269.

[47] S. Han, X. Qiao, F. Kemp, J. Bogden, Lead exposure at an early age substantially increases lead retention in the rat, Environmental Health Perspectives, (1997) 412-417.

[48] R. Ronchetti, P. Van den Hazel, G. Schoeters, W. Hanke, Z. Rennezova, M. Barreto, M.P. Villa, Lead neurotoxicity in children: Is prenatal exposure more important than postnatal exposure?, Acta Paediatrica, 95 (2006) 45-49.

[49] M. Rabinowitz, G. Wetherill, J. Kopple, Kinetic-analysis of lead metabolism in healthy humans, The Journal of Clinical Investigation, 58 (1976) 260-270.

[50] R. Kehoe, Studies of lead administration and elimination in adult volunteers under natural and experimentally induced conditions over extended periods of time, Food and Chemical Toxicology, 25 (1987) 425-493.

[51] J.C. Barton, M.E. Conrad, L. Harrison, S. Nuby, Effects of vitamin-D on the absorption and retention of lead, American Journal of Physiology, 238 (1980) G124-G130.

[52] R.L. Canfield, C.R. Henderson, D.A. Cory-Slechta, C. Cox, T.A. Jusko, B.P. Lanphear, Intellectual impairment in children with blood lead concentrations below 10 microg per deciliter., N Engl J Med, 348 (2003) 1517-1526.

[53] J. Schwartz, C. Angle, H. Pitcher, Relationship between childhood blood lead levels and stature., Pediatrics, 77 (1986) 281-288.

[54] J. Schwartz, D. Otto, Blood lead, hearing thresholds, and neurobehavioral development in children and youth., Arch Environ Health, 42 (1987) 153-160.

[55] B.L. Carson, H.V. Ellis, J.L. McCann, Toxicology and biological monitoring of metals in humans : including feasibility and need, Lewis, Chelsea, Mich., 1986.

[56] S. Toplan, D. Ozcelik, T. Gulyasar, M. Akyolcu, Changes in hemorheological parameters due to lead exposure in female rats., J Trace Elem Med Biol, 18 (2004) 179-182.

[57] T. Ma, H. Chen, D. Lim, A. Hume, I. Ho, Effects of subacute lead exposure on [H-3]MK-801 binding in hippocampus and cerebral cortex in the adult rat, Brain Research, 760 (1997) 187-192.

[58] L. Gerhardsson, N. Lundstrom, G. Nordberg, S. Wall, Mortality and lead-exposure - A retrospective cohort study of swedish smelter workers, British Journal of Industrial Medicine, (1986) 707-712.

[59] H. Hu, Poisoning, drug, overdose and envenomation, in: Harrison's Principles of Internal Medicine, New York, 2002, pp. 2577-2580.

[60] J. Pearce, Burton's line in lead poisoning, European Neurology, 57 (2007) 118-119.

[61] R.A. Goyer, Renal changes associated with lead exposure, in: M. KR (Ed.) Dietary and environmental lead: Human health effects, Elsevier Science Publishers B.V., Amesterdam, The Netherlands, 1985, pp. 315-338.

[62] M. Sallmen, M. Lindbohm, M. Nurminen, Paternal exposure to lead and infertility, Epidemiology, (2000) 148-152.

[63] S. Kumar, S. Jain, C.S. Aggarwal, G.K. Ahuja, Encephalopathy due to inorganic lead exposure in an adult., Jpn J Med, 26 (1987) 253-254.

[64] L. Gerhardsson, N. Lundstrom, G. Nordberg, S. Wall, Mortality and lead-exposure - a retrospective cohort study of swedish smelter workers, British Journal of Industrial Medicine, 43 (1986) 707-712.

[65] E. Boyland, C. Dukes, P. Grover, B. Mitchley, The induction of renal tumours by feeding lead acetate to rats, British Journal of Cancer, 16 (1962) 283-288.

[66] K. Steenland, P. Boffetta, Lead and cancer in humans: Where are we now?, American Journal of Industrial Medicine, (2000) 295-299.

[67] N. Castellino, P. Lamanna, B. Grieco, Biliary excretion of lead in the rat, British Journal of Industrial Medicine, 23 (1966) 237-239.

[68] L. Davidson, H. Fullerton, H. Rae, A. Henderson, Lead poisoning in the North-East of Scotland, Lancet, 2 (1933) 374-377.

[69] A.J. Vander, D.L. Taylor, K. Kalitis, D.R. Mouw, W. Victery, Renal handling of lead in dogs: clearance studies., Am J Physiol, 233 (1977) F532-538.

[70] L. Gerhardsson, D. Chettle, V. Englyst, G. Nordberg, H. Nyhlin, M. Scott, A. Todd, O. Vesterberg, Kidney effects in long-term exposed lead smelter workers, British Journal of Industrial Medicine, 49 (1992) 186-192.

[71] W. Mortada, M. Sobh, M. El-Defrawy, S. Farahat, Study of lead exposure from automobile exhaust as a risk for nephrotoxicity among traffic policemen, American Journal of Nephrology, 21 (2001) 274-279.

[72] J. Lin, D. Tan, K. Hsu, C. Yu, Environmental lead exposure and progressive renal insufficiency, Archives of Internal Medicine, 161 (2001) 264-271.

[73] R. Lilis, N. Gavriles, B. Nestores, C. Dumitriu, A. Roventa, Nephropathy in chronic lead poisoning, British Journal of Industrial Medicine, 25 (1968) 196-&.

[74] L. Vasil'eva, I. Grinshtein, S. Gucer, B. Izgi, Determination of lead and cadmium in urine by electrothermal atomization atomic absorption spectrometry, Journal of Analytical Chemistry, 63 (2008) 649-654.

[75] D. Brune, G. Nordberg, P. Wester, Distribution of 23 elements in the kidney, liver and lungs of workers from a smeltery and refinery in north Sweden exposed to a number of elements and of a control-group, Science of the Total Environment, 16 (1980) 13-35.

[76] G. Conterato, P. Augusti, S. Somacal, L. Einsfeld, R. Sobieski, J. Torres, T. Emanuelli, Effect of lead acetate on cytosolic thioredoxin reductase activity and oxidative stress parameters in rat kidneys, Basic & Clinical Pharmacology & Toxicology, 101 (2007) 96-100.

[77] M. Jurczuk, J. Moniuszko-Jakoniuk, M. Brzoska, Involvement of some low-molecular thiols in the peroxidative mechanisms of lead and ethanol action on rat liver and kidney, Toxicology, 219 (2006) 11-21.

[78] M. Hermeslima, V. Valle, A. Vercesi, E. Bechara, Damage to rat-liver mitochondria promoted by delta-aminolevulinic acid-generated reactive oxygen species - connections with acute intermittent porphyria and lead-poisoning, Biochimica Et Biophysica Acta, 1056 (1991) 57-63.

[79] A. Bernard, R. Lauwerys, Metal-induced alterations of delta-aminolevulinic-acid dehydratase, Annals of the New York Academy of Sciences, 514 (1987) 41-47.

[80] H. Gonick, Lead, renal disease and hypertension., Am J Kidney Dis, 40 (2002) 202-204.

[81] J. Rader, J. Peeler, K. Mahaffey, Comparative toxicity and tissue distribution of lead acetate in weanling and adult-rats, Environmental Health Perspectives, 42 (1981) 187-195.

[82] R.A. Goyer, D.L. Leonard, J.F. Moore, B. Rhyne, M.R. Krigman, Lead dosage and the role of the intranuclear inclusion body. An experimental study., Arch Environ Health, 20 (1970) 705-711.

[83] H. de Assis, A. Sanchez-Chardi, R. dos Reis, L. Nicaretta, C. Mencinauski, S. Jakobi, P. da Silva, A. Zampronio, E. Pelletier, C. Ribeiro, Subchronic toxic effects of tributyltin (TBT) and inorganic lead (PbII) in rats, Environmental Toxicology and Pharmacology, (2005) 113-120.

[84] R.A. Goyer, C.D. Klaassen, M.P. Waalkes, Metal toxicology, Academic Press, San Diego ; London, 1995.

[85] B. Gulson, C. Jameson, K. Mahaffey, K. Mizon, M. Korsch, G. Vimpani, Pregnancy increases mobilization of lead from maternal skeleton, Journal of Laboratory and Clinical Medicine, 130 (1997) 51-62.

[86] B. Gulson, J. Pounds, P. Mushak, B. Thomas, B. Gray, M. Korsch, Estimation of cumulative lead releases (lead flux) from the maternal skeleton during pregnancy and lactation, Journal of Laboratory and Clinical Medicine, 134 (1999) 631-640.

[87] B. Gulson, K. Mizon, M. Korsch, J. Palmer, J. Donnelly, Mobilization of lead from human bone tissue during pregnancy and lactation - a summary of long-term research, Science of the Total Environment, 303 (2003) 79-104.

[88] A. Aufderheide, L. Wittmers, Selected aspects of the spatial-distribution of lead in bone, Neurotoxicology, 13 (1992) 809-819.

[89] U. Nilsson, R. Attewell, J. Christoffersson, A. Schutz, L. Ahlgren, S. Skerfving, S. Mattsson, Kinetics of lead in bone and blood after end of occupational exposure, Pharmacology & Toxicology, 68 (1991) 477-484.

[90] F. Gerr, R. Letz, L. Stokes, D. Chettle, F. McNeill, W. Kaye, Association between bone lead concentration and blood pressure among young adults, American Journal of Industrial Medicine, 42 (2002) 98-106.

[91] S. Korrick, D. Hunter, A. Rotnitzky, H. Hu, F. Speizer, Lead and hypertension in a sample of middle-aged women, American Journal of Public Health, 89 (1999) 330-335.

[92] M. Weisskopf, J. Weuve, H. Nie, M. Saint-Hilaire, L. Sudarsky, D. Simon, B. Hersh, J. Schwartz, R. Wright, H. Hu, Association of Cumulative Lead Exposure with Parkinson's Disease, Environmental Health Perspectives, (2010) 1609-1613.

[93] M. Weisskopf, H. Hu, R. Mulkern, R. White, A. Aro, S. Oliveira, R. Wright, Cognitive deficits and magnetic resonance spectroscopy in adult monozygotic twins with lead poisoning, Environmental Health Perspectives, 112 (2004) 620-625.

[94] A. Escribano, M. Revilla, E. Hernandez, C. Seco, J. GonzalezRiola, L. Villa, H. Rico, Effect of lead on bone development and bone mass: A morphometric, densitometric, and histomorphometric study in growing rats, Calcified Tissue International, 60 (1997) 200-203.

[95] M. Ronis, J. Aronson, G. Gao, W. Hogue, R. Skinner, T. Badger, C. Lumpkin, Skeletal effects of developmental lead exposure in rats, Toxicological Sciences, 62 (2001) 321-329.

[96] J. Hamilton, E. O'Flaherty, Influence of lead on mineralization during bone-growth, Fundamental and Applied Toxicology, 26 (1995) 265-271.

[97] F. Were, W. Njue, J. Murungi, R. Wanjau, Use of human nails as bio-indicators of heavy metals environmental exposure among school age children in Kenya, Science of the Total Environment, 393 (2008) 376-384.

[98] R. Cespon-Romero, M. Yebra-Biurrun, Flow injection determination of lead and cadmium in hair samples from workers exposed to welding fumes, Analytica Chimica Acta, 600 (2007) 221-225.

[99] J. Manzoori, A. Bavili-Tabrizi, Cloud point preconcentration and flame atomic absorption spectrometric determination of Cd and Pb in human hair, Analytica Chimica Acta, 470 (2002) 215-221.

[100] H. Delves, A micro-sampling method for rapid determination of lead in blood by atomic-absorption spectrophotometry, Analyst, 95 (1970) 431-438.

[101] A. Steenhout, M. Pourtois, Lead accumulation in teeth as a function of age with different exposures, British Journal of Industrial Medicine, 38 (1981) 297-303.

[102] H. Günzler, A. Williams, Handbook of analytical techniques, Wiley-VCH, Weinheim ; Chichester, 2001.

[103] V. Lagesson, L. Andrasko, Direct determination of lead and cadmium in blood and urine by flameless atomic-absorption spectrophotometry, Clinical Chemistry, 25 (1979) 1948-1953.

[104] F. Kummrow, F. Silva, R. Kuno, A. Souza, P. Oliveira, Biomonitoring method for the simultaneous determination of cadmium and lead in whole blood by electrothermal atomic absorption spectrometry for assessment of environmental exposure, Talanta, 75 (2008) 246-252.

[105] E. Daftsis, G. Zachariadis, Analytical performance of ETAAS method for Cd, Co, Cr and Pb determination in blood fractions samples, Talanta, (2007) 722-730.

[106] N. Campillo, P. Vinas, I. Lopez-Garcia, M. Hernandez-Cordoba, Rapid determination of lead and cadmium in biological fluids by electrothermal atomic absorption spectrometry using Zeeman correction, Analytica Chimica Acta, 390 (1999) 207-215.

[107] T. Maranhao, E. Martendal, D. Borges, E. Carasek, B. Weiz, A. Curtius, Cloud point extraction for the determination of lead and cadmium in urine by graphite furnace atomic absorption spectrometry with multivariate optimization using Box-Behnken design, Spectrochimica Acta Part B-Atomic Spectroscopy, 62 (2007) 1019-1027.

[108] M. Wilhelm, I. Lombeck, D. Hafner, F.K. Ohnesorge, Hair lead levels in young-children from the FRG, Journal of Trace Elements and Electrolytes in Health and Disease, 3 (1989) 165-170.

[109] T. Ozden, G. Gokcay, H. Ertem, O. Suoglu, A. Kilic, S. Sokucu, G. Saner, Elevated hair levels of cadmium and lead in school children exposed to smoking and in highways near schools, Clinical Biochemistry, 40 (2007) 52-56.

[110] W. Mortada, M. Sobh, M. El-Defrawy, S. Farahat, Reference intervals of cadmium, lead, and mercury in blood, urine, hair, and nails among residents in Mansoura city, Nile delta, Egypt, Environmental Research, 90 (2002) 104-110.

[111] B. Batista, J. Rodrigues, J. Nunes, L. Tormen, A. Curtius, F. Barbosa, Simultaneous determination of Cd, Cu, Mn, Ni, Pb and Zn in nail samples by inductively coupled plasma mass spectrometry (ICP-MS) after tetramethylammonium hydroxide solubilization at room temperature: Comparison with ETAAS, Talanta, 76 (2008) 575-579.

[112] J. Ortel, Accumulation of Cd and Pb in successive stages of galleria-mellonella and metal transfer to the pupal parasitoid pimpla-turionellae, Entomologia Experimentalis et Applicata, 77 (1995) 89-97.

[113] Z. Gyori, B. Kovacs, P. Daniels, P. Szabo, C. Phillips, Cadmium and lead in Hungarian porcine products and tissues, Journal of the Science of Food and Agriculture, 85 (2005) 1049-1054.

[114] W. Cybulski, A. Chalabis-Mazurek, A. Jakubczak, L. Jarosz, K. Kostro, K. Kursa, Content of lead, cadmium, and mercury in the liver and kidneys of silver foxes (Vulpes Vulpes) in relation to age and reproduction disorders Bulletin of the Veterinary Institute in Pulawy, 53 (2009) 65-69.

[115] G.A. Drasch, J. Bohm, C. Baur, Lead in human bones. Investigations on an occupationally non-exposed population in sothern bavaria (F.R.G) I. Adults, Science of the Total Environment, (1987) 303-315.

[116] Z.W. Zhang, S. Shimbo, N. Ochi, M. Eguchi, T. Watanabe, C.S. Moon, M. Ikeda, Determination of lead and cadmium in food and blood by inductively coupled plasma mass spectrometry: a comparison with graphite furnace atomic absorption spectrometry., Sci Total Environ, 205 (1997) 179-187.

[117] H.T. Delves, M.J. Campbell, Measurement of total lead concentrations and of lead isotope ratios in whole blood by use of inductively coupled plasma, Journal of Analytical and Atomic Spectrometry, 3 (1988) 343-348.

[118] A. Bazzi, J.O. Nriagu, A.M. Linder, Determination of toxic and essential elements in children's blood with inductively coupled plasma-mass spectrometry., J Environ Monit, 10 (2008) 1226-1232.

[119] J.P. Goullé, E. Saussereau, L. Mahieu, D. Bouige, S. Groenwont, M. Guerbet, C. Lacroix, Application of inductively coupled plasma mass spectrometry multielement analysis in fingernail and toenail as a biomarker of metal exposure., J Anal Toxicol, 33 (2009) 92-98.

[120] J.L. Rodrigues, B.L. Batista, J.A. Nunes, C.J. Passos, F. Barbosa, Evaluation of the use of human hair for biomonitoring the deficiency of essential and exposure to toxic elements., Sci Total Environ, 405 (2008) 370-376.

[121] F.X. Lesage, F. Deschamps, H. Millart, Lead levels in fur of rats treated with inorganic lead measured by inductively coupled argon plasma mass spectrometry., Interdiscip Toxicol, 3 (2010) 118-121.

[122] J. Wang, E. Harald Hansen, B. Gammelgaard, Flow injection on-line dilution for multi-element determination in human urine with detection by inductively coupled plasma mass spectrometry., Talanta, 55 (2001) 117-126.

[123] P. Schramel, I. Wendler, J. Angerer, The determination of metals (antimony, bismuth, lead, cadmium, mercury, palladium, platinum, tellurium, thallium, tin and tungsten) in urine samples by inductively coupled plasma-mass spectrometry., Int Arch Occup Environ Health, 69 (1997) 219-223.

[124] B. Zlateva, R. Djingova, I. Kuleff, On the possibilities of ICP-AES for analysis of archaeological bones, Central European Journal of Chemistry, 1 (2003) 201-221.

[125] E. Engstrom, A. Stenberg, S. Senioukh, R. Edelbro, D. Baxter, I. Rodushkin, Multi-elemental characterization of soft biological tissues by inductively coupled plasma-sector field mass spectrometry, Analytica Chimica Acta, 521 (2004) 123-135.

[126] S.S.Q. Hee, J.R. Boyle, Simultaneous multielemental analysis of some environmental and biological samples by inductively coupled plasma atomic emission-spectrometry, Analytical Chemistry, 60 (1988) 1033-1042.

[127] E. Sanna, A. Liguori, L. Palmas, M. Soro, G. Floris, Blood and hair lead levels in boys and girls living in two Sardinian towns at different risks of lead pollution, Ecotoxicology and Environmental Safety, 55 (2003) 293-299.

[128] R.W. Thatcher, M.L. Lester, R. Mcalaster, R. Horst, Effects of low-levels of cadmium and lead on cognitive-functioning in children, Archives of Environmental Health, 37 (1982) 159-166.

[129] B. Nowak, J. Chmielnicka, Relationship of lead and cadmium to essential elements in hair, teeth, and nails of environmentally exposed people, Ecotoxicology and Environmental Safety, 46 (2000) 265-274.

[130] M. Farago, I. Thornton, N. White, I. Tell, M. Martensson, Environmental impacts of a secondary lead smelter in Landskrona, southern Sweden, Environmental Geochemistry and Health, 21 (1999) 67-82.

[131] H. Kuo, S. Kuo, C. Chou, T. Lee, Determination of 14 elements in Taiwanese bones, Science of the Total Environment, 255 (2000) 45-54.

[132] M. Carvalho, A. Marques, X-ray fluorescence spectrometry: applications in trace elements studies in human tissues from patients with cirrhosis, X-Ray Spectrometry, 30 (2001) 397-402.

[133] M. Carvalho, J. Brito, M. Barreiros, Study of trace element concentrations in human tissues by EDXRF spectrometry, X-Ray Spectrometry, 27 (1998) 198-204.

[134] J. Brito, F. McNeill, D. Chettle, C. Webber, C. Vaillancourt, Study of the relationships between bone lead levels and its variation with time and the cumulative blood lead index, in a repeated bone lead survey, Journal of Environmental Monitoring, (2000) 271-276.

[135] J.A.A. Brito, D.E.B. Fleming, D.R. Chettle, A review of EDXRS in the study of human lead, X-Ray Spectrometry, 37 (2008) 84-88.

[136] H. Nie, P. Parsons, D. Bellis, A. Todd, D. Chettle, R. Wright, Accuracy and Precision of an Advanced K-x Ray Fluorescence (KXRF) in vivo Bone Lead Measurement System, Epidemiology, 19 (2008) S304-S304.

[137] D. Chettle, Three decades of in vivo x-ray fluorescence of lead in bone, X-Ray Spectrometry, 34 (2005) 446-450.

[138] U. Nilsson, S. Skerfving, In-vivo X-Ray Fluorescence measurements of cadmium and lead, Scandinavian Journal of Work Environment & Health, 19 (1993) 54-58.

[139] T. Magalhaes, A. von Bohlen, M. Carvalho, M. Becker, Trace elements in human cancerous and healthy tissues from the same individual: A comparative study by TXRF and EDXRF, Spectrochimica Acta Part B-Atomic Spectroscopy, (2006) 1185-1193.

[140] D. vonCzarnowski, E. Denkhaus, K. Lemke, Determination of trace element distribution in cancerous and normal human tissues by total reflection X-ray fluorescence analysis, Spectrochimica Acta Part B-Atomic Spectroscopy, 52 (1997) 1047-1052.

[141] L. Benninghoff, D. vonCzarnowski, E. Denkhaus, K. Lemke, Analysis of human tissues by total reflection X-ray fluorescence. Application of chemometrics for diagnostic cancer recognition, Spectrochimica Acta Part B-Atomic Spectroscopy, 52 (1997) 1039-1046.

[142] M. Mages, S. Woelfl, M. Ovari, W. Von Tumpling, F. Encina, The use of a portable total reflection X-ray fluorescence spectrometer for trace element determination in freshwater microcrustaceans (Daphnia), Spectrochimica Acta Part B-Atomic Spectroscopy, 59 (2004) 1265-1272.

[143] M. Carvalho, P. Custodio, U. Reus, A. Prange, Elemental analysis of human amniotic fluid and placenta by total-reflection X-ray fluorescence and energy-dispersive X-ray fluorescence: child weight and maternal age dependence, Spectrochimica Acta Part B-Atomic Spectroscopy, 56 (2001) 2175-2180.

[144] V. Bezel, K. Koutzenogii, S. Mukhacheva, O. Chankina, T. Savchenko, Using of Synchrotron radiation for study of multielement composition of the small mammals diet and tissues, Nuclear Instruments & Methods in Physics Research Section a-Accelerators Spectrometers Detectors and Associated Equipment, 575 (2007) 218-220.

[145] K. Koutzenogii, T. Savchenko, O. Chankina, G. Kovalskaya, L. Osipova, A. Bgatov, Synchrotron radiation X-ray fluorescence analysis (SRXRF) for measuring the multielement composition of samples of biogenic nature, Journal of Trace and Microprobe Techniques, 21 (2003) 311-325.

[146] O. Chankina, G. Kovalskaya, K. Koutzenogii, L. Osipova, T. Savchenko, SRXRF determination of the multielement composition of the hair and blood of the children of Tundra Nenetz population, Nuclear Instruments & Methods in Physics Research Section a-Accelerators Spectrometers Detectors and Associated Equipment, 470 (2001) 448-451.

[147] W.C. Röntgen, On a new kind of rays, Nature, 53 (1896).

[148] R. Tertian, F. Claisse, Principles of quantitative X-ray fluorescence analysis, Heyden, London, 1982.

[149] R. Jenkins, X-ray fluorescence spectrometry, 2nd ed. ed., Wiley, New York ; Chichester, 1999.

[150] R. Wittkopp, V.L. Da Gragano, Fundamentals of X-Ray Fluorescence, 1 st ed., Kevex Corporation, California, 1973.

[151] D.A. Skoog, F.J. Holler, S.R. Crouch, D.A.P.o.i.a. Skoog, Principles of instrumental analysis, 6th ed. / Douglas A. Skoog, F. James Holler, Stanley R. Crouch. ed., Brooks/Cole ; London : Thomson Learning [distributor], Pacific Grove, Calif., 2007.

[152] S.A.E. Johansson, J.L. Campbell, K.G. Malmqvist, Particle-induced X-ray emission spectrometry (PIXE), Wiley, New York ; Chichester, 1995.

[153] L. Salgueiro, J.G. Ferreira, Introdução à Física Atómica e Nuclear: Física Atómica, 1970.

[154] H.Z. Berlin, Applied Materials: XRD, in, 2009.

[155] D.E. Porter, High intensity excitation sources for X-ray energy spectroscopy, X ray Spectrometry, 2 (1973) 85-89.

[156] C. Barkla, Energy of secondary rontgen radiation., Proceedings of the Physical Society of London, 19 (1905) 185-204.

[157] C. Barkla, Polarisation in secondary rontgen radiation, Proceedings of the Royal Society of London Series a-Containing Papers of a Mathematical and Physical Character, 77 (1906) 247-255.

[158] R. Jenkins, R.W. Gould, D. Gedcke, Quantitative x-ray spectrometry, M. Dekker, New York, 1981.

[159] A. Compton, C. Hagenow, A measurement of the polarization of secondary X-rays, Journal of the Optical Society of America and Review of Scientific Instruments, 8 (1924) 487-491.

[160] P. Standzenieks, E. Selin, Background reduction of X-Ray-Fluorescence spectra in a secondary target energy dispersive spectrometer, Nuclear Instruments & Methods, 165 (1979) 63-65.

[161] G.F. Knoll, Radiation detection and measurement, 4th ed. ed., Wiley, Hoboken, N.J., 2010.

[162] C. Vandecasteele, C.B. Block, Modern methods for trace element determination, Wiley, Chichester, 1993.

[163] D. Newbury, The new X-ray mapping: X-ray spectrum imaging above 100 kHz output count rate with the silicon drift detector, Microscopy and Microanalysis, 12 (2006) 26-35.

[164] C. Whiston, F.E. Prichard, X-ray methods, Published on behalf of ACOL by Wiley, Chichester, 1987.

[165] D.H. Wilkinson, Breit-Wigners viewed through Gaussians, Nuclear Instruments & Methods, 95 (1971) 259-264.

[166] G.W. Corder, D.I. Foreman, Nonparametric statistics for non-statisticians : a step-by-step approach, Wiley-Blackwell, Oxford, 2009.

[167] A. Rindby, Software for Energy-Dispersive X-Ray Fluorescence, X-Ray Spectrometry, 18 (1989) 113-118.

[168] A. Rindby, X-ray spectroscopy with applications in trace element analysis, in: Department of Physics, Göteborg University, Sweden, 1983.

[169] P. Custodio, M. Carvalho, F. Nunes, S. Pedroso, A. Campos, Direct analysis of human blood (mothers and newborns) by energy dispersive X-ray fluorescence, Journal of Trace Elements in Medicine and Biology, 19 (2005) 151-158.

[170] Y. Yoneda, T. Horiuchi, Optical flats for use in X-ray spectrochemical microanalysis, Review of Scientific Instruments, 42 (1971) 1069-1072.

[171] H. Aiginger, P. Wobrauschek, Method for quantitative X ray Fluorescence analysis in nanogram region Nuclear Instruments & Methods, 114 (1974) 157-158.

[172] R. Klockenkamper, A. vonBohlen, Elemental analysis of environmental samples by total reflection X-ray fluorescence: A review, X-Ray Spectrometry, 25 (1996) 156-162.

[173] P. Wobrauschek, Total reflection x-ray fluorescence analysis - a review, X-Ray Spectrometry, 36 (2007) 289-300.

[174] R. Pepelnik, B. Erbsloh, W. Michaelis, A. Prange, Determination of trace element deposition into a forest ecosystem using total reflection X-ray fluorescence, Spectrochimica Acta Part B-Atomic Spectroscopy, 48 (1993) 223-229.

[175] R. Schmeling, F. Alt, R. Klockenkamper, D. Klockow, Multielement analysis by total reflection X-ray fluorescence spectrometry for the certification of lichen research material, Fresenius Journal of Analytical Chemistry, (1997) 1042-1044.

[176] A. Prange, A. Knochel, W. Michaelis, Multi-element determination of dissolved heavy metal traces in sea-water by total reflection X-ray fluorescence spectrometry, Analytica Chimica Acta, 172 (1985) 79-100.

[177] L.M. Muia, F.L. Razafindramisa, R.E. Van Grieken, Total reflection X-Ray fluorescence analysis using an extended focus tube for the determination of dissolved elements in rain water, Spectrochimica Acta Part B-Atomic Spectroscopy, 46 (1991) 1421-1427.

[178] A. von Bohlen, R. Klockenkämper, H. Otto, G. Tolg, B. Wiecken, Qualitative survey analysis of thin-layers of tissue samples - heavy metal traces in human lung tissue, International Archives of Occupational and Environmental Health, 59 (1987) 403-411.

[179] A. Prange, K. Kramer, U. Reus, Determination of trace-element impurities in ultrapure reagents by total reflection X-Ray spectrometry, Spectrochimica Acta Part B-Atomic Spectroscopy, 46 (1991) 1385-1393.

[180] J.S. Chen, H. Berndt, R. Klockenkämper, G. Tölg, Trace analysis of high-purity iron by total reflection X-ray fluorescence spectrometry, Fresenius Journal of Analytical Chemistry, 338 (1990) 891-894.

[181] K. Freitag, U. Reus, J. Fleischhauer, The application of TXRF spectrometry for the determination of trace-metals in lubricating oils, Fresenius Zeitschrift Fur Analytische Chemie, 334 (1989) 675-675.

[182] M. Schirmacher, P. Freimann, D. Schmidt, G. Dahlmann, Trace metal determination by total reflection X-ray fluorescence (TXRF) for the differentiation between pure fuel-oil (bunker oil) and waste oil (sludge) in maritime shipping legal cases, Spectrochimica Acta Part B-Atomic Spectroscopy, 48 (1993) 199-205.

[183] D.K.G. de Boer, A.J.G. Leenaers, W.W. Vandenhoogenhof, Glancing-incidence X-ray analysis of thin-layered materials - a review X-Ray Spectrometry, 24 (1995) 91-102.

[184] I.U.o.P.a.A. Chemistry, Comission on spectrochemical and other optical procedures for analysis - Nomenclature, symbols, units and their usage in spectrochemical analysis. II. Data Interpretation, Pure and Applied Chemistry, 45 (1976) 99-103.

[185] A. Lagalante, Atomic absorption spectroscopy: A tutorial review, Applied Spectroscopy Reviews, (1999) 173-189.

[186] E. Metcalfe, F.E. Prichard, Atomic absorption and emission spectroscopy, Wiley on behalf of ACOL, Chichester, 1987.

[187] D.C. Harris, Quantitative chemical analysis, 7th ed. ed., W. H. Freeman ; [Basingstoke : Palgrave, distributor], New York, 2007.

[188] J.J. Brehm, W.J. Mullin, Introduction to the structure of matter : a course in modern physics, Wiley, New York, 1989.

[189] B.V. L'vov, The analytical use of atomic absorption spectra Spectrochimica Acta, 17 (1961) 761-770.

[190] H. Massmann, Vergleich von atomabsorption und atomfluoreszenz in der graphitküvette, Spectrochimica Acta B: Atomic Spectroscopy, 23 (1968) 215-226.

[191] A. Volynskii, Chemical modiflers in modern electrothermal atomic absorption spectrometry, Journal of Analytical Chemistry, 58 (2003) 905-921.

[192] J. Sardans, F. Montes, J. Penuelas, Determination of As, Cd, Cu, Hg and Pb in biological samples by modern electrothermal atomic absorption spectrometry, Spectrochimica Acta Part B-Atomic Spectroscopy, (2010) 97-112.

[193] B. Tariba, A. Pizent, Z. Kljakovia-Gaspic, Determination of lead in croatian wines by graphite furnace atomic absorption spectrometry, Arhiv Za Higijenu Rada I Toksikologiju, 62 (2011) 25-31.

[194] P. Correia, C. Nomura, P. Oliveira, Multielement determination of cadmium and lead in urine by simultaneous electrothermal atomic absorption spectrometry with an end-capped graphite tube., Anal Sci, 19 (2003) 1519-1523.

[195] E. Lima, F. Barbosa, F. Krug, Lead determination in slurries of biological materials by ETAAS using a W-Rh permanent modifier, Fresenius Journal of Analytical Chemistry, 369 (2001) 496-501.

[196] J.C. Miller, J.N. Miller, Statistics and chemometrics for analytical chemistry, 4th ed. ed., Prentice Hall, Harlow, 2000.

[197] K. Srogi, A review: Application of microwave techniques for environmental analytical chemistry, Analytical Letters, 39 (2006) 1261-1288.

[198] M. Burguera, J. Burguera, Microwave sample pretreatment in analytical systems. A review, Quimica Analitica, 15 (1996) 112-122.

[199] J. Millos, M. Costas-Rodríguez, I. Lavilla, C. Bendicho, Multielemental determination in breast cancerous and non-cancerous biopsies by inductively coupled plasma-mass spectrometry following small volume microwave-assisted digestion., Anal Chim Acta, 622 (2008) 77-84.

[200] K.S. Suslick, Sonochemistry, Science, 247 (1990) 1439-1445.

[201] K.S. Suslick, Applications of ultrasound to materials chemistry, Mrs Bulletin, 20 (1995) 29-34.

[202] J. Capelo, S. Catarino, A. Curvelo-Garcia, M. Vaiao, Focused ultrasound versus microwave digestion for the determination of lead in must by electrothermal-atomic absorption spectrometry, Journal of Aoac International, 88 (2005) 585-591.

[203] K.S. Suslick, Ultrasonic physical mechanisms and chemical effects, in: Wiley Encyclopedia of Electrical and Electronics Engineering, John Wiley & Sons, Inc, 1999, pp. 646-657.

[204] W. Lauterborn, A. Vogel, Modern optical techniques in fluid-mechanics, Annual Review of Fluid Mechanics, 16 (1984) 223-244.

[205] J. Capelo, C. Maduro, C. Vilhena, Discussion of parameters associated with the ultrasonic solid-liquid extraction for elemental analysis (total content) by electrothermal atomic absorption spectrometry. An overview., Ultrason Sonochem, 12 (2005) 225-232.

[206] L. Amoedo, J. Capelo, I. Lavilla, C. Bendicho, Ultrasound-assisted extraction of lead from solid samples: a new perspective on the slurry-based sample preparation methods for electrothermal atomic absorption spectrometry, Journal of Analytical Atomic Spectrometry, 14 (1999) 1221-1226.

[207] J. Capelo, M. Galesio, G. Felisberto, C. Vaz, J. Pessoa, Micro-focused ultrasonic solid-liquid extraction (mu FUSLE) combined with HPLC and fluorescence detection for PAHs determination in sediments: optimization and linking with the analytical minimalism concept, Talanta, 66 (2005) 1272-1280.

[208] B. Batista, J. Rodrigues, V. Souza, F. Barbosa, A fast ultrasound-assisted extraction procedure for trace elements determination in hair samples by ICP-MS for forensic analysis, Forensic Science International, 192 (2009) 88-93.

[209] P. Bermejo-Barrera, A. Moreda-Pineiro, A. Bermejo-Barrera, Factorial designs for Cd, Cr, Hg, Pb and Se ultrasound-assisted acid leaching from human hair followed by atomic absorption spectrometric determination, Journal of Analytical Atomic Spectrometry, 15 (2000) 121-130.

[210] J. Capelo, I. Lavilla, C. Bendicho, Ultrasound-assisted extraction of cadmium from slurried biological samples for electrothermal atomic absorption spectrometry, Journal of Analytical Atomic Spectrometry, (1998) 1285-1290.

[211] I. Lavilla, J. Capelo, C. Bendicho, Determination of cadmium and lead in mussels by electrothermal atomic absorption spectrometry using an ultrasound-assisted extraction method optimized by factorial design, Fresenius Journal of Analytical Chemistry, 365 (1999) 283-288.

[212] D. Halls, Analytical minimalism applied to the determination of trace-elements by atomic spectrometry, Journal of Analytical Atomic Spectrometry, 10 (1995) 169-175.

[213] K. Ashley, R. Andrews, L. Cavazos, M. Demange, Ultrasonic extraction as a sample preparation technique for elemental analysis by atomic spectrometry, Journal of Analytical Atomic Spectrometry, 16 (2001) 1147-1153.

[214] M. Romdhane, C. Gourdon, Investigation in solid-liquid extraction: influence of ultrasound, Chemical Engineering Journal, 87 (2002) 11-19.

[215] P. Chow, R. Ng, B. Ogden, Using Animal Models in Biomedical Research: A Primer for the investigator, World Scientific, New Jersey, 2008.

[216] H. Bielarczyk, X. Tian, J. Suszkiw, Cholinergic denervation-like changes in rat hippocampus following developmental lead exposure., Brain Res, 708 (1996) 108-115.

[217] A. Thompson, D. Attwood, E. Gullikson, M. Howells, K. Kim, J. Kirz, J. Kortright, I. Lindau, Y. Liu, P. Pianetta, A. Robinson, J. Scofield, J. Underwood, G. Williams, X-Ray Data Booklet, 3rd ed., Lawrence Berkeley National Laboratory, 2009.

[218] R.W. Ryon, Polarization for background reduction in EDXRF - the technique that does indeed work, in: Advances in X-Ray Analysis, Denver, 2003, pp. 352-362.

[219] J. Boman, J. Isakson, Comparison between 2 X-ray-analysis software packages, X-Ray Spectrometry, 20 (1991) 305-314.

[220] G.V. Iyengar, W.E. Kollmer, H.J.M. Bowen, The elemental composition of human tissues and body fluids : a compilation of values for adults, Verlag Chimie, Weinheim ; New York, 1978.

[221] R. Klockenkämper, A. von Bohlen, B. Wiecken, Quantification in Total Reflection X-Ray Fluorescence analysis of microtome sections, Spectrochimica Acta Part B-Atomic Spectroscopy, 44 (1989) 511-517.

[222] C. Burrini, A. Cagnini, Determination of mercury in urine by ET-AAS using complexation with dithizone and extraction with cyclohexane, Talanta, 44 (1997) 1219-1223.

[223] A. Volynsky, B. Spivakov, Y. Zolotov, Solvent-extraction Electrothermal Atomic Absorption analysis, Talanta, 31 (1984) 449-458.

[224] E. Tserovsky, S. Arpadjan, Behavior of various organic-solvents and analytes in Electrothermal Atomic-Absorption Spectrometry, Journal of Analytical Atomic Spectrometry, 6 (1991) 487-491.

[225] G. Vale, S. Pereira, A. Mota, L. Fonseca, J. Capelo, Enzymatic probe sonication as a tool for solid-liquid extraction for total selenium determination by electrothermal-atomic absorption spectrometry., Talanta, 74 (2007) 198-205.

[226] X. Hu, Rapid coprecipitation-separation and flame atomic absorption spectrometric determination of lead and cadmium in water with cobalt (II) and ammonium pyrrolidine dithiocarbamate, International Journal of Environmental Analytical Chemistry, 91 (2011) 263-271.

[227] K. Provazi, B. Campos, D. Espinosa, J. Tenorio, Metal separation from mixed types of batteries using selective precipitation and liquid-liquid extraction techniques, Waste Management, 31 (2011) 59-64.

[228] I. Lavilla, A. Mosquera, J. Millos, J. Cameselle, C. Bendicho, Ultrasound-assisted extraction technique for establishing selenium contents in breast cancer biopsies by Zeeman-electrothermal atomic absorption spectrometry using multi-injection, Analytica Chimica Acta, 566 (2006) 29-36.

[229] T. Agusa, T. Matsumoto, T. Ikemoto, Y. Anan, R. Kubota, G. Yasunaga, T. Kunito, S. Tanabe, H. Ogi, Y. Shibata, Body distribution of trace elements in black-tailed gulls from

Rishiri Island, Japan: age-dependent accumulation and transfer to feathers and eggs., Environ Toxicol Chem, 24 (2005) 2107-2120.

[230] P. Bustamante, P. Bocher, Y. Chérel, P. Miramand, F. Caurant, Distribution of trace elements in the tissues of benthic and pelagic fish from the Kerguelen Islands., Sci Total Environ, 313 (2003) 25-39.

[231] D.C. Montgomery, Design and analysis of experiments, 6th ed. ed., Wiley, Hoboken ; [Great Britain], 2005.

[232] A.I. Khuri, T. Mathew, B.K. Sinha, Statistical tests for mixed linear models, Wiley, New York ; Chichester, 1998.

[233] P.R. Hinton, SPSS explained, Routledge, London, 2004.

[234] R.D. Andrews, L.A. Standridge, Understanding Statistics as a Language, Hope House Press, United States, 2010.

[235] T.A. Reddy, Applied Data Analysis and Modeling for Energy Engineers and Scientists, 1st ed., Springer, 2011.

[236] P. Barry, Comparison of concentrations of lead in human tissues, British Journal of Industrial Medicine, 32 (1975) 119-139.

[237] M. Moreira, E. Neves, Use of urine lead level as an exposure indicator and its relationship to blood lead, Cadernos de Saúde Pública, 24 (2008) 2151-2159.

[238] J. Quarterman, E. Morrison, Effect of age on absorption and excretion of lead, Environmental Research, 17 (1978) 78-83.

[239] A. Marques, J. Marques, C. Casaca, M. Carvalho, X-ray microprobe synchroton radiation X-ray fluorescence application on human teeth of renal insufficiency patients, Spectrochimica Acta Part B-Atomic Spectroscopy, 59 (2004) 1675-1680.

[240] C. Mason, S. MacDonald, Levels of cadmium, mercury and lead in otter and mink feces from the United-Kingdom, Science of the Total Environment, 53 (1986) 139-146.

[241] H. Mykkanen, J. Dickerson, M. Lancaster, Effect of age on the tissue distribution of lead in the rat, Toxicology and Applied Pharmacology, 51 (1979) 447-454.

[242] H. Schroeder, J. Balassa, W. Vinton, Chromium cadmium and lead in rats - effects on life span tumours and tissue levels, Journal of Nutrition, 86 (1965) 51-66.

[243] C. Gardella, Lead exposure in pregnancy: A review of the literature and argument for routine prenatal screening, Obstetrical & Gynecological Survey, (2001) 231-238.

[244] K. Mahaffey, J. Rader, J. Schaefer, S. Kramer, Comparative toxicity to rats of lead acetate from food or water, Bulletin of Environmental Contamination and Toxicology, 25 (1980) 541-546.

[245] W. Victery, C. Miller, S. Zhu, R. Goyer, Effect of different levels and periods of lead-exposure on tissue-levels and excretion of lead, zinc, and calcium in the rat, Fundamental and Applied Toxicology, 8 (1987) 506-516.

[246] F. Sonmez, O. Donmez, H. Sonmez, A. Keskinoglu, C. Kabasakal, S. Mir, Lead exposure and urinary N-acetyl beta D glucosaminidase activity in adolescent workers in auto repair workshops, Journal of Adolescent Health, 30 (2002) 213-216.

[247] B. Momcilovic, K. Kostial, Kinetics of lead retention and distribution in suckling and adult rats, Environmental Research, 8 (1974) 214-220.

[248] J.I. Rader, E.M. Celesk, J.T. Peeler, K.R. Mahaffey, Retention of lead acetate in weanling and adult rats, Toxicology and Applied Pharmacology, 67 (1983) 100-109.

[249] R.W. Leggett, An age-specific kinetic model of lead metabolism in humans, Environmental Health Perspectives, 101 (1993) 598-616.

[250] H. Schroeder, I. Tipton, Human body burden of lead, Archives of Environmental Health, 17 (1968) 965-978.

[251] R.B. Holtzman, Measurement of the natural contents of RaD (Pb210) and RaF (Po210) in human bone--estimates of whole-body burdens., Health Phys, 9 (1963) 385-400.

[252] R.G. Smith, J. Szajnar, L. Hecker, Study of lead levels in experimental animals, Environmental Science & Technology, 4 (1970) 333-338.

[253] R.N. Khandekar, S.J. Anand, Measurement of Pb-210 (RaD) in human bone at Bombay, India, Health Physics, 20 (1971) 83-85.

[254] N. Adams, R. Boice, Development of dominance in domestic rats in laboratory and seminatural environments, Behavioural Processes, 19 (1989) 127-142.

[255] N. Adams, R. Boice, A longitudinal-study of dominance in an outdoor colony of domestic rats, Journal of Comparative Psychology, 97 (1983) 24-33.

[256] J. Leeder, G. Kearns, Pharmacogenetics in pediatrics - Implications for practice, Pediatric Clinics of North America, 44 (1997) 55-77.

[257] R. Jenkins, R. Manne, R. Robin, C. Senemaud, Nomenclature, symbols, units and their usage in spectrochemical analysis .8. Nomenclature system for X-Ray Spectroscopy - (Recommendations 1991) Pure and Applied Chemistry, 63 (1991) 735-746.

[258] M.M. R. Martoja, Initiation aux tecniques de l'histologie animal, Masson and Cie, Paris, 1967.

[259] R.D. Lillie, Histopathologic technic and practical histochemistry, Blakiston, New York, 1954.

[260] P.R. Wheater, H.G. Burkitt, Functional histology : a text and colour atlas, 2nd ed. / revised and edited by Paul R. Wheater and H. George Burkitt / drawings by Philip J. Deakin. ed., Churchill Livingstone, Edinburgh, 1987.

[261] P. Kuisma-Kursula, Accuracy, precision and detection limits of SEM-WDS, SEM-EDS and PIXE in the multi-elemental analysis of medieval glass, X-Ray Spectrometry, 29 (2000) 111-118.

[262] S.A.E. Johansson, J.L. Campbell, PIXE : a novel technique for elemental analysis, Wiley, Chichester, 1988.

[263] M. Araujo, L. Alves, J. Cabral, Comparison of EDXRF and PIXE in the analysis of ancient gold coins, Nuclear Instruments & Methods in Physics Research Section B-Beam Interactions With Materials and Atoms, 75 (1993) 450-453.

[264] M. Reis, P. Chaves, V. Corregidor, N. Barradas, E. Alves, F. Dimroth, A. Bett, Detection angle resolved PIXE and the equivalent depth concept for thin film characterization, X-Ray Spectrometry, 34 (2005) 372-375.

[265] M. Reis, L. Alves, DATTPIXE, a computer package for TTPIXE data-analysis, Nuclear Instruments & Methods in Physics Research Section B-Beam Interactions With Materials and Atoms, 68 (1992) 300-304.

[266] C. Pascual-Izarra, N. Barradas, M. Reis, LibCPIXE: A PIXE simulation open-source library for multilayered samples, Nuclear Instruments & Methods in Physics Research Section B-Beam Interactions With Materials and Atoms, 249 (2006) 820-822.